AD-A165 916 CALIBRATED L-BAND TERRAIN MEASUREMENTS AND ANALYSIS PROGRAM. (U) ENVIRONMENTAL RESEARCH INST OF MICHIGAN ANN ARBOR R W LARSON ET AL. FEB 86 ERIM-174200-5-P 1/2

UNCLASSIFIED RADC-TR-85-266 F19628-84-C-0081 F/G 8/6 NL

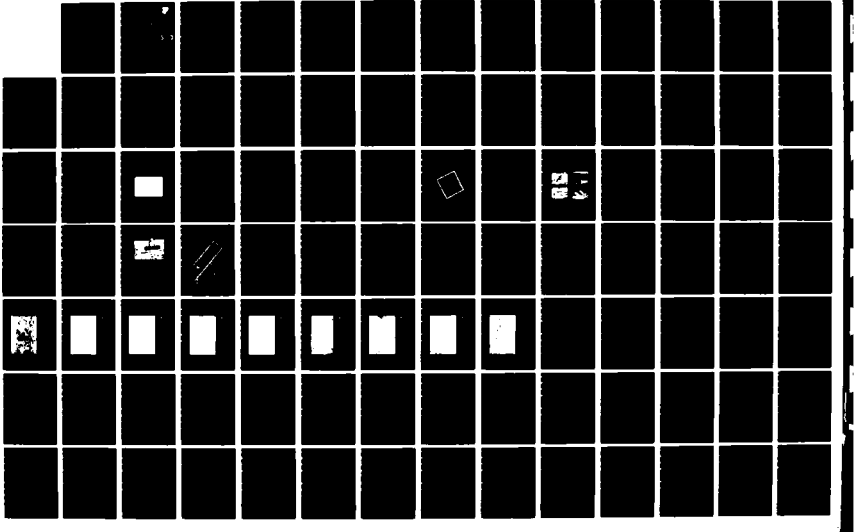

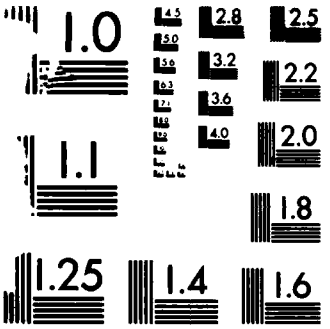

RADC-TR-85-266
Interim Report
February 1986

CALIBRATED L-BAND TERRAIN MEASUREMENTS AND ANALYSIS PROGRAM

Environmental Research Institute of Michigan

R. W. Larson
E. S. Kasischke
A. Maffett

ROME AIR DEVELOPMENT CENTER
Air Force Systems Command
Griffiss Air Force Base, NY 13441-5700

This report has been reviewed by the RADC Public Affairs Office (PA) and is releasable to the National Technical Information Service (NTIS). At NTIS it will be releasable to the general public, including foreign nations.

RADC-TR-85-266 has been reviewed and is approved for publication.

APPROVED: K V N Rao

K. V. N. RAO
Project Engineer

APPROVED: Allan C. Schell

ALLAN C. SCHELL
Chief, Electromagnetic Sciences Division

FOR THE COMMANDER: John A. Ritz

JOHN A. RITZ
Plans & Programs Division

If your address has changed or if you wish to be removed from the RADC mailing list, or if the addressee is no longer employed by your organization, please notify RADC (EECT) Hanscom AFB MA 01731-5000. This will assist us in maintaining a current mailing list.

Do not return copies of this report unless contractual obligations or notices on a specific document requires that it be returned.

UNCLASSIFIED
SECURITY CLASSIFICATION OF THIS PAGE

ADA 165916

REPORT DOCUMENTATION PAGE

1a REPORT SECURITY CLASSIFICATION UNCLASSIFIED	1b RESTRICTIVE MARKINGS N/A
2a SECURITY CLASSIFICATION AUTHORITY N/A	3 DISTRIBUTION / AVAILABILITY OF REPORT Approved for public release; distribution unlimited.
2b DECLASSIFICATION / DOWNGRADING SCHEDULE N/A	
4 PERFORMING ORGANIZATION REPORT NUMBER(S) 174200-5-P	5 MONITORING ORGANIZATION REPORT NUMBER(S) RADC-TR-85-266
6a NAME OF PERFORMING ORGANIZATION Environmental Research Institute of Michigan 6b OFFICE SYMBOL (If applicable)	7a NAME OF MONITORING ORGANIZATION Rome Air Development Center (EECT)
6c ADDRESS (City, State, and ZIP Code) P.O. Box 8618 Ann Arbor MI 48107	7b ADDRESS (City, State, and ZIP Code) Hanscom AFB MA 01731-5700
8a NAME OF FUNDING / SPONSORING ORGANIZATION Rome Air Development Center 8b OFFICE SYMBOL (If applicable) EECT	9 PROCUREMENT INSTRUMENT IDENTIFICATION NUMBER F19628-84-C-0081
8c ADDRESS (City, State, and ZIP Code) Hanscom AFB MA 01731-5000	10 SOURCE OF FUNDING NUMBERS PROGRAM ELEMENT NO: 62702F; PROJECT NO: 4600; TASK NO: 15; WORK UNIT ACCESSION NO: 73

11 TITLE (Include Security Classification)
CALIBRATED L-BAND TERRAIN MEASUREMENTS AND ANALYSIS PROGRAM

12 PERSONAL AUTHOR(S)
R. W. Larson, E. S. Kasischke, A. Maffett

13a TYPE OF REPORT	13b TIME COVERED	14 DATE OF REPORT (Year, Month, Day)	15 PAGE COUNT
Interim	FROM Apr 84 TO Apr 85	February 1986	164

16 SUPPLEMENTARY NOTATION
N/A

17 COSATI CODES		
FIELD	GROUP	SUB-GROUP
17	09	
20	14	

18 SUBJECT TERMS (Continue on reverse if necessary and identify by block number)
Electromagnetic Scattering, Ground Truth, Terrain Cross Section Measurements, Soil Moisture, Dielectric Constant, (See Reverse)

19 ABSTRACT (Continue on reverse if necessary and identify by block number)
This report presents the initial results of a three year program for the collection and analysis of L-band calibrated backscatter data from various terrain types. During the first year advantage was taken of two SAR data collection programs to obtain ground measurements simultaneously with the SAR flights. These data collection flights were conducted in North Carolina during April 1984 sponsored by USGS and during August - September 1984 in Long Island, sponsored by ONR. Ground data were collected at specific sites during both SAR flights and included measurement of dielectric constant, surface roughness and moisture. The reduction of ground data and the calibration of the SAR are described. Calibration of the SAR has been verified and an error of less than 3 dB in absolute calibration of the L-band channel demonstrated.

20 DISTRIBUTION / AVAILABILITY OF ABSTRACT ☐ UNCLASSIFIED/UNLIMITED ☒ SAME AS RPT ☐ DTIC USERS	21 ABSTRACT SECURITY CLASSIFICATION UNCLASSIFIED
22a NAME OF RESPONSIBLE INDIVIDUAL K.V.N. Rao	22b TELEPHONE (Include Area Code) (617) 861-3106 22c OFFICE SYMBOL RADC (EECT)

DD FORM 1473, 84 MAR 83 APR edition may be used until exhausted
All other editions are obsolete

SECURITY CLASSIFICATION OF THIS PAGE
UNCLASSIFIED

17. COSATI CODES (Continued)

Field	Group
09	03

18. SUBJECT TERMS (Continued)

L-band
SAR Data

PREFACE

The work described in this report was conducted by personnel in the Radar Division of the Environmental Research Institute of Michigan. The work reported covers the period April 1984 through April 1985 and discusses the results of the first year of a three-year program. This work is supported by the Electronic Systems Division, Air Force Systems Command, USAF, Hanscom AFB, MA under Contract No. F19628-84-0081. The Air Force technical monitor is Dr. K.V.N. Rao, Hanscom AFB. The SAR data utilized in the research discussed herein were collected for programs sponsored by the U.S. Geological Survey (USGS) under Contract No. 14-08-0001-21748 and the Office of Naval Research (ONR) under Contract No. N00014-81-C-0692.

The principal investigator for this work is Richard W. Larson. The work described in this report was performed by R.W. Larson, A. Maffett and E.S. Kasischke.

ACKNOWLEDGEMENTS

The accomplishments discussed in this report would not have been possible without the cooperation and help of a number of people and organizations. It is a pleasure to acknowledge the help of the following individuals from ERIM: Mr. T. Kladzyk for his efforts in assisting in the installation of the calibration reflector arrays, in the collection of ground measurements and in performing the laboratory dielectric constant measurements; Mr. Brian Denemy for assisting in the reduction of the ground measurement data; Mr. C. Wackerman and Dr. P. Jackson for digitally processing the SAR data and to Mr. P. Paus for digital analysis of the SAR data.

Special acknowledgement and thanks are given to Mr. John Jones, technical monitor of the USGS SAR data program in North Carolina and to Mr. Robert Winokur, ONR technical monitor of the SARSEX program in Long Island, for permission to use the SAR data for this research effort.

Also, the contribution of Dr. Sandy Davidson of Duke University Forestry Department for his help in obtaining ground data for the Duke Forest sites is gratefully acknowledged. And special thanks are given to Lt. C. Watts and Mr. R. Rasmussen of the Grumman Aerospace Corp. facilities at Peconic Airport, Long Island for permitting the use of the Peconic Airport as the location for the extensive SAR calibration reference reflector array.

TABLE OF CONTENTS

LIST OF FIGURES

LIST OF FIGURES
(Continued)

LIST OF FIGURES
(Continued)

LIST OF FIGURES
(Continued)

LIST OF FIGURES
(continued)

LIST OF FIGURES
(Concluded)

LIST OF TABLES

CALIBRATED L-BAND TERRAIN MEASUREMENTS AND ANALYSIS PROGRAM

1
INTRODUCTION

This report presents the initial results of a three-year program being conducted by the Environmental Research Institute of Michigan (ERIM) for the Electronics Systems Division of the U.S. Air Force Systems Command. The goal of this program is to collect, process and statistically analyze calibrated L-band clutter data.

This report gives the results from the first year of this three-year program. It also outlines the procedures which will be used to further reduce and analyze the calibrated L-band terrain data. This program was designed to use existing calibrated synthetic aperture radar (SAR) data, as well as SAR data collected during two flight programs in 1984. During these programs, ground measurements of surface roughness and dielectric characteristics were obtained simultaneously with the SAR overflights. SAR data from one of these data collection programs has been digitally processed into imagery, and using an existing calibration algorithm, L-band terrain clutter statistics generated. Ground measurements made in test areas during the data gathering period have been reduced to obtain surface roughness statistics and dielectric constant values.

This report is divided into six chapters, including this introduction. Chapter 2 presents an executive summary, which includes a discussion of the overall approach, the specific tasks of the three-year program, and the significant achievements of the past year. Chapter 3 discusses the sources of data used for this program. Chapter 4 presents the data analysis and reduction techniques used to produce calibrated L-band terrain measurements from L-band SAR imagery and outlines the techniques used to reduce the ground measurements. Chapter 5 presents the data analysis and reduction techniques to be used during the remainder of this program. Finally,

Chapter 6 discusses recommended research areas for analysis of L-band terrain measurements beyond the end of this program. An appendix to this report presents the results from the ground measurements, including data products from reduction of the surface roughness measurements and photographs of test sites.

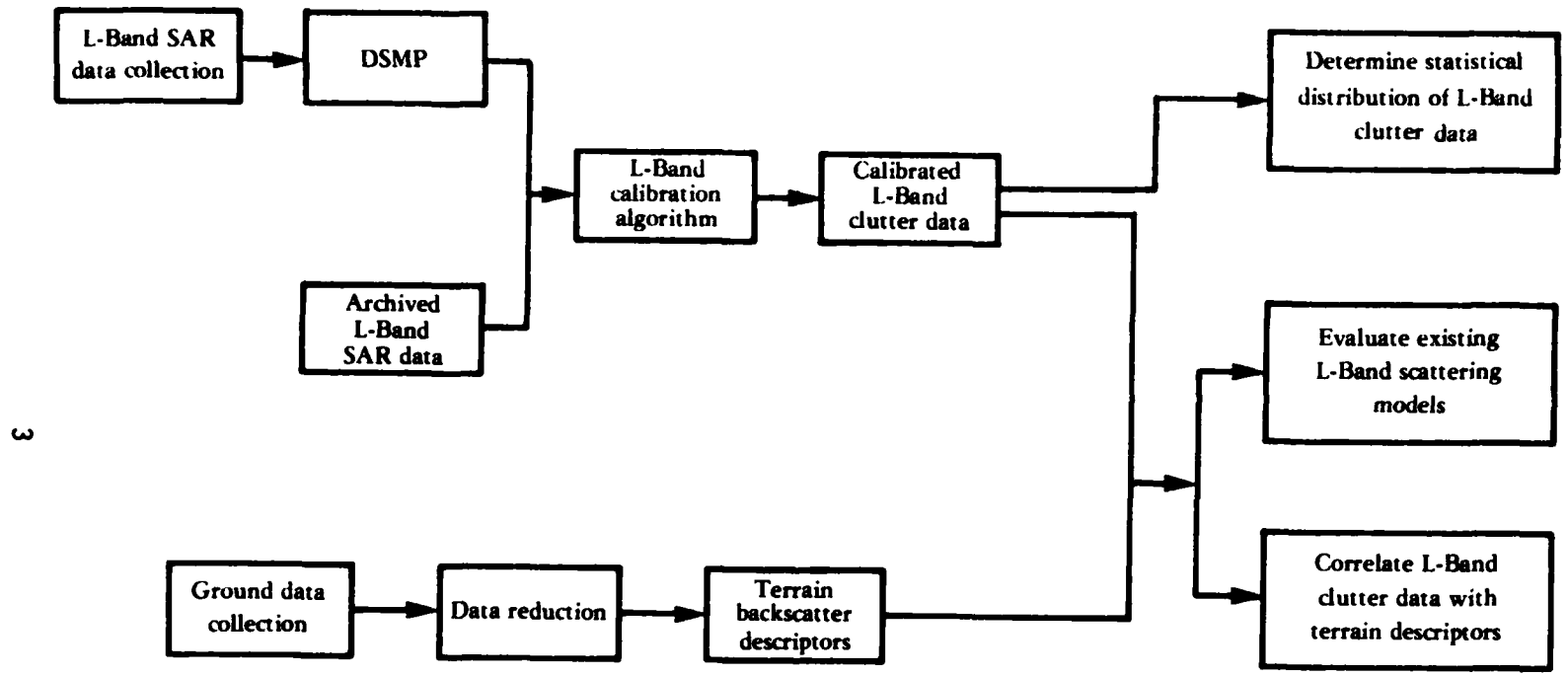

Figure 1. Approach to the Calibrated L-Band Terrain Measurements and Analysis Program

2
EXECUTIVE SUMMARY

This report discusses the results of the first of a three-year program to collect, process and analyze L-band clutter data. The goals of this program are to:

- Determine the statistical distribution of L-band clutter data as a function of terrain types,
- Evaluate existing L-band clutter or scattering models, and
- Correlate L-band clutter measurements with terrain scattering descriptors.

The program was designed to address the above objectives using existing or recently collected calibrated SAR imagery. Figure 1 outlines the overall approach of the program.

The program contains six distinct tasks:

1. SAR data collection and ground measurements,
2. SAR data processing,
3. Ground data reduction,
4. Determination of the statistical distribution of L-band clutter data,
5. Evaluation of L-band clutter/scattering models, and
6. Correlation of L-band clutter data to ground measurements.

Table 1 summarizes the elements of each of these tasks and presents a schedule for their completion.

During the past year, advantage was taken of two SAR data collection missions which were conducted using the CV-580 SAR system. These missions were carried out near Durham, North Carolina during April 1984 and at and around the Peconic River Airport on Long

Table 1

Task Summary and Schedule for the

Calibrated L-Band SAR Terrain Measurements

and Analysis Program

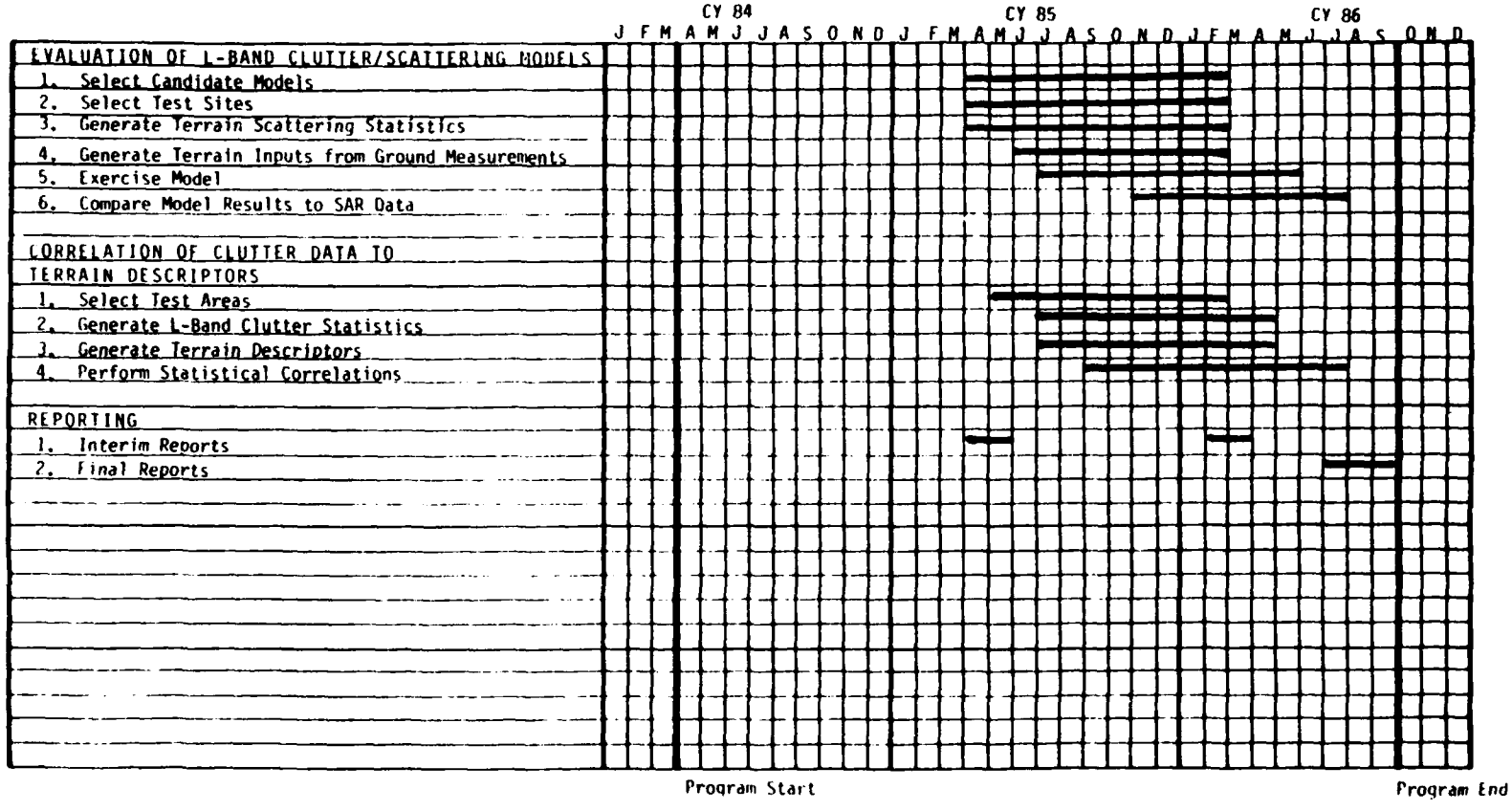

Island, NY during late August and early September 1984. The North Carolina mission was sponsored by the U.S. Geological Survey (USGS), and the Long Island mission was sponsored by the Office of Naval Research (ONR). Extensive SAR calibration and ground measurements were obtained coincident with these data collection missions. These latter efforts were supported by this program and are described in this report.

Descriptions of the SAR calibration reference reflector arrays are given along with examples of calibration relationships for the SAR L-band channel. As many as 21 reference reflectors were used to calculate each SAR calibration curve for L-band. Results from the initial calibration verification analysis indicate that a calibration accuracy of less than 3 dB was achieved. Initial results obtained from applying calibration data to determine scattering coefficients are given. Average values of calculated σ_0 (HH polarization, 63° incidence angle) included 0.005 for grass fields, 0.015 for forested sites and 0.020 for corn fields.

Ground measurements obtained included surface height profiles, dielectric constant values, moisture content and plant density. Surface height profile data have been used to obtain height spectra, slope, radii of curvature statistics and correlation length. Examples of these data are presented.

An example of the statistical analysis procedure is given along with preliminary results. An inverse Gaussian (IG) distribution was selected to model the histogram of the scattering coefficients. A three parameter description has been derived for an IG distribution using emperical data.

Future plans include continuation of the analysis using the I.G. distribution to determine distinct signatures that can be related to the surface measurements. Also, surface profile and electrical properties of the surface will be used to evaluate models that describe the scattering characteristics observed from SAR data.

Several surface scattering models have been selected from the literature as candidates for initial comparison to measured scattering data. Each model utilizes a particular description of the scattering surface that can be derived from available measured ground data. Future analysis to verify or to justify modifications to existing models will be conducted. SAR data from selected areas will be used to extend the range of incident angles over which the scattering response is available.

3
DATA SETS

The approach taken to achieve the objectives of this program was to obtain L-band radar cross section statistics using data collected by the ERIM/Canadian Centre for Remote Sensing (CCRS) CV-580 SAR System. During the past year, terrain roughness characteristics were obtained simultaneously with two SAR data collection missions being performed for the U.S. Geological Survey (USGS) and the Office of Naval Research (ONR). In addition, archived, calibrated L-band SAR data are also available for determining clutter statistics of terrain types not present in the above data sets.

In this chapter, we will first discuss the characteristics of the CV-580 SAR System and the steps taken to achieve calibration for this system. This will be followed by a description of the two test sites where SAR and surface roughness measurements were obtained. In addition, the ground measurements themselves will be described.

3.1 ERIM/CCRS CV-580 SAR SYSTEM

From 1978 through 1984, ERIM operated a multifrequency and multipolarization SAR in conjunction with CCRS. This SAR system was maintained through a leasing agreement between ERIM and CCRS and is called the CV-580 SAR System. This facility was used extensively over the past six years in a variety of oceanographic and terrestrial research programs. The leasing agreement between ERIM expired at the end of CY84. At this time, the CV-580 SAR System is not available for U.S. Government sponsored research programs. Efforts are underway to transfer this system into a U.S.-owned aircraft.

The CV-580 SAR System was essentially an X-band radar to which an L-band and a C-band capability was added. Because of this configuration, the X-band channels were always available, and, in addition, one could operate either the L-band or the C-band channels

simultaneously with the X-band channel. For each frequency band, two orthogonal polarizations were available. The radar could transmit either horizontal or vertical polarization and receive both the parallel- and perpendicular-polarized returns. The radar antenna could be pointed so as to image on either side of the aircraft. Table 2 summarizes the relevant radar parameters for this system.

Figure 2 presents a functional diagram of the CV-580 SAR System. The major components of the SAR are its antennas, the transmitters and receivers, the calibration signal generator, the optical film recorders, the digital tape recorder and the X-band real-time processor.

Figure 3 presents a more detailed diagram of the reference oscillators, transmitters and receivers of the SAR system. This diagram shows how the L-band and C-band wavelengths are converted to X-band.

Figure 4 presents a diagram of the calibration signal generator (CSG) system, which is used as a monitoring and reference source for the periodic verification of the SAR's system transfer function. The calibration signal generator produces synthetic target signals which are added into the radar receiver (Walker and Larson, 1981; Larson, et al., 1981; 1982; 1985). The form of the synthetic target corresponds to a given range, and the intensity is controlled by an accurately calibrated R.F. attenuator. At specific times during the imaging flight, the calibration signals are inserted into the receiver at the antenna terminals, so that the radar receiver detects them as a radar return. Using a sequence of such signals with different intensities, along with the processed signals from the corner reflectors, a calibration curve can be produced of output signal power versus radar cross section (σ_0). When combined with measurements of precision corner reflectors, CSG measurements can be used to achieve absolute calibration of the SAR (see Walker and Larson, 1981; or Larson, et al., 1985). The synthetic targets from the CSG

TABLE 2
CV-580 SAR SYSTEM PARAMETERS

Parameter	X-Band	C-Band	L-Band
Center Frequency	9.35 GHz	5.3 GHz	1.185 GHz
Wavelength	3.2 cm	5.7 cm	23.5 cm
Nominal Altitude	7 km	7 km	7 km
Nominal Platform Velocity	250 knots	250 knots	250 knots
Swath Width/Channel (slant range)	5.2 km	5.2 km	5.2 km
Incidence Angle	0° - 90°	0° - 90°	0° - 90°
FM Rate	33.3 MHz/μsec	33.3 MHz/μsec	33.3 MHz/μsec
Pulse Length	2.7 μsec	2.7 μsec	1.8 μsec
Bandwidth	89 MHz	89 MHz	60 MHz
Azimuth Beamwidth	1.15°	2.5°	8°
Nominal Slant Range Resolution	3 m	3 m	3 m
Nominal Azimuth Resolution	3 m	3 m	3 m
Azimuth Scale Factor (Approx.)	15,000	15,000	41,500
Range Scale Factor (Approx.)	196,000	196,000	196,000
Data Recording	Real Time Image	Real Time Image	
	Opt. Sig. Film	Optical Signal Film	Optical Signal Film
	Dig.Tape (HDDT)	Digital Tape	Digital Tape

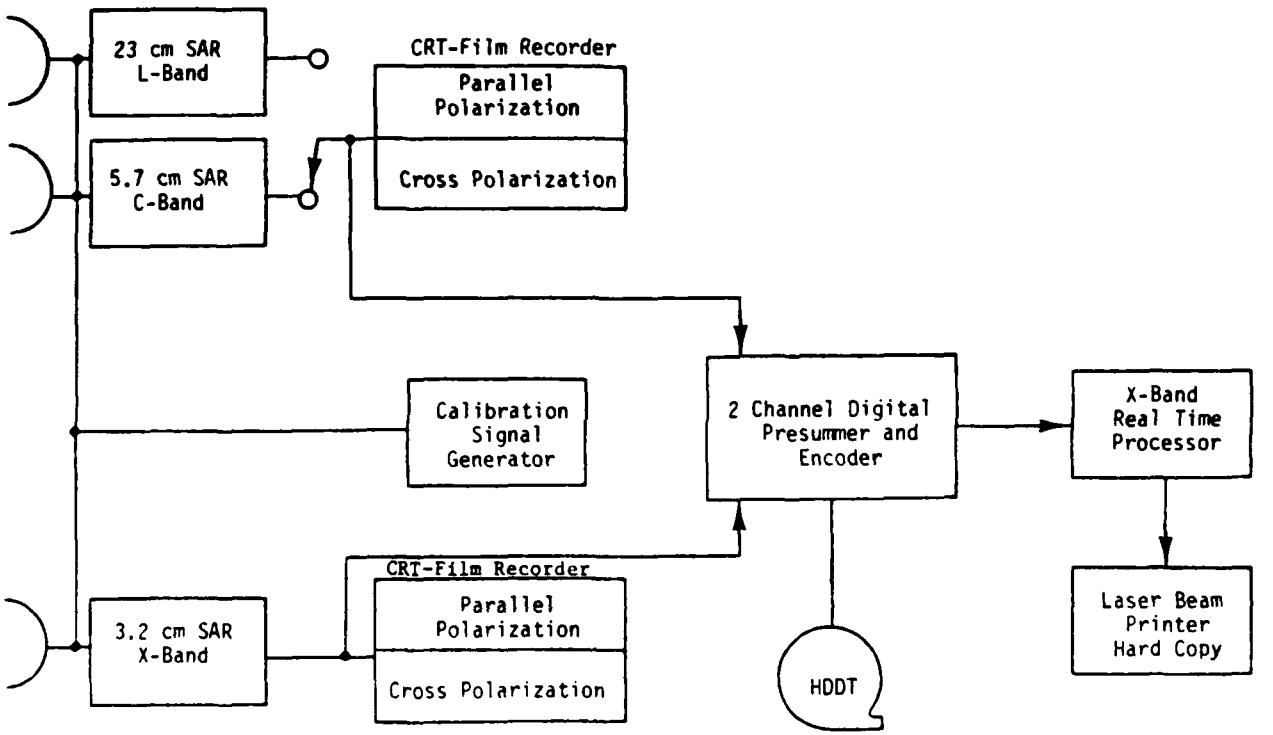

Figure 2. Schematic Diagram of ERIM/CCRS X/C/L Band SAR System

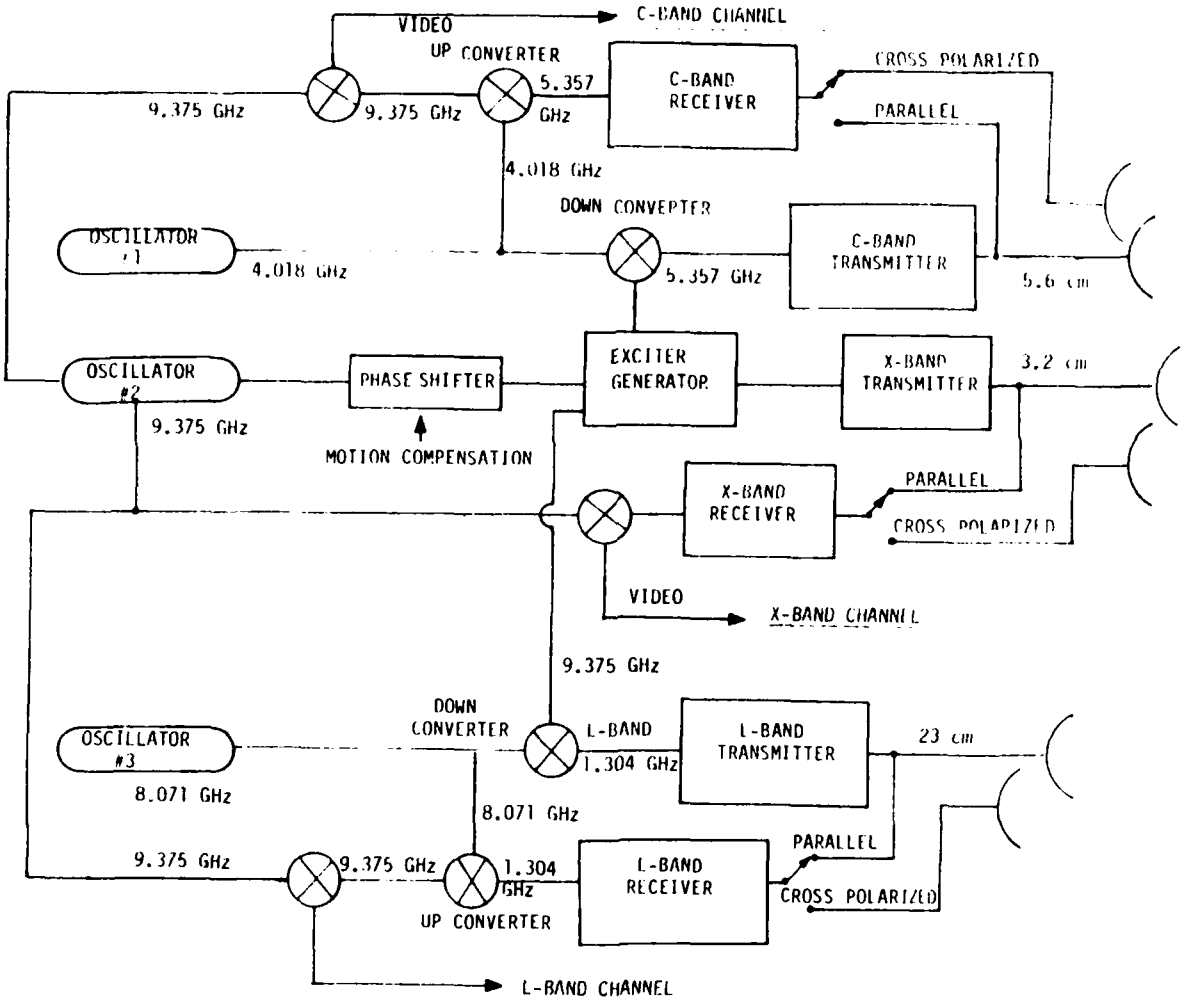

Figure 3. Schematic Diagram of CV-580 SAR Receiver/Transmitter

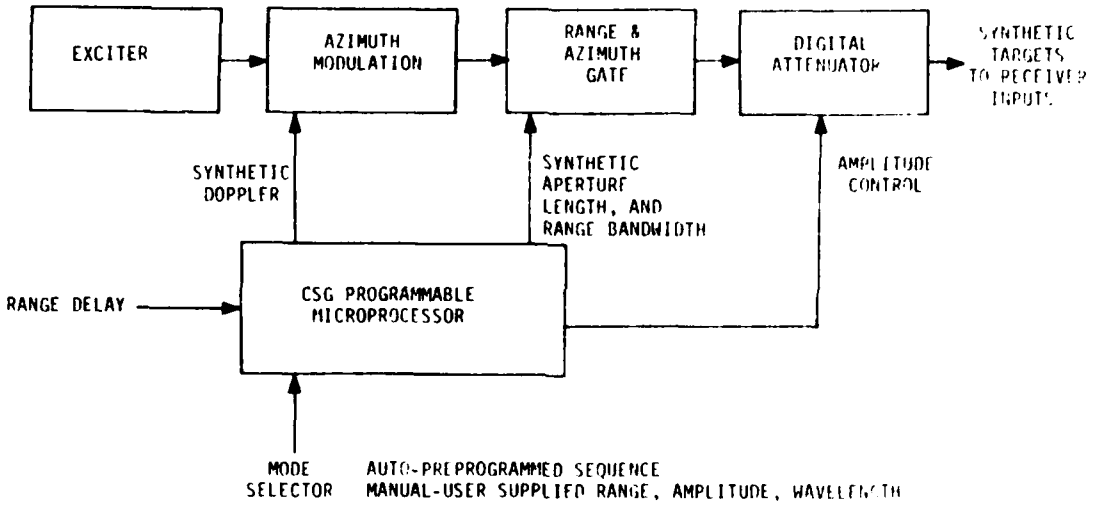

Figure 4. Schematic Diagram of CV-580 SAR X/L Calibration Signal Generator

can be recorded both optically and digitally, but only at X- and L-band.

Figure 5 presents an optically processed L-band image of the calibration signals. Table 3 summarizes the signal power and equivalent radar cross sections for these calibration signals.

The three SARs which comprised the CV-580 SAR System are similar in that they all use the synthetic aperture technique to produce imagery with fine cross-range resolution. These SARs used pulse compression to achieve fine resolution in the range dimension. Each recording channel was adjusted to produce imagery of a selected swath parallel to the flight direction. The width of the imaged swath was determined by the range increment of signals displayed on the recording system. The displacement of the recorded swath from the flight line was adjustable by the radar operator. The CV-580 SAR System is extensively described by Rawson, et al. (1975) and CCRS (1983).

The SAR phase histories were recorded onboard the aircraft both optically on 70 mm film and digitally on high density digital tape (HDDT). The optical recording system recorded four data channels, while the digital system was restricted to recording only two of the four data channels during data collection. In addition to the optical and digital recorders, a real-time digital SAR processor onboard the CV-580 generated X-band imagery. The real-time imagery was not intended to be of high quality, but provided "quick-look" data necessary for system performance evaluation and planning purposes during data collection missions. It was also used to select digital data of interest for subsequent processing and analysis. Table 4 presents the various data recording options available on the system. Figure 6 schematically illustrates the various SAR data recording and processing options.

L-BAND CALIBRATION SIGNALS

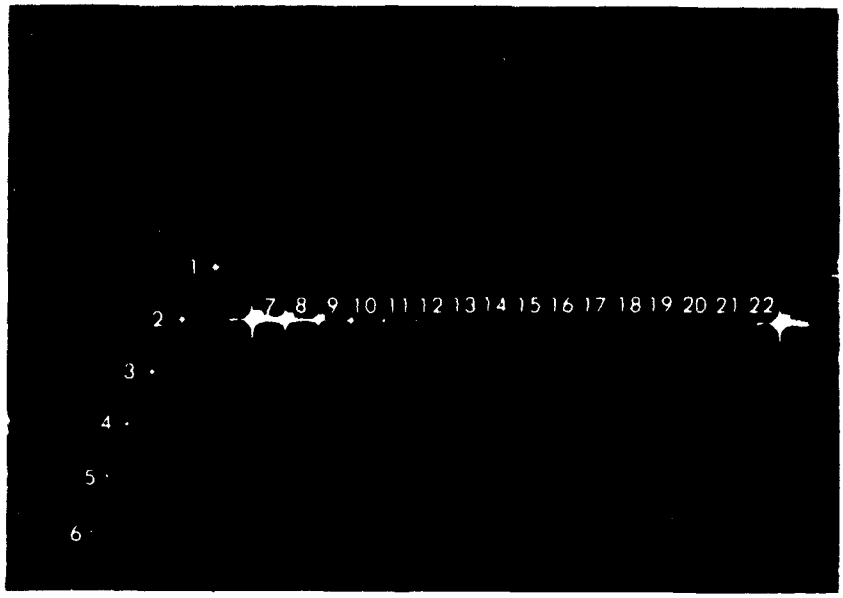

Figure 5. Image of L-Band Calibration Signals

TABLE 3
INTERNAL CALIBRATION SIGNAL POWER AND EQUIVALENT RADAR CROSS SECTIONS AT A RANGE OF 10 KM

Cal. Signal Number	Cal. Signal Power in dB Relative to 1 mW	Equivalent Cross Section 10 km in dB Relative to 1 m^2
1-6*	-95	15
7	-65	45
8	-70	40
9	-75	35
10	-80	30
11	-85	25
12	-90	20
13	-95	15
14	-100	10
15	-105	5
16	-110	0
17	-115	-5
18	-120	-10
19	-125	-15
20	-130	-20
21	-135	-25
22	-95	15

*Calibration signals 1-6 have the same power and are injected at a variable range. Signals 7-22 are at the same range.

TABLE 4
PRESENT X-, C- AND L-BAND SAR DATA RECORDING CAPABILITY

SAR Mode	Optical Recording (2 Recorders) Channels	Swath	Digital Recording (A+B) Channels	Swath	Resolution	Real-Time Processor Channels	Swath	Comments
X-band wide swath	1 (2 films)	20 km	A and B	12 km 20 km	3 m 6 m	Near range 12 km	6 km	Data buffer required
4 channel X, C or X, L	4	5.2 km	A any channel B X, C, L, like, cross	6 km	3 m	X- or C-band Channel A only	6 km	Scene illumination depends on altitude and incidence angle range
3 channel X, C or X, L	3	10 km 5.2 km	A and B, wide swith channel or A, B independent assignment	12 km 6 km	3 m 6 m	X- or C-band Channel A only	6 km	Wide swath channel illumination strongly affected by antenna pattern and imaging geometry
2 channel X, C or X, L	2	10 km	A and B (either channel)	12 km	3 m	Channel A if not L-band	6 km	As above

Notes: 1. The extended swath recording modes enhance the system signal to noise for weak returns on the optical recordings only.

2. An X band signal film will contain approximately 215 nautical miles of data, a high density digital tape will contain approximately 130 nautical miles of data.

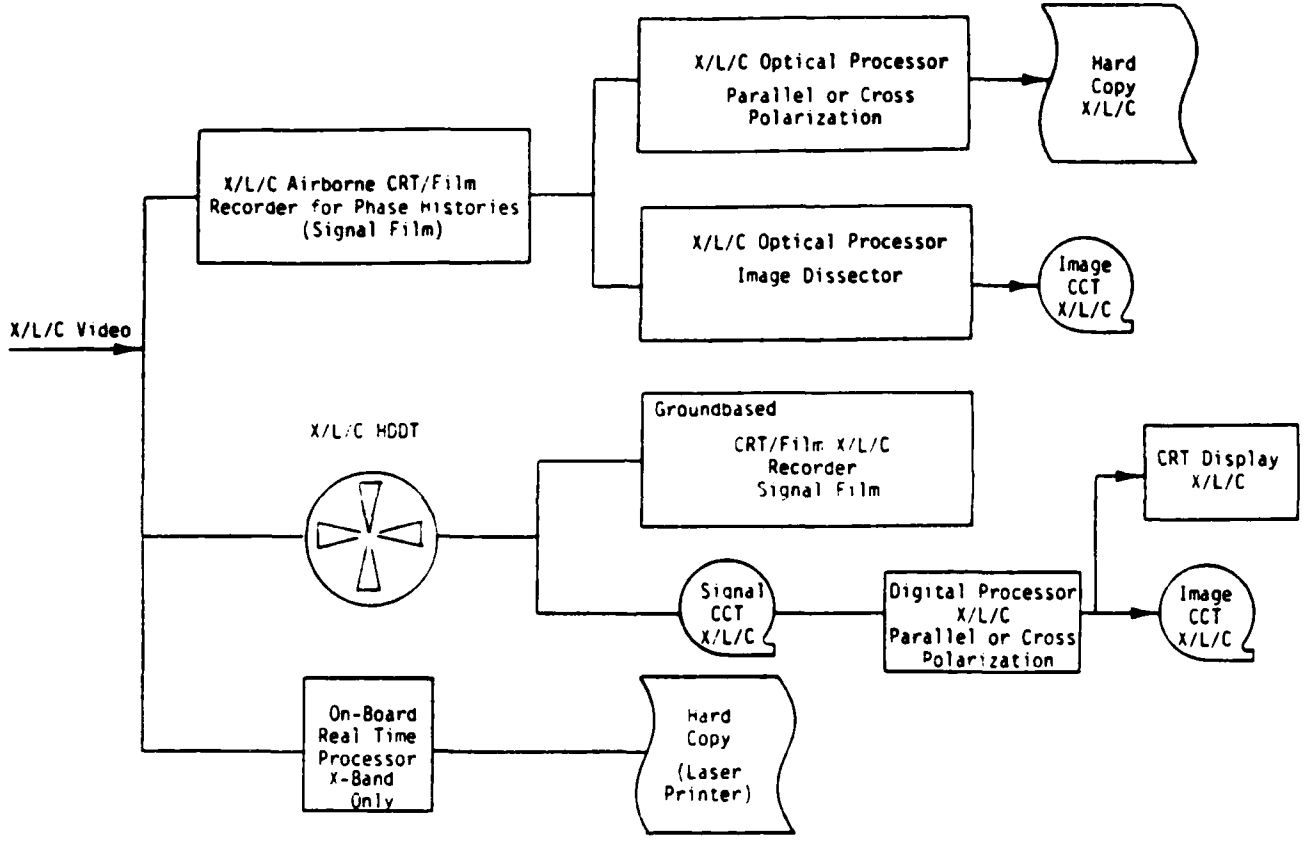

Figure 6. CV-580 SAR Signal Recording and Processing Options

3.2 DATA SETS

There are three sources of data for calibrated L-band terrain measurements which will be used in this program: (1) data collected during a USGS program in April 1984; (2) data collected during an ONR-sponsored program in August/September 1984; and (3) L-band SAR imagery archived at ERIM. These data sets are discussed in this section.

3.2.1 USGS SAR DATA

In April 1984, the U.S. Geological Survey sponsored a series of SAR data collection flights near Durham, N.C. In conjunction with these flights, a series of test passes were made over a forested area in order to verify the operational readiness of the SAR. This area consisted primarily of research forests owned and maintained by Duke University and is collectively known as the Duke Forest (see Figure 7). This forest consists primarily of pure and mixed 1 to 50 hectare plots of pine (southern, Loblolly and Virginia), whose ages range from one to over 100 years old. There are also mixed stands of hardwoods (red gum, yellow poplar, river birch, sycamore, beech and white, red, black, post and blackjack oak) scattered throughout the area.

Duke University researchers and foresters actively manage this forest and records of tree species, age and density are maintained for each plot within the forest. A total of five flights were made over the Duke Forest test site and 11 flights over other sites in this area. Both horizontally- and vertically-polarized imagery were collected. Table 5 summarizes the SAR flights.

During both the USGS and ONR flight programs, a set of calibrated reference reflectors were deployed to provide calibration references for the SAR imagery. The types of reflectors are pictured in Figure 8. A series of corner reflectors were deployed at a site within

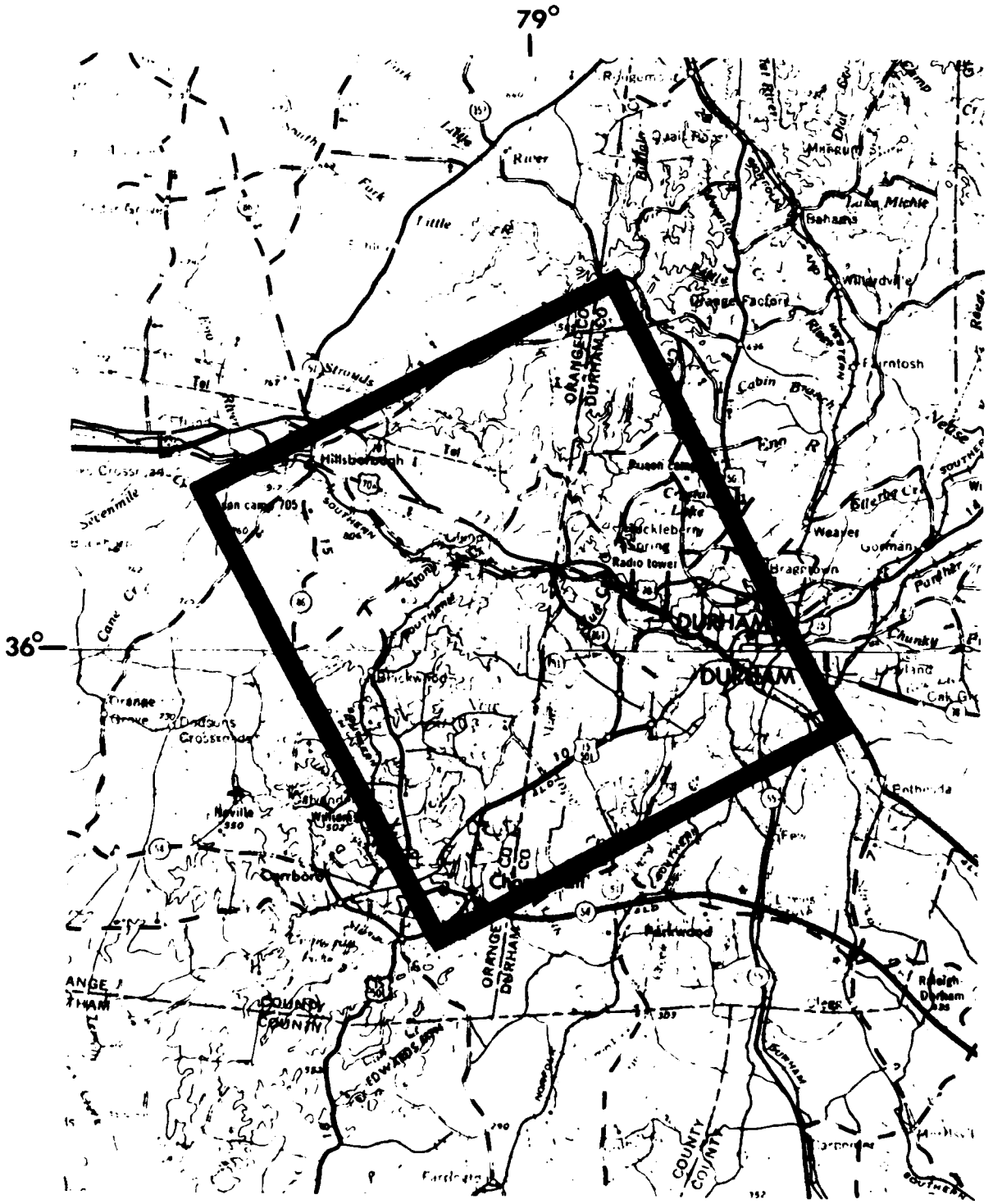

Figure 7. Location of Duke Forest SAR Test Area

TABLE 5
SUMMARY OF USGS MULTICHANNEL SAR FLIGHTS

Date	Mission	Pass	Area*	Time (EST)	Frequency and Polarization**							
					X-VV	X-HH	X-VH	X-HV	L-VV	L-HH	L-VH	L-HV
8 April 1984	USGS-1	1	T	13:06-13:10	±		±		+		+	
		2	T	13:34-13:40	±		+		±		+	
		3	B	13:56-13:59	±		+		±		+	
		4	B	14:20-14:25	±		+		±		+	
		5	A	14:41-14:46	±		+		±		+	
		6	A	15:05-15:09	±		+		±		+	
		7	A/B	15:27-15:31	±		+		±		+	
		8	T	15:50-15:56		±		+		±		+
		9	A	16:21-16:24	+		+		+		+	
9 April 1984	USGS-2	1	T	11:27-11:31		±		±		+		+
		2	T	11:51-11:56		+		+		±		±
		3	B	12:13-12:18	±		+		±		+	
		4	A	12:33-12:40	±		+		±		+	
		5	B	12:59-13:04	±		+		±		+	
		6	D	13:28-13:32	±		+		±		+	
		7	C	13:43-13:45	±		+		±		+	

*Areas

A - Caraway/Cedar Rock/Coolers Rock Mountains
B - Pilot/Needums Mountains
A/B - Cedar Rock/Coolers Rock/Pilot Mountains
C - White/Bowlings Mountains
D - Jackson Creek/Daniels Mountains
T - Test Flight

**

\+ - Data Recorded Optically
± - Data Recorded Optically and Digitally

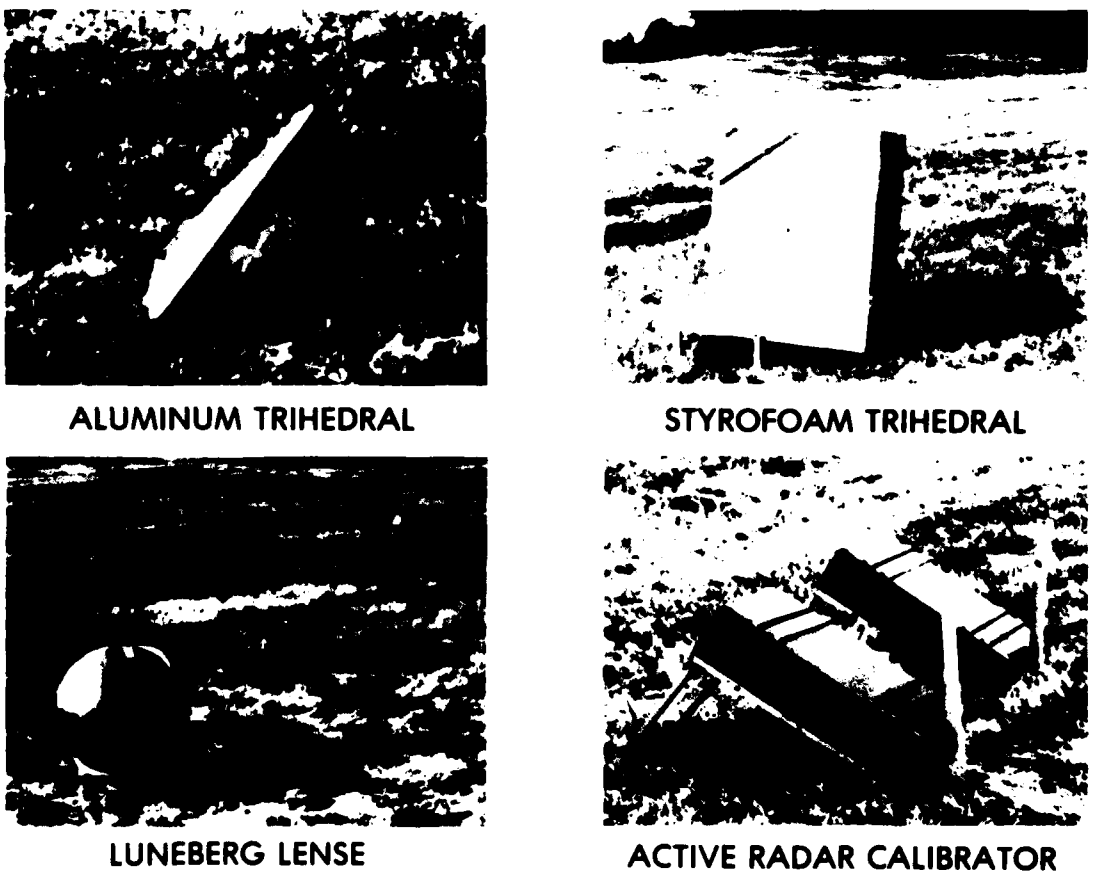

Figure 8. Typical Calibrated Reflectors Deployed During the USGS and ONR SAR Data Collection Flights

Duke Forest as well as at the Asheboro Airport. The position of these reflectors are presented in Figure 9, while their sizes are presented in Table 6.

A set of ground measurements were obtained from 14 separate sites in the Duke Forest. These sites are presented in Figures 10a and 10b and are summarized in Table 7. Data collected at each of the selected test sites consisted of surface roughness measurements, dielectric constant values, soil density and soil moisture. A measure of surface roughness was obtained by "tracing" the surface profile on graph paper. A four foot section of chart paper was taped to a plywood board. A water-resistant pen was then attached firmly to a wooden rod and used to trace the surface contour on the chart paper. Several four-foot long tracings of the surface contour were obtained from each field. A photograph illustrating the surface contour tracing method is presented in Figure 11.

Soil samples were obtained from each test site and used to determine soil density, moisture content and dielectric constant. In addition, a portable instrument was used to obtain a measurement of dielectric constant on site. This instrument consists of a "Q" meter operating at 100 MHz and a coaxial cavity resonator for measurements at L-band, 1200 MHz.

3.2.2 ONR DATA COLLECTION

In August/September 1984, the Office of Naval Research sponsored a series of data collection flights near and over Long Island, New York. As part of the program, a series of 24 passes were made over a calibration array located a Grumman's Peconic River Airport (see Figure 12) during eight separate missions. The terrain surrounding the Peconic River Airport consists primarily of agricultural fields, but also contains some forested land, swamps, and coastal marshes. Both horizontally- and vertically-polarized data were collected over a wide variety of incidence angles (see Table 8).

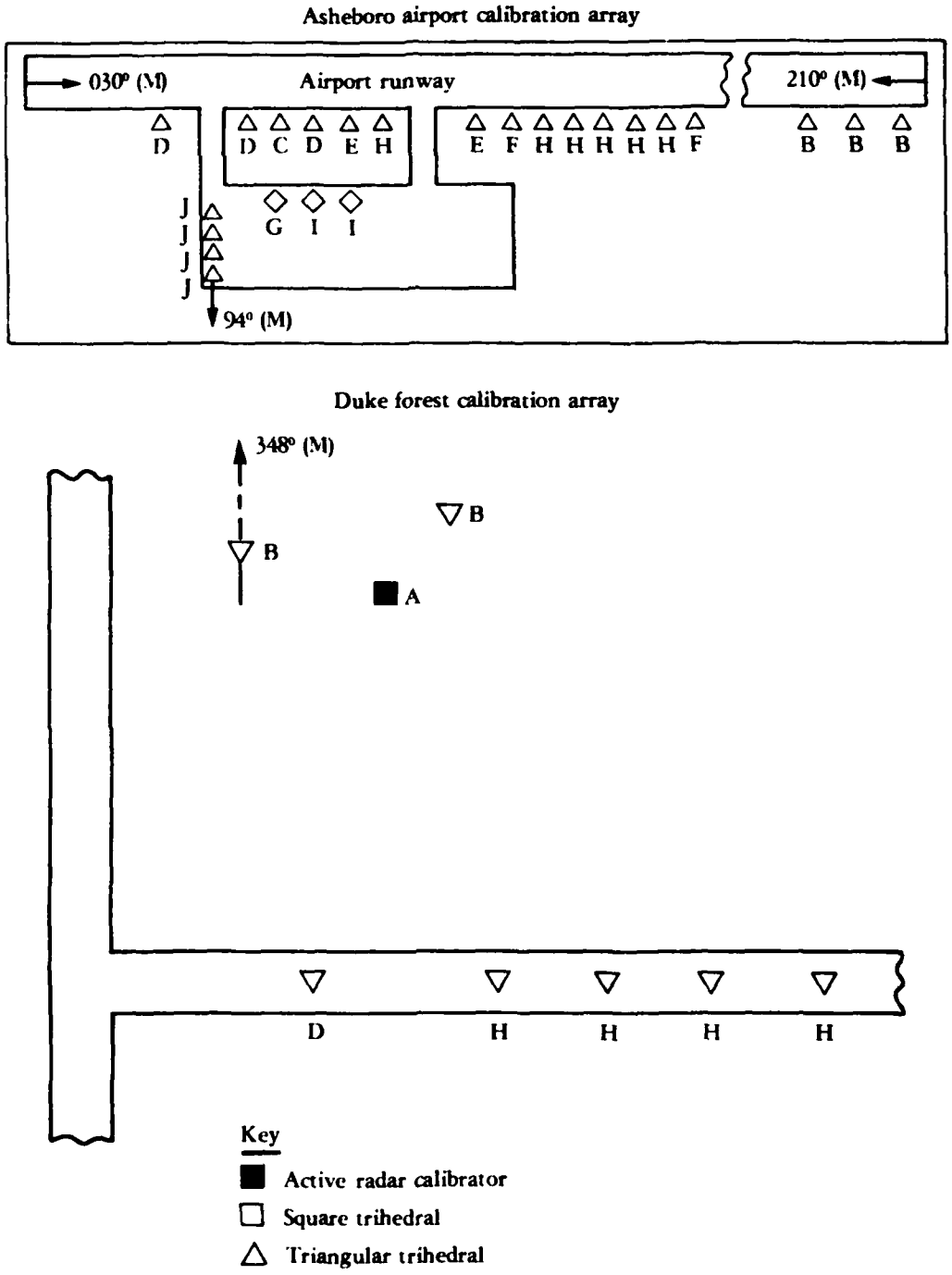

Figure 9. Reflector Positions at Asheboro and Duke Forest Calibration Arrays

TABLE 6
SUMMARY OF REFLECTORS DEPLOYED AT ASHBORO AIRPORT AND
DUKE FOREST, NORTH CAROLINA DURING APRIL 1984

Designation	Number of Reflectors	Reflector Types	Reflector Size (cm)	X-Band (m^2)	L-Band (m^2)
A	1	ART	---	---	---
B	5	TRA	119	8200	159
C	1	TRA	68	874	17
D	4	TRA	61	566	11
E	2	TRA	52	300	6
F	2	TRA	45	168	3
G	1	SQA	22	89	2
H	9	TRA	38	35	1.5
I	2	SQA	17	30	---
J	4	TRA	23	11	---

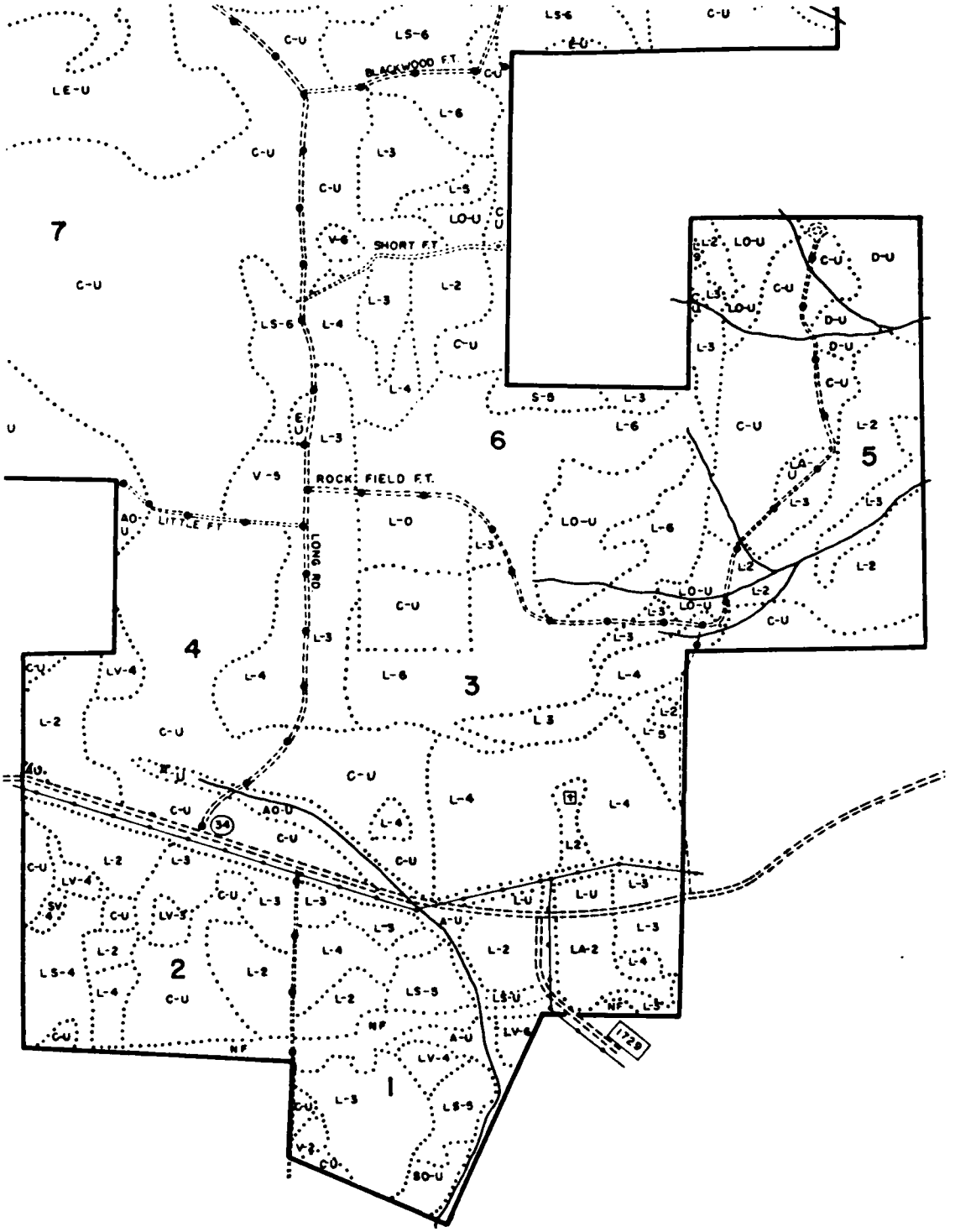

BLACKWOOD DIVISION

Figure 10a. Location of Duke Forest Ground Measurement Sites

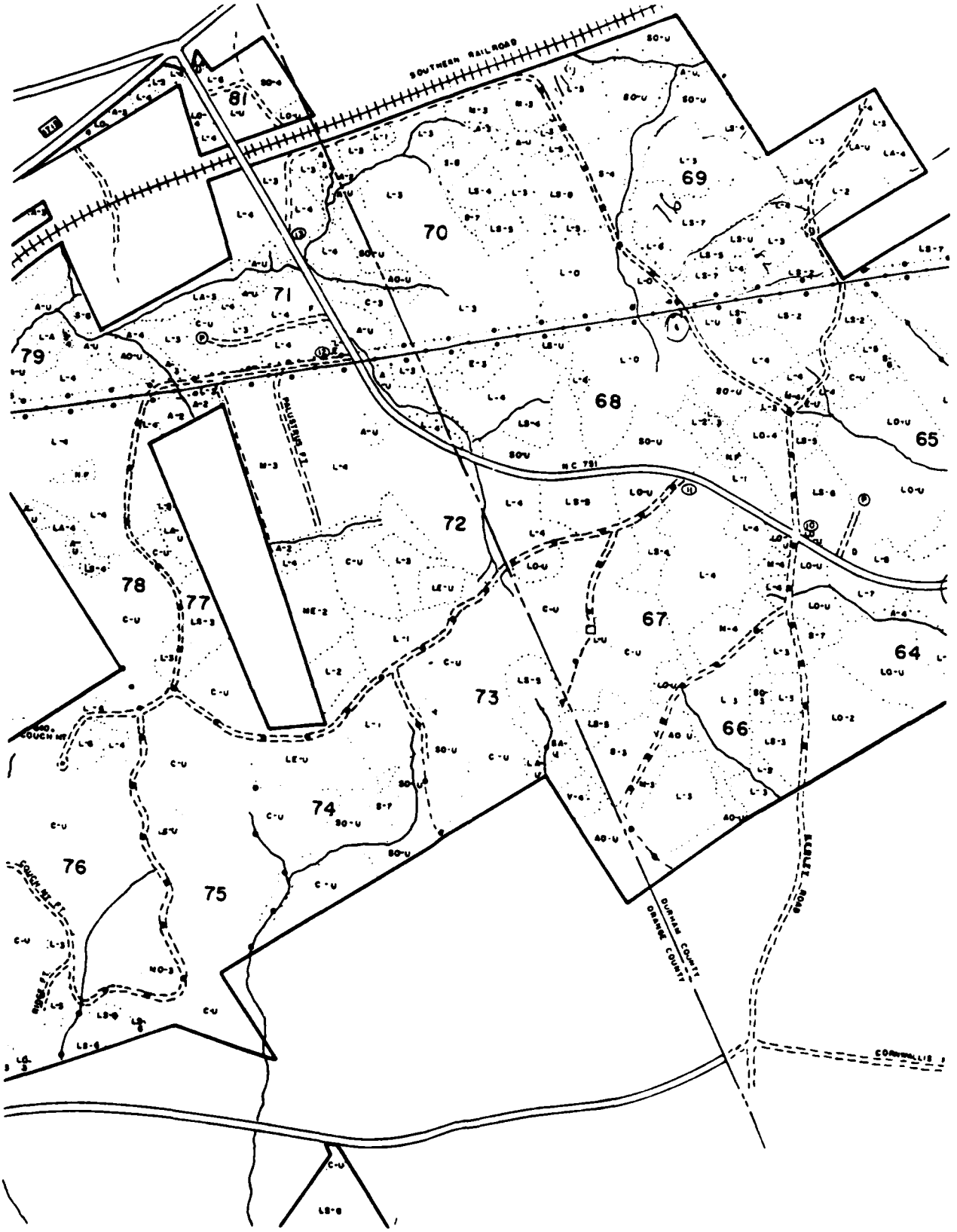

Figure 10b. Location of Duke Forest Ground Measurement Sites

TABLE 7
DUKE FOREST TEST SITES

Site Designation	Site Description
L-3	Duke Forest (Blackwood Division) Grass Field Additional Moisture 10-15 - 16 percent 15-20 - 15 percent
L-3W	Blackwood Rough - Short Pine - Trees - Weeds Additional Moisture - Different Times
Duke I	No. of L-3 (Blackwood Rd.) Cut - Rough Area Fallen Trees - One Year Growth
R1	LSG Area Reflector Site - Ashville Airport
R2	Reflector Site - L-3
4	Forest Sites (Korstian Division) 30-Year Lobolly Pines
5	Deciduous Trees - 30-50 Years
L-4	26-50 Year Lobolly Pines
LS-7	70 Year Lobolly Pines
L-1	20 Year Lobolly Pines
M	Dense Young Pines
E	Hardwoods - 20 Feet Tall
M-3	20 Feet - Pines
C-U	White-Red Oak - 60-80 Feet

Figure 11. Illustration of a Surface Contour Tracing Used to Measure Surface Roughness

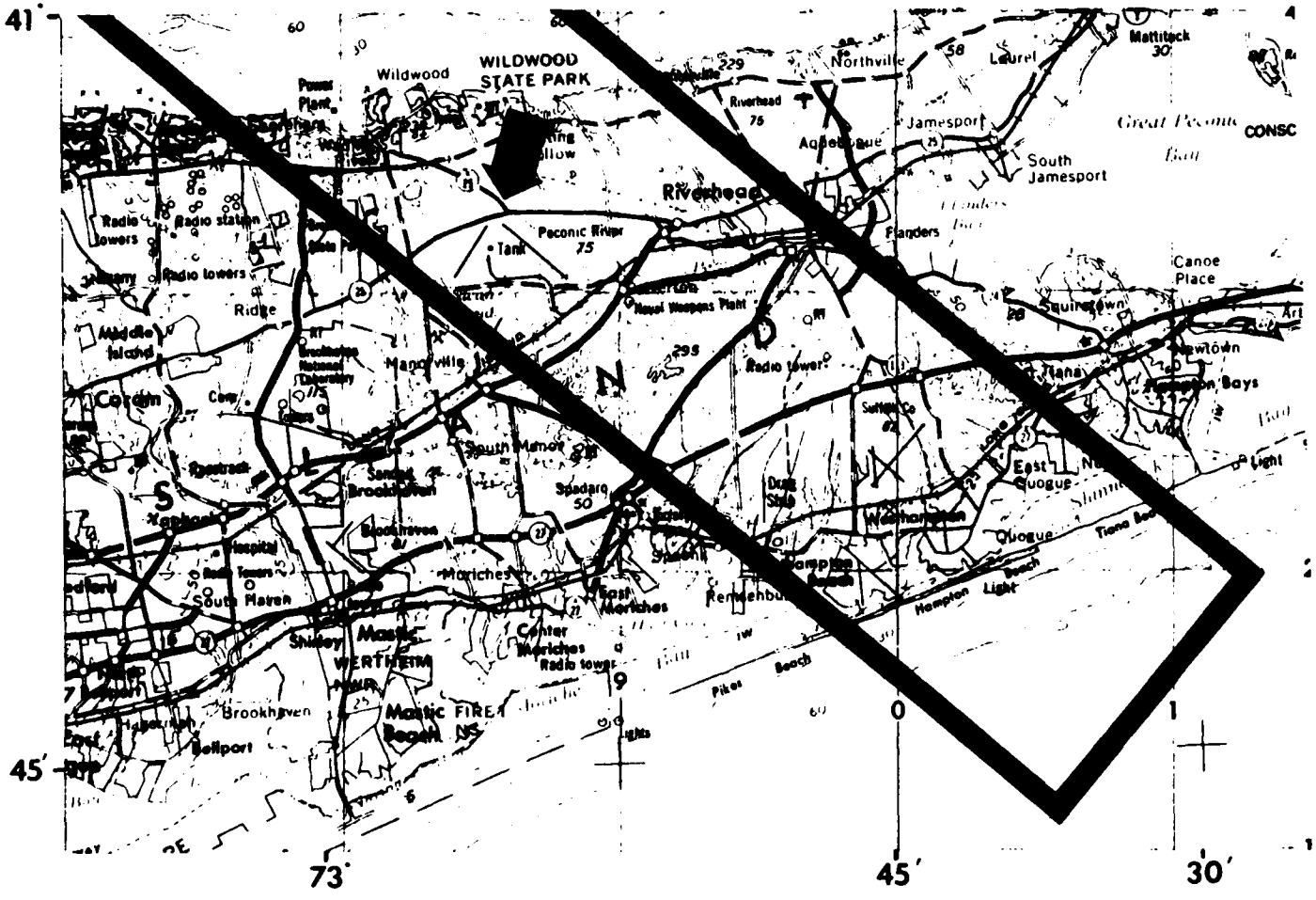

Figure 12. Location of Peconic River, Long Test Area

TABLE 8
SUMMARY OF ONR MULTICHANNEL SAR FLIGHTS

Date	Mission	Pass	Area*	Time (EST)	Frequency and Polarization - Digital Reader							
					X-VV	X-HH	X-VH	X-HV	L-VV	L-HH	L-VH	L-HV
26 August	1	1-7	O	1435-1544		X		X		X		X
28 August	2	1-4	O	2044-2126		X		X		X		X
30 August	3	1-2	P	1804-1828		X		X		X		X
30 August	3	3-9	O	1837-2116		X		X		X		X
31 August	4	1-9	O	2026-2300		X		X		X		X
31 August	4	1-12	P	2315-2357		X		X		X		X
3 September	5	1-2	P	1726-1815		X		X		X		X
	5	3-12	O	1832-2110		X		X		X		X
4 September	6	1-4	P	1853-2014		X		X		X		X
	6	5-11	O	2029-2237		X		X		X		X
5 September	7	1-3	P	1718-1802		X		X		X		X
5 September	7	3-12	O	1821-2136		X		X		X		X
6 September	8	1-2	P	1246-1309		X		X		X		X
6 September	8	3-10	O	1304-1614		X		X		X		X
6 September	9	1-2	P	1835-1902		X		X		X		X
6 September	9	3-6	O	1921-1951		X		X		X		X
7 September	10	1-2	P	1405-1502		X		X		X		X
7 September	10	3-4	P	1517-1541	X		X		X		X	
7 September	10	5-8	O	1550-1657	X		X		X		X	
7 September	11	1-	M	2030-2036	X		X		X		X	
		2-	M	2051-2055		X		X		X		X

* Areas

P - Peconic River area
O - Ocean areas
M - Mountain, N.Y.

An extensive array of calibrated reference reflectors were deployed at the Peconic River Airport. The positions of these reflectors are presented in Figures 13 through 15, and the size of these reflectors are summarized in Table 9.

The ground measurements discussed in the previous section were also collected at various test sites out and around the Peconic River Airport. These test sites are listed in Table 10 and are identified on the diagrams given in Figure 16.

3.3 ARCHIVED SAR DATA

There is an extensive set of calibrated L-band SAR imagery archived at ERIM which is available for use in this program. Of particular interest are the data sets listed in Table 11. All these data sets were collected after 1979, when the CV-580 SAR System underwent an extensive system modification to improve the system's calibration capability. All the imagery from the missions listed in Table 11 contain calibration signals, which will enable calibration of the terrain signatures from the targets of interest.

A number of different terrain types were imaged during the data collections listed in Table 11. These experiments are discussed in more detail by de Ritter, et al. (1984), Burns, et al. (1984) Kasischke, et al. (1983), and Shuchman, et al. (1983). Table 11 summarizes the different terrain types and incidence angles which potentially can be used in this program using the recently collected and archived L-band SAR data.

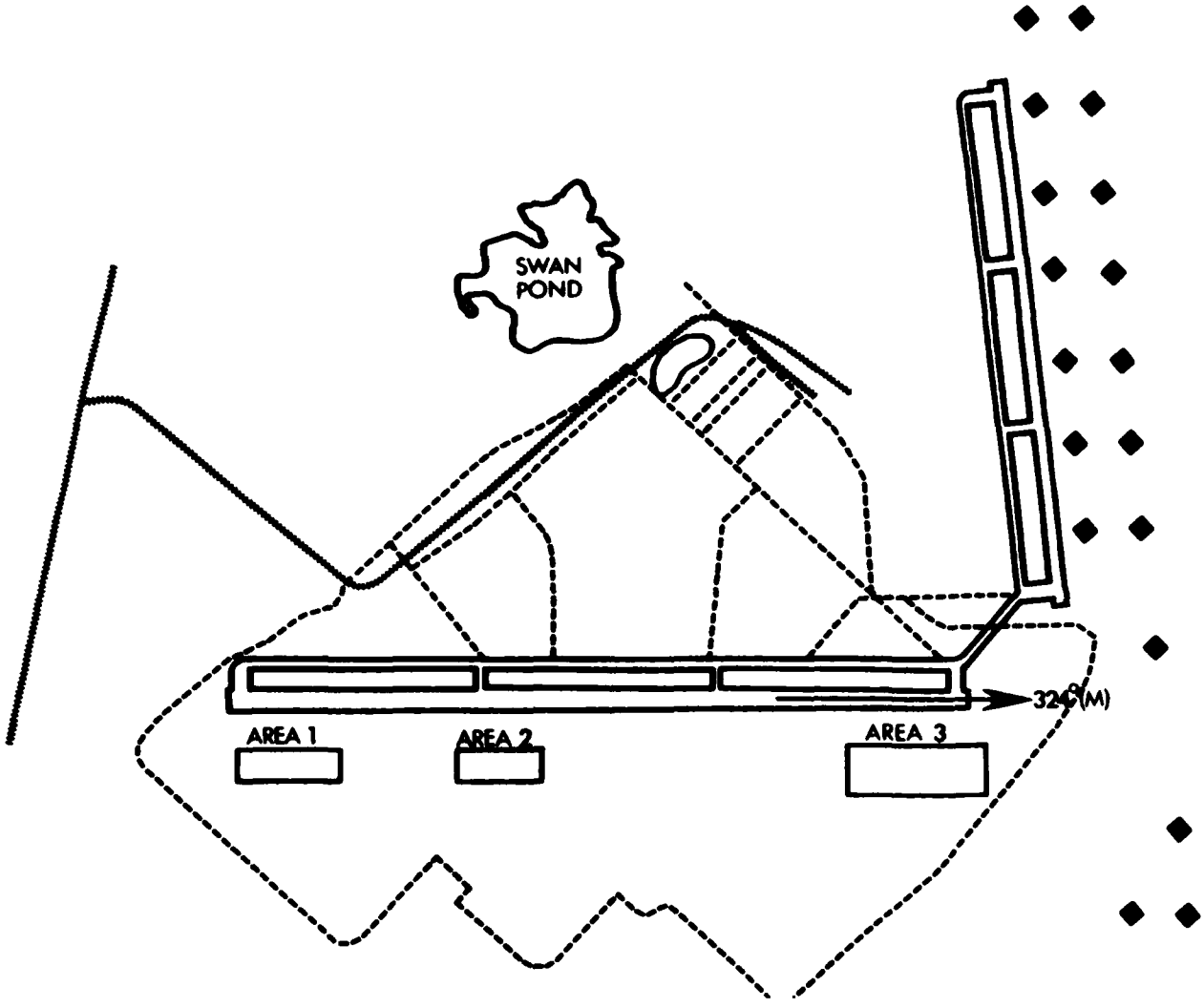

Figure 13. Location of Calibrated Reflector Sites at Peconic River Airport

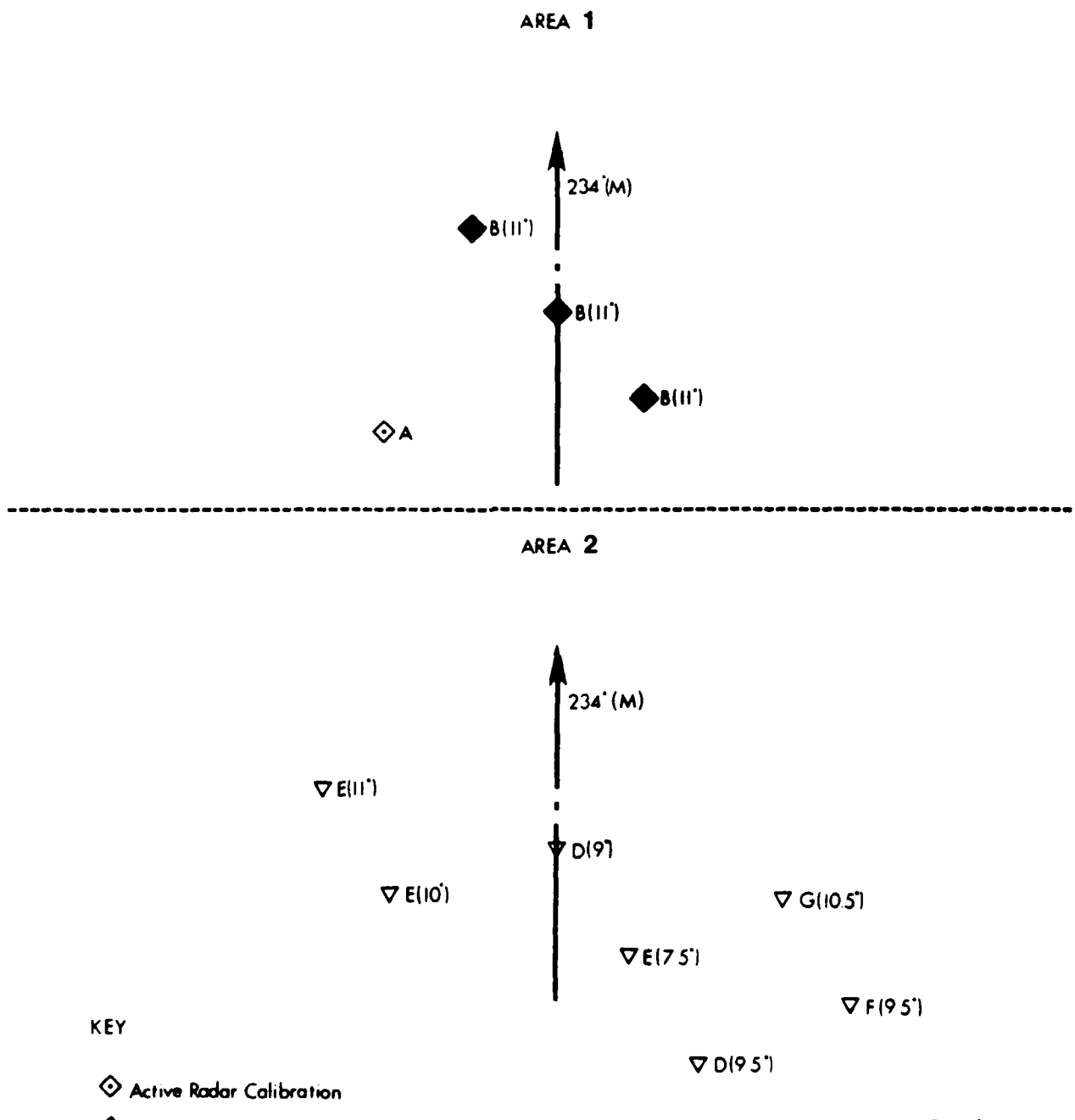

Figure 14. Location of Calibrated Reflectors at Areas 1 and 2

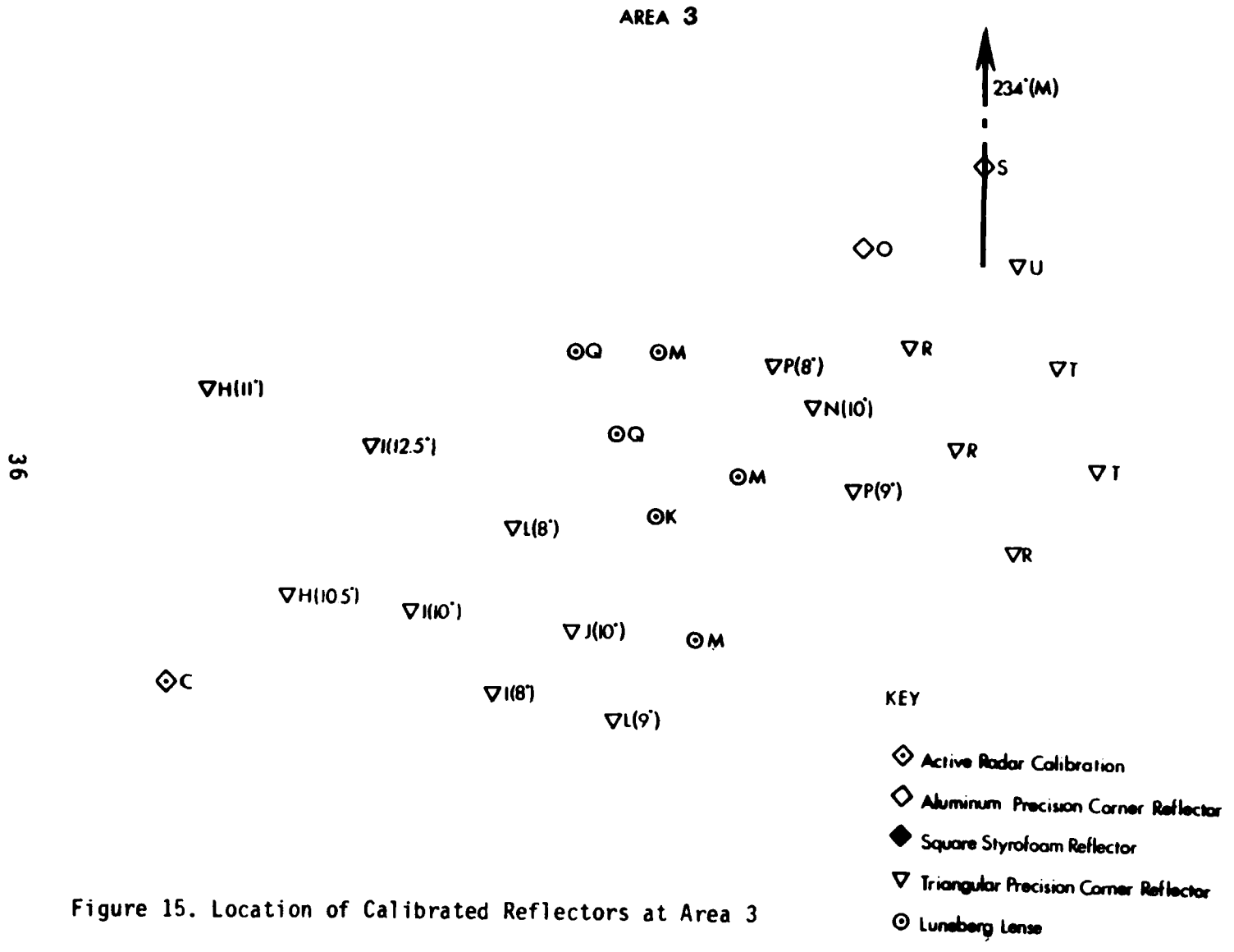

Figure 15. Location of Calibrated Reflectors at Area 3

TABLE 9
SUMMARY OF CORNER REFLECTORS DEPLOYED AT PECONIC RIVER AIRPORT DURING AUGUST/SEPTEMBER 1984

Designation	Number of Reflectors	Reflector Type*	Reflector Size (cm)	Radar Cross Section X-Band (m^2)	Radar Cross Section L-Band (m^2)
A	1	AR1	—	—	1538
B	3	SQS	119	73828	1429
C	1	AR2	—	—	631
D	2	TRA	119	8200	159
E	3	TRA	116	7406	143
F	2	TRA	91	2805	54
G	1	TRA	88	2453	48
H	2	TRA	68	874	17
I	3	TRA	61	566	11
J	1	TRA	52	300	6
K	1	LLS	—	262	--
L	2	TRA	45	168	3
M	3	LLS	—	104	--
N	1	TRA	39	95	2
O	1	SQA	22	89	2
P	2	TRA	38	85	1.5
Q	2	LLS	—	32	--
R	3	TRA	29	30	--
S	1	SQA	17	30	--
T	1	TRA	23	11	--
U	2	TRA	22	10	--
V	20	SQS	61	5097	99

*AR1 - Single Polarization Active Radar Calibration
AR2 - Dual Polarization Active Radar Calibration
LLS - Luneberg Lens
SQA - Square Aluminum Precision Corner Reflector
SQS - Square Styrofoam Corner Reflector (Aluminum Coated)
TRA - Triangular Aluminum Precision Corner Reflector

TABLE 10
LONG ISLAND TEST SITES

Site Designation	Site Description
A	Strawberry Field
B	Orchard
C	Smooth Field
D	Smooth Field - Near Sound Rd. Potatoes - South Side
E O 8	Potatoes - Row N-S Row N-S Row Direction - 345°
F	Grass
G	Corn - Stocks - Picked but Standing Dry Stocks
H	Cut Corn
I	Grass
J	Cabbage
K	Grass Field (VOR, Reflectors)
RF1	Grumman Reflector Site - 4 Reflectors
RF2	Grumman Reflector Site - 8 Reflectors
RF3	Grumman Reflector Site - 26 Reflectors
L	Short Pine Trees - Weeds (Similar to "West of L-3, North Carolina)
M	Smooth Field
N	Smooth Field
O	Smooth Field
P	Smooth Field
3	Potatoes
4	Smooth Field
Q	Sod
R	Sod
W	Sod
Z	Bare, Smooth Field N-S Furrows
	Mountains Upper N.Y. State

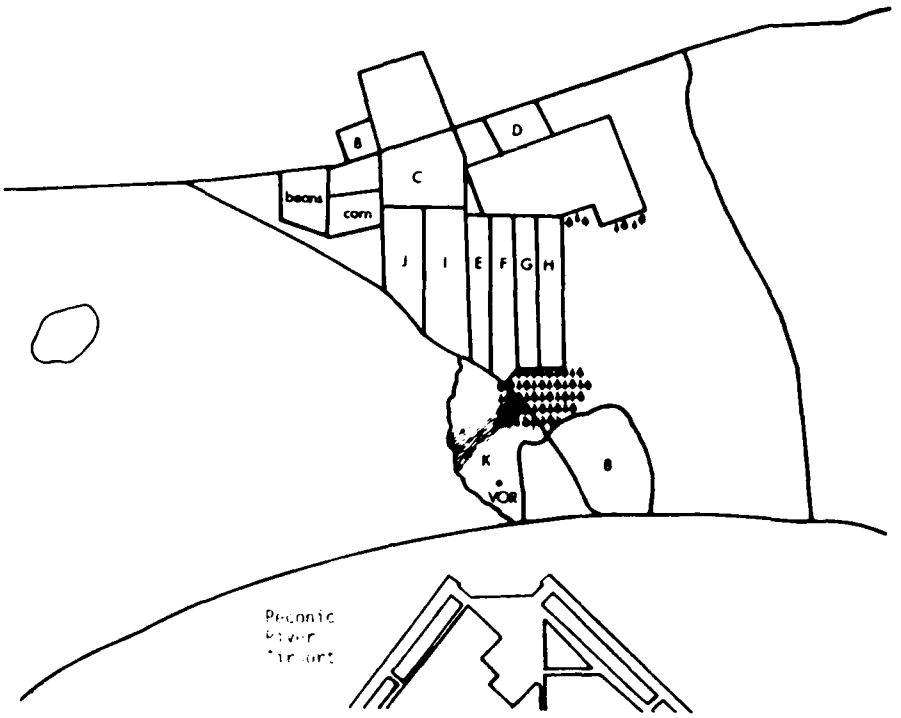

16 (a)

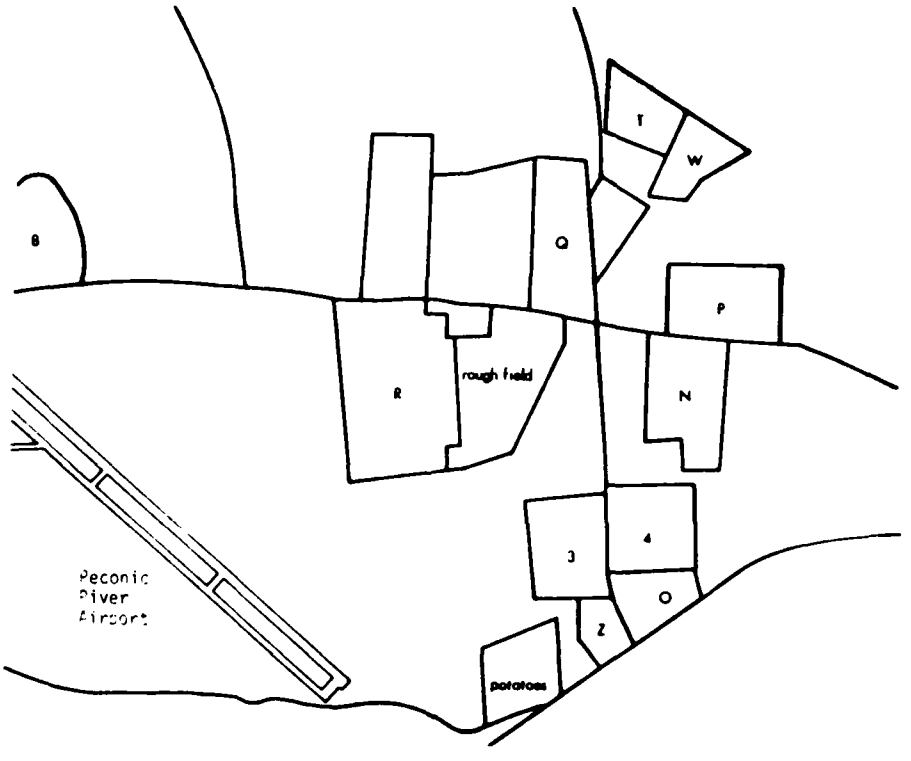

16 (b)

Figure 16. Location of Peconic River Airport Ground

TABLE 11
AVAILABLE L-BAND SAR DATA SETS

Date of Data Collection	Location - Description of Sites	Incidence Angle Range
June-July 1983, 84	Sea ice and ocean	30°-80°
June-August 1983	SE Michigan, urban, rural areas, Victoria, B.C.; mountains, ocean	40°-85°
September 1980	Michigan; cultivated areas; forests; lakes	35°-85°
September 1980	Central Canada - ground truth available; cultivated field with caps, base fields, tundra; forests; deciduous and coniferous prairie lands	40°-80°

4
DATA REDUCTION

This chapter discusses the techniques and procedures used to reduce the SAR and ground truth data collected during the USGS and ONR experiments. A section is devoted to each data set.

4.1 SAR DATA

The SAR data recorded during the two missions were optically processed into imagery using ERIM's tilted-plane optical processor (Kozma, et al., 1972). An engineering assessment was performed on the data to determine which passes met minimum image quality standards. From the optically-processed imagery, specific scenes were selected and digitally-processed into imagery using ERIM's Digital Strip Map Processing facility (Jackson, et al., 1974).

Figure 17a and 17b present representative examples of optically-processed L-band imagery collected during the USGS flights. These images include the portion of the Duke Forest where the corner reflectors were deployed. Figures 18a and b present L-band SAR imagery of the Asheboro Airport Calibration Array.

Figures 19a, b and c present digitally-processed L-band imagery of the Peconic River Airport gathered during the ONR data collection mission. These images contain the corner reflector array as well as the ground test sites (see Figures 13 and 16). Figures 20a and 20b present optically-processed L-band imagery collected over a forested mountain region in upper New York for horizontal and vertical polarization, respectively.

In the remainder of this section, we will discuss the techniques used to calibrate the digital L-band SAR data and present examples of calibrated terrain measurements.

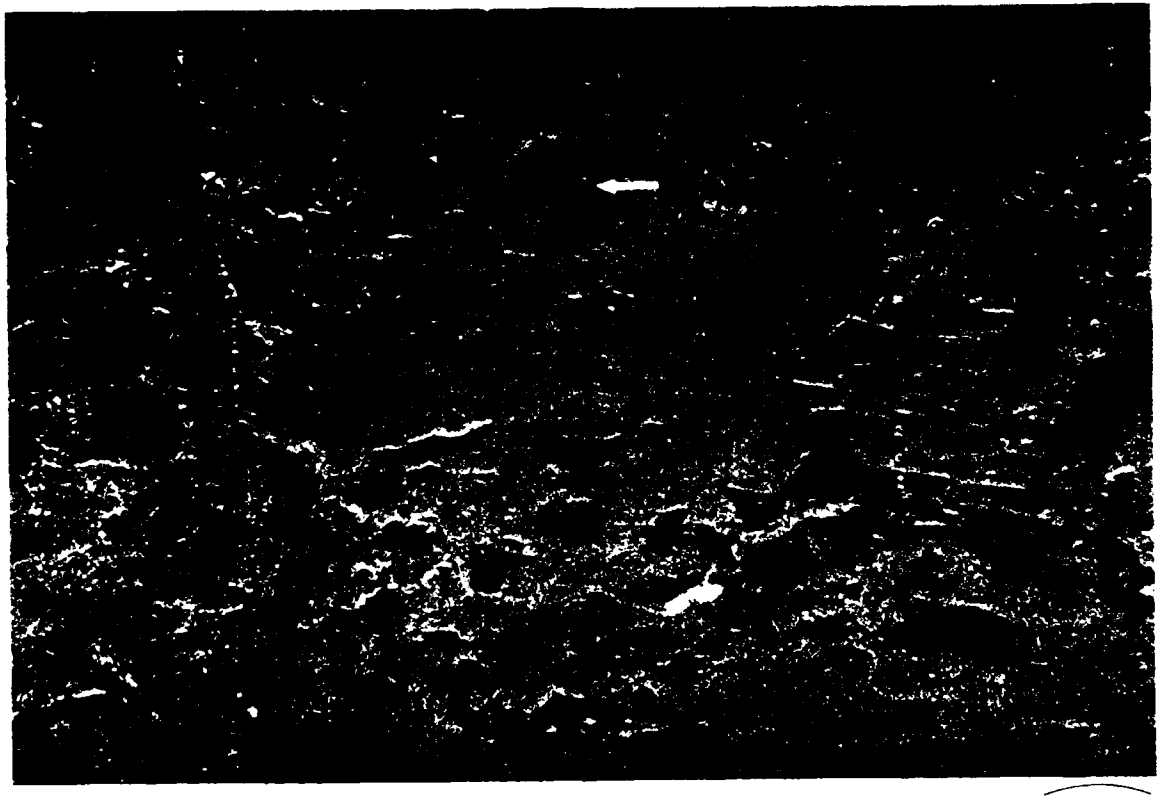

FIGURE 17A. OPTICALLY-PROCESSED L-BAND (HH) SAR IMAGERY OF DUKE FOREST TEST SITE (USGS-2, PASS 2, APRIL 9, 1984; ARROW INDICATES CALIBRATION ARRAYS LOCATION)

FIGURE 17B. OPTICALLY-PROCESSED L-BAND (VV) SAR IMAGERY OF DUKE FOREST TEST SITE (USGS-1, PASS L, APRIL 8, 1984; ARROW INDICATES CALIBRATION ARRAY LOCATION)

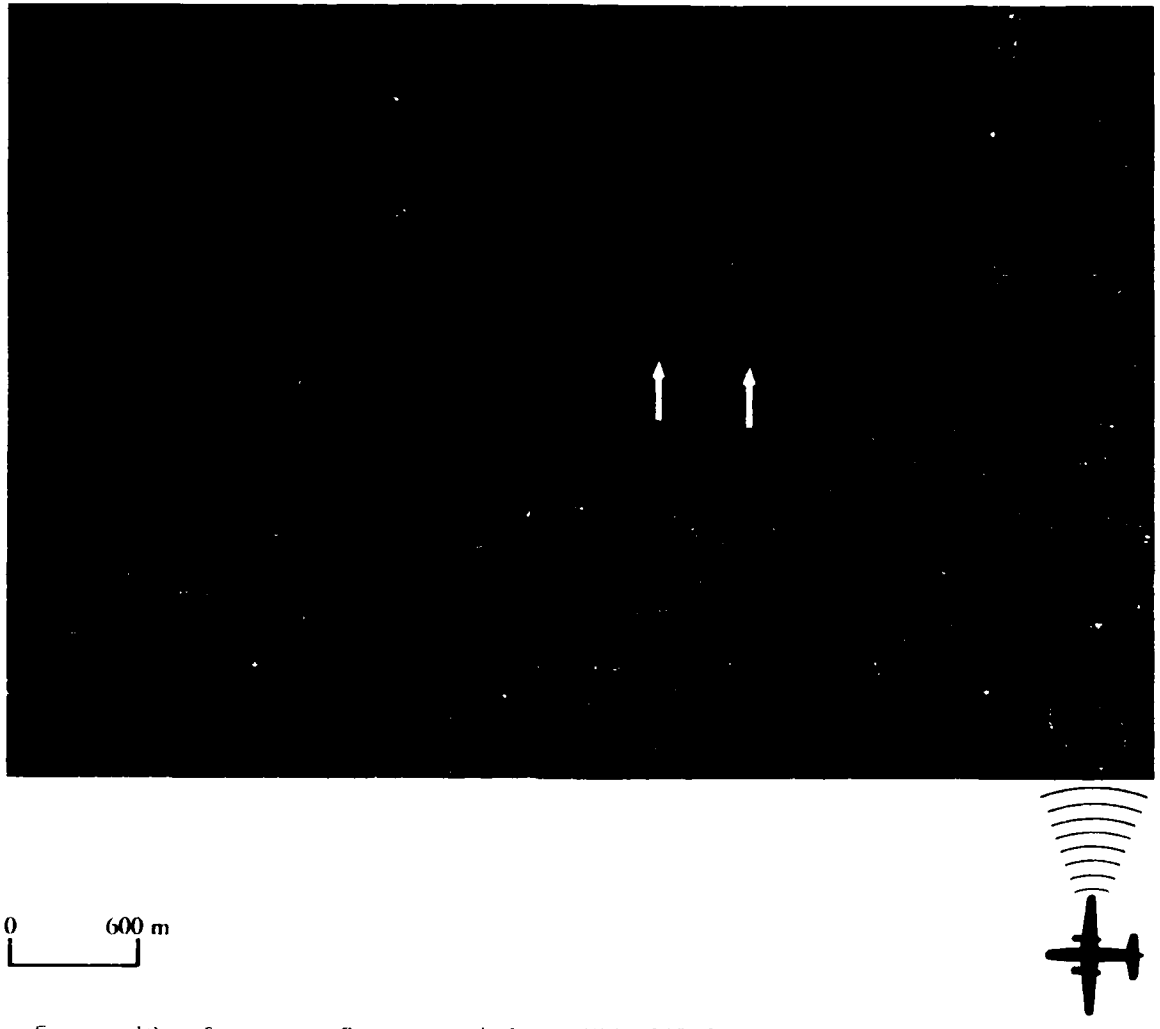

FIGURE 18A. OPTICALLY-PROCESSED L-BAND (HH) SAR IMAGERY AT ASHEBORO AIRPORT CALIBRATION ARRAY (USGS-1, PASS 8, APRIL 8, 1984; ARROWS INDICATE ARRAY LOCATION)

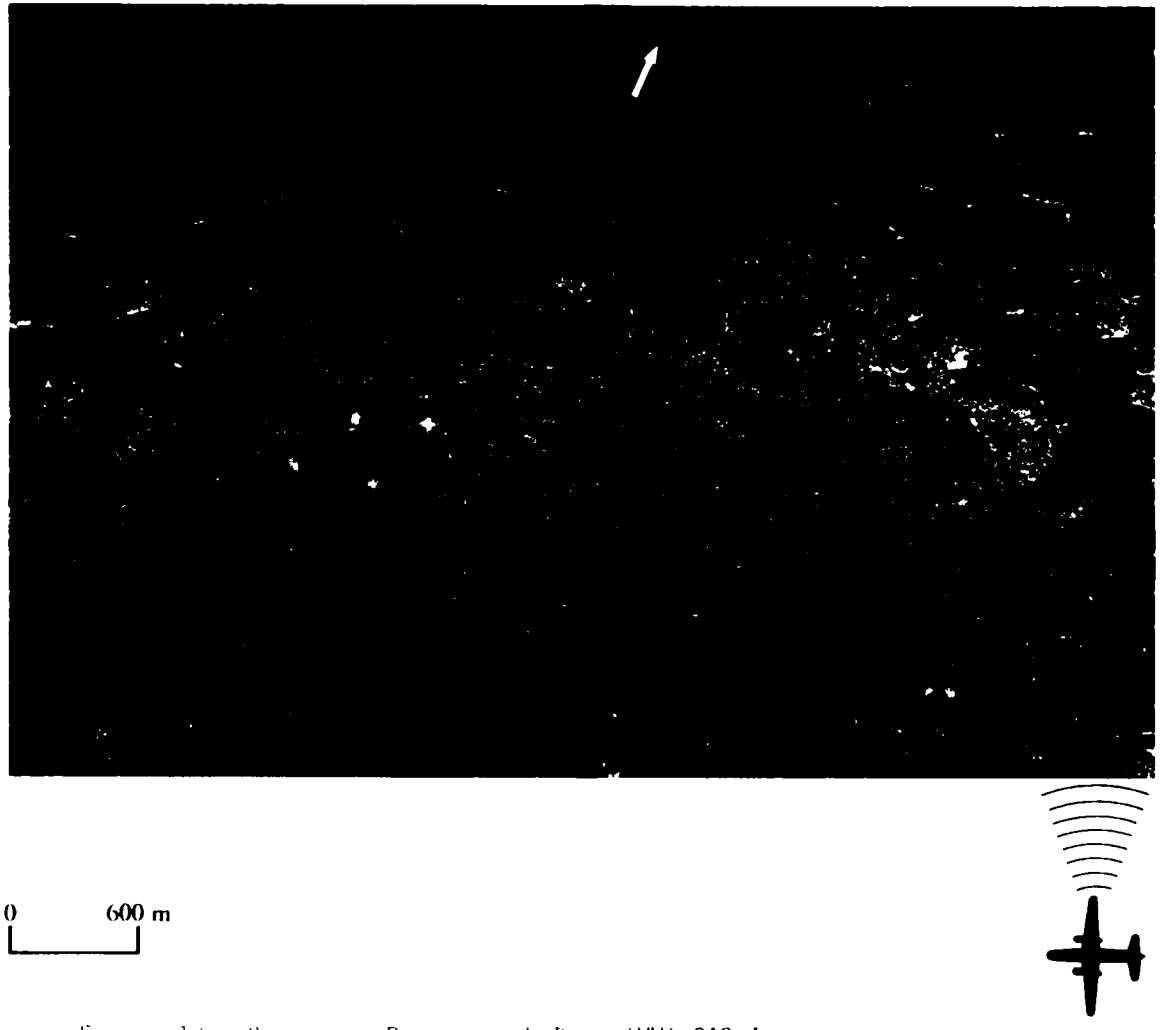

FIGURE 18B. OPTICALLY-PROCESSED L-BAND (VV) SAR IMAGERY OF ASHEBORO AIRPORT CALIBRATION ARRAY (USGS-1, PASS 3, APRIL 8, 1984; ARROWS INDICATE ARRAY LOCATION)

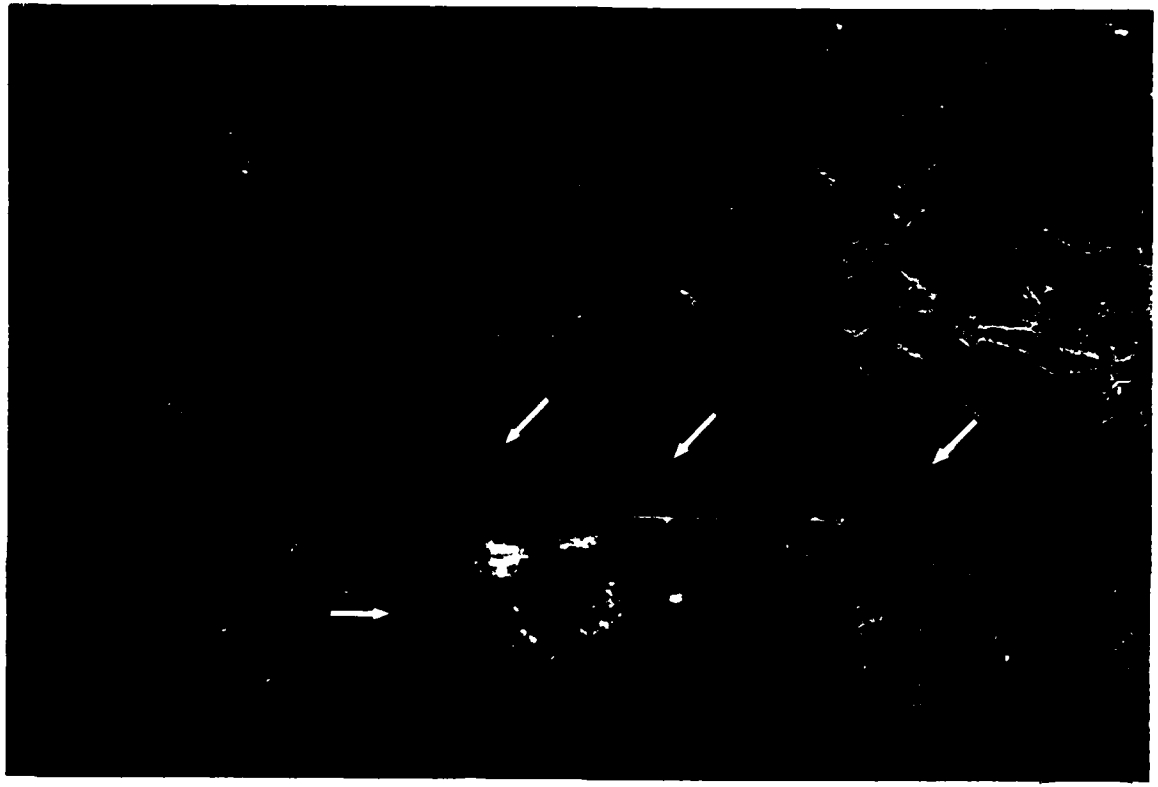

FIGURE 19A. DIGITALLY-PROCESSED L-BAND (HH) SAR IMAGERY OF PECONIC RIVER CALIBRATION ARRAY (SARSEX-10, PASS 1, SEPTEMBER 7, 1984; ARROWS INDICATE REFLECTOR LOCATION)

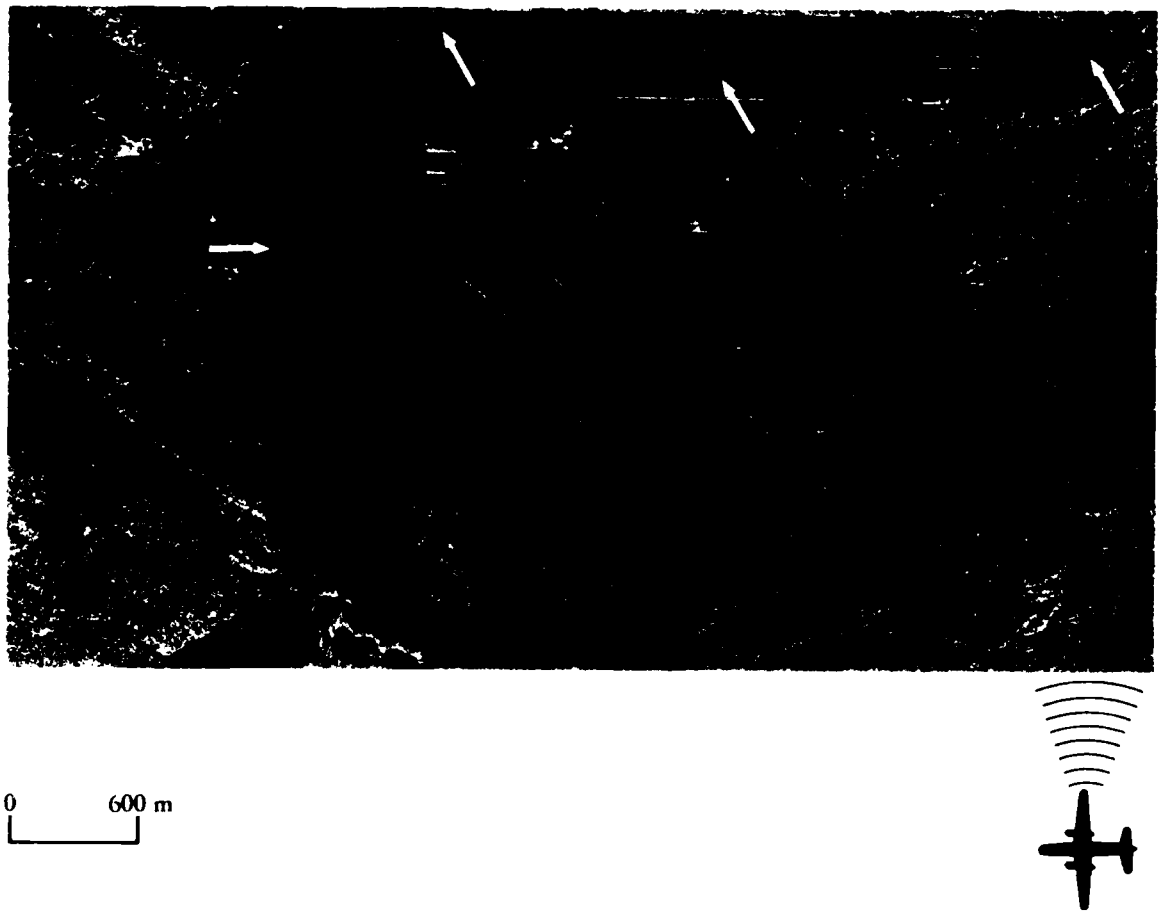

FIGURE 19B. DIGITALLY-PROCESSED L-BAND (VV) SAR IMAGERY OF PECONIC RIVER CALIBRATION ARRAY (SARSEX-10, PASS 4, SEPTEMBER 7, 1984; ARROWS INDICATE REFLECTOR LOCATION)

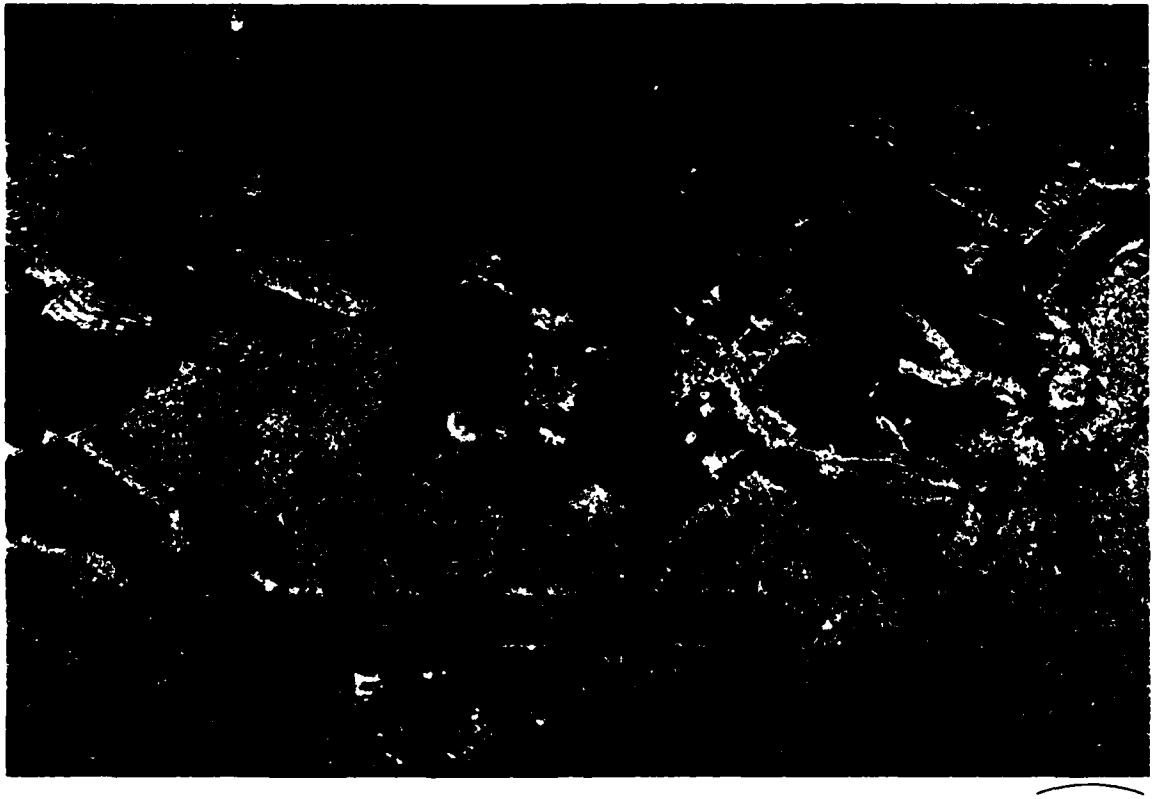

FIGURE 19c. DIGITALLY-PROCESSED L-BAND (HH) SAR IMAGERY OF GROUND MEASUREMENT SITES NEAR PECONIC RIVER AIRPORT (SARSEX-10, PASS 2, SEPTEMBER 7, 1984)

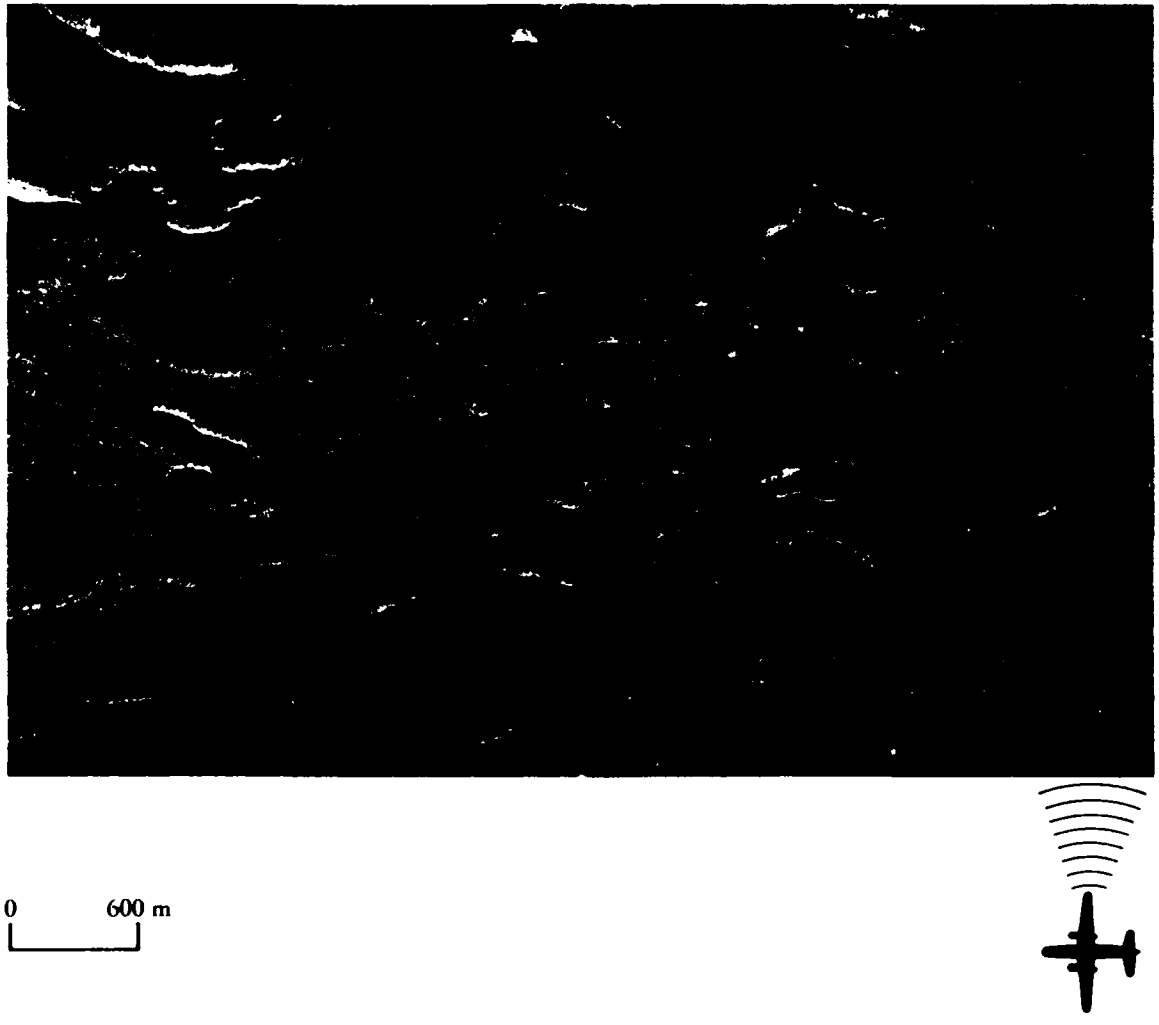

FIGURE 20A. OPTICALLY-PROCESSED L-BAND (HH) SAR IMAGERY OF UPPER NEW YORK (SARSEX-11, PASS 1, SEPTEMBER 7, 1984

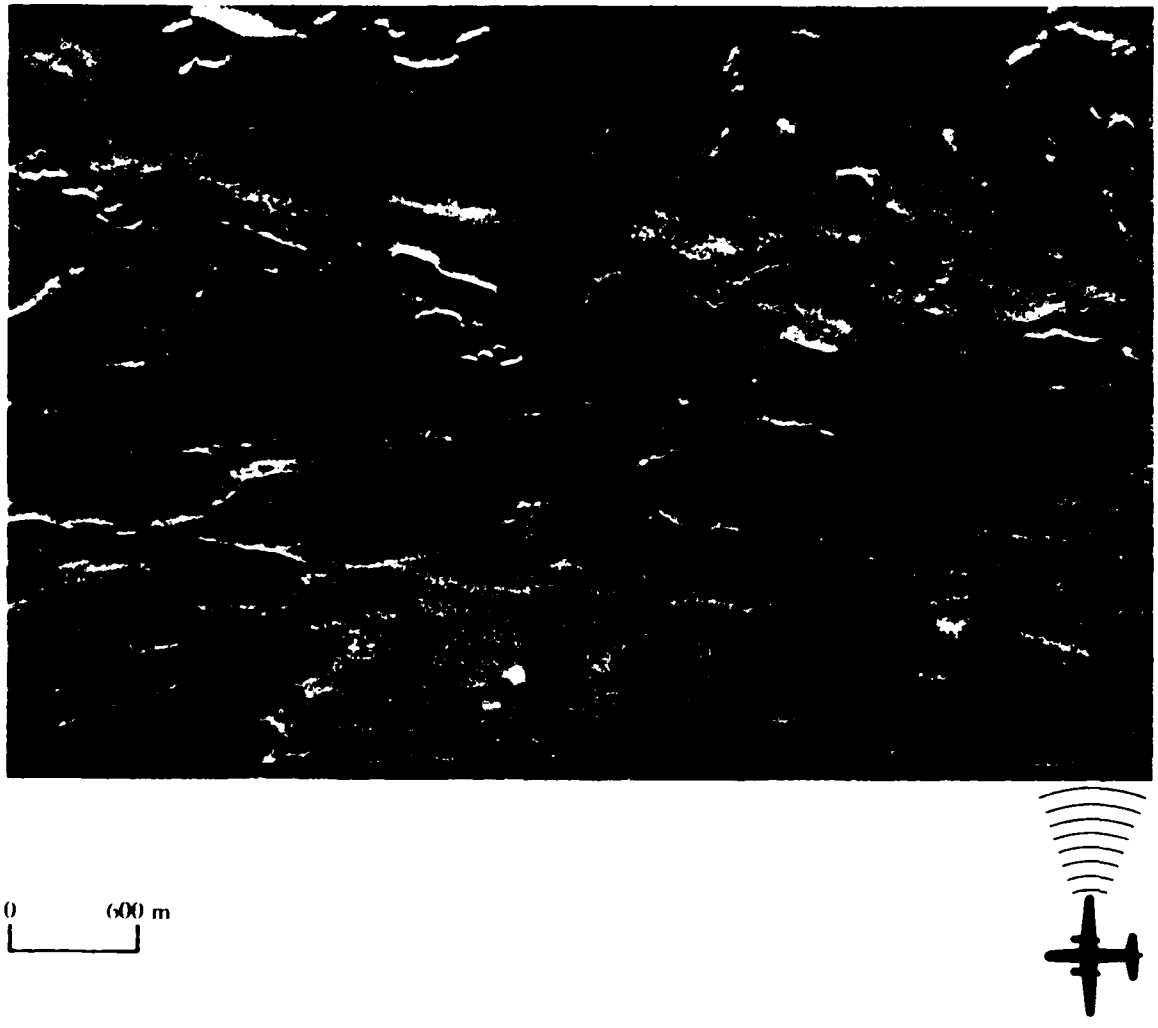

FIGURE 2UB. OPTICALLY-PROCESSED L-BAND (VV) SAR IMAGERY OF UPPER NEW YORK (SARSEX-II, PASS 2, SEPTEMBER 7, 1984)

4.1.1 CALIBRATION OF SAR DATA

The procedure to convert the recorded SAR image intensities into radar cross-section actually involves two steps: image calibration and radiometric corrections. This procedure is carried out in the slant range plane. If a calibrated image in ground plane coordinates is desired, a slant-to-ground range conversion can be subsequently performed. The algorithms to accomplish calibration are described in the following paragraphs.

Image Calibration

The image calibration algorithm translates the image intensity values into actual radar cross-sections. This is accomplished by comparing the image intensities of the SAR data to be calibrated with known image intensities produced by the "reference" calibrated reflectors.

The calibration of a SAR image begins with the well known radar return equation

$$P = \frac{HP_t G^2(\theta)\lambda\sigma}{4\pi^3 R^4} + P_N \qquad (1)$$

where P is the measured image power,
P_N is the system noise power,
R is the slant range,
λ is SAR wavelength,
P_t is the transmitter power,
$G(\theta)$ is the antenna gain,
θ is the incidence angle,
σ is the radar cross-section, and
H is the SAR gain from receiver input to image.

An R^3 term is used rather than an R^4 term because a 1/R factor is applied to the image during the azimuth compression stage of SAR image processing. Equation (1) can be rewritten as

$$\sigma = \frac{(P - P_N)(4\pi)^3 R^4}{H\lambda P_t G^2(\theta)} \tag{2}$$

If a SAR images a scene with a series of targets with known radar cross-sections of different values, then a relationship between σ and P can be established, and H_r can be calculated, provided the transmitted power (P_t) and antenna gain ($G(\theta)$) are known

The procedure used to calibrate aircraft SAR imagery is to relate the data to be calibrated (σ_i, where the i subscript denotes the scene to be calibrated) to the reference scene radar cross-sections (σ_r, where the r subscript denotes the reference scene), i.e.,

$$\frac{\sigma_i}{\sigma_r} = \frac{(P_i - P_{Ni})\, H_r P_{tr} R_i^3 G_r^2(\theta)}{(P_r - P_{Nr})\, H_i P_{ti} R_r^3 G_i^2(\theta)} \tag{3}$$

or

$$\sigma_i = (P_i - P_{Ni})\, \frac{\sigma_r}{(P_r - P_{Nr})}\, \frac{H_r}{H_i}\, \frac{P_{tr} R_i^3 G_r^2(\theta)}{P_{ti} R_r^3 G_i^2(\theta)} \tag{4}$$

The calibration procedure determines all the terms in Eq. (4), and thus allows for calculation of σ_i for any P_i in the scene. In Eq. (4), all the terms are known or can be calculated except for $\sigma_r/(P_r - P_{Nr})$ and H_i/H_r. The relationship between σ_r and P_r is determined by measuring the intensities of a set of calibrated retroreflectors deployed in the calibration array and

imaged by the SAR. The measured power intensity (P_r) values are then regressed against the radar cross-section (σ_r) values,

$$P_r = a\,\sigma_r + b \tag{5}$$

where a is the linear regression coefficient and b is the y-intercept. If we assume the y-intercept, b, is equivalent to the system noise, P_{Nr}, then Eq. (5) can be rewritten as

$$a = \frac{(P_r - P_{Nr})}{\sigma_r} \tag{6}$$

or,

$$\frac{1}{a} = \frac{\sigma_r}{(P_r - P_{Nr})} \tag{7}$$

The next step in the calibration procedure is to calculate H_r and H_i. Using Eqs. (1) and (6), H_r can be calculated. H_i is determined by using the intensities of the synthetic targets generated by the calibration signal generator. The CSG produces a series of synthetic point targets, each target with a different attenuation setting. The CSG signal is the same transmitted pulse as used for the data. Therefore, the CSG signals also monitor the transmitted waveform. The calibration signals are inserted at the antenna prior to and after each data collection pass, and are recorded on the digital tape in the same fashion as the SAR phase histories. They are then processed into images. Thus any differences in the intensity in the processed image of a specific signal between passes represents a change in the SAR system gain (H).

The power intensity of the calibration signals generated after the calibration reference pass and the image to be calibrated are measured. These intensities are then plotted on a curve, using the input power from the CSG as the axis. This plotting results in two straight lines (one for each pass), each with the same slope. The

vertical, relative difference between these two lines represents the amount the system gain for the reference pass (H_r) has to be adjusted to obtain a system gain for the image to be calibrated (H_i).

In the implementation of Eq. (4) to calculate radar cross-sections, logarithms of the values are usually taken, and all plots and computations are carried out in dB for convenient numerical evaluation.

4.1.2 INITIAL RESULTS

To date, two calibration data sets have been processed and calibration relationships obtained. Examples of the calibration relationships are given in Figure 21. Figure 21 presents the L-band calibration relationship obtained for the Long Island flights of 31 August and 7 September 1984 using the calibrated reflectors to provide the reference for calibration RCS values.

As initial verification of the L-band calibration algorithm, the SAR data obtained on 7 September 1984 was used to calibrate the SAR data of 31 August 1984. Both SAR data sets include the reflector array at the Peconic Airport, Long Island. The values for each reflector of the 31 August data were determined using the 7 September calibration curve. These values were then compared to the known nominal values for each reference reflector; the results are presented in Figure 22. A standard deviation of about 3 dB is obtained using values from 21 reference reflectors.

Using the calibration relationship, the values of σ_0 for several of the fields selected for initial analysis were determined. Values of σ_0 are given in Table 12 for several test sites. These values are obtained by evaluation of a histogram of the radar cross sections for these sites. The histograms of RCS values for the area near the reference reflector array is given in Figure 23; other RCS histograms are included in the Appendix.

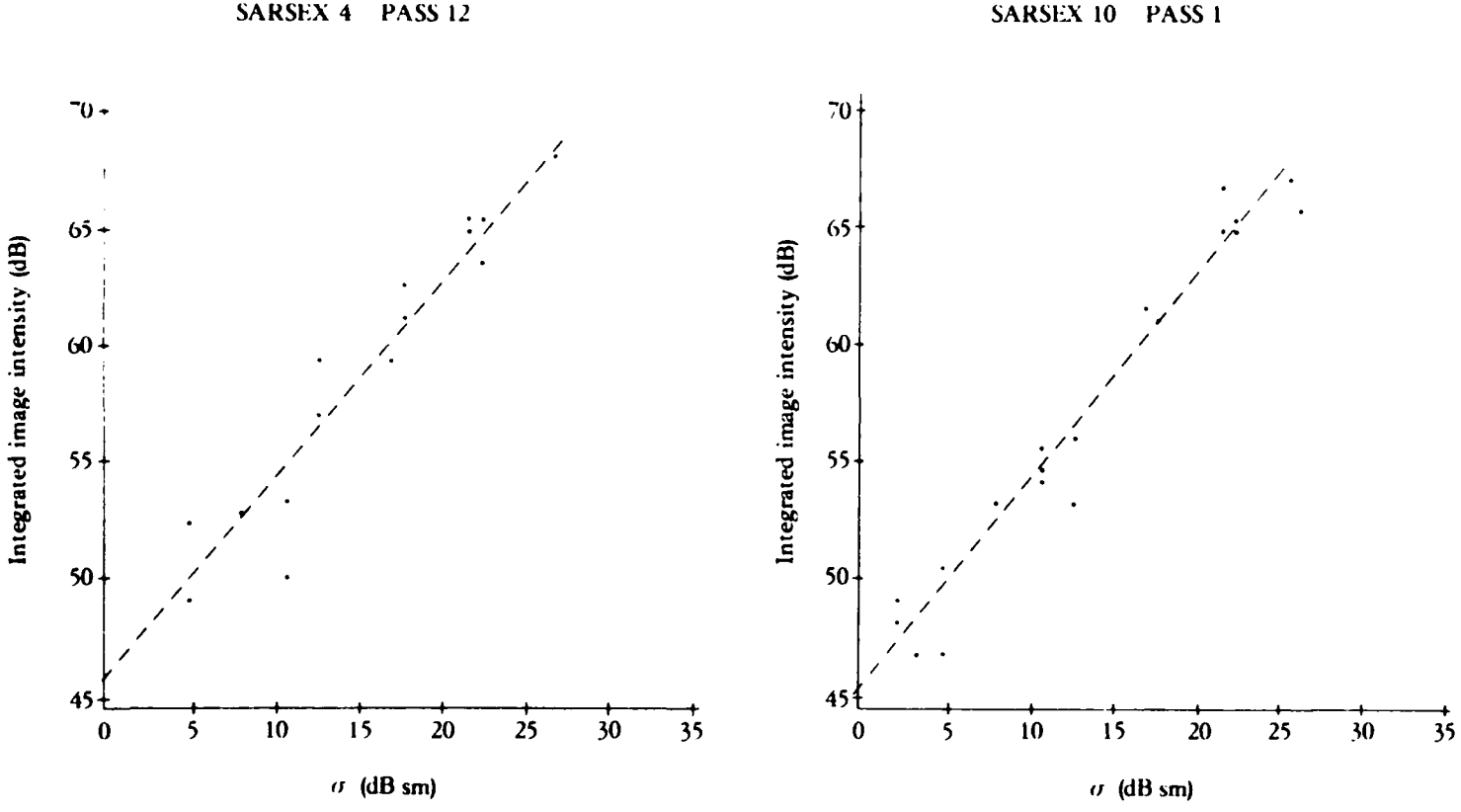

Figure 21. Image Intensity Versus Radar Cross Section of Calibrated Reflectors Located at the Peconic River Calibration Array

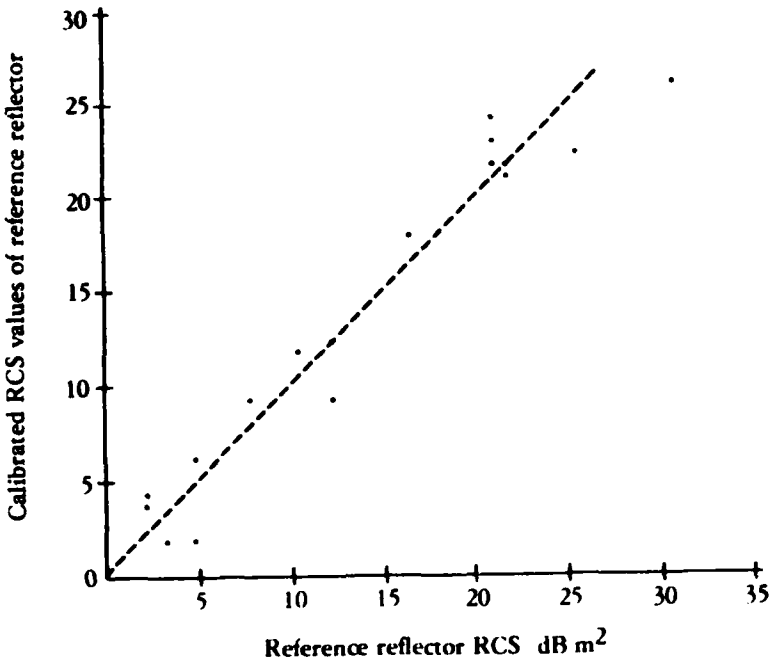

Figure 22. Plot of Predicted versus Actual Radar Cross Section Values for L-Band Corner Reflectors

TABLE 12
VALUES OF RADAR CROSS SECTION (σ_o) FOR SEVERAL TEST SITES IN THE PECONIC RIVER AIRPORT TEST AREA

(L-Band Horizontal, Polarization, 63.9° Incidence Angle)

Field	σ (dBm^2)*	σ_o	σ_o (S.D.)
Forest Area			
Near Reflector Site			
1	-16.6	0.012	0.013
2	-15.0	0.014	0.014
3	-14.2	0.017	0.018
Grass RF2	-23.0	0.002	0.002
Grass RF3	-19.9	0.004	0.004
Grass RF3	-20.4	0.004	0.004
E2	-12.3	0.023	0.022
E1	-11.0	0.029	0.030
F1			
F2	-17.6	0.008	0.008
F1		0.008	0.007
G2	-14.9	0.015	0.016
G1	-11.9	0.003	0.028

*Total Radar Cross Section is in dB with reference to one square meter for one pixel. Pixel size = $2.16m^2$.

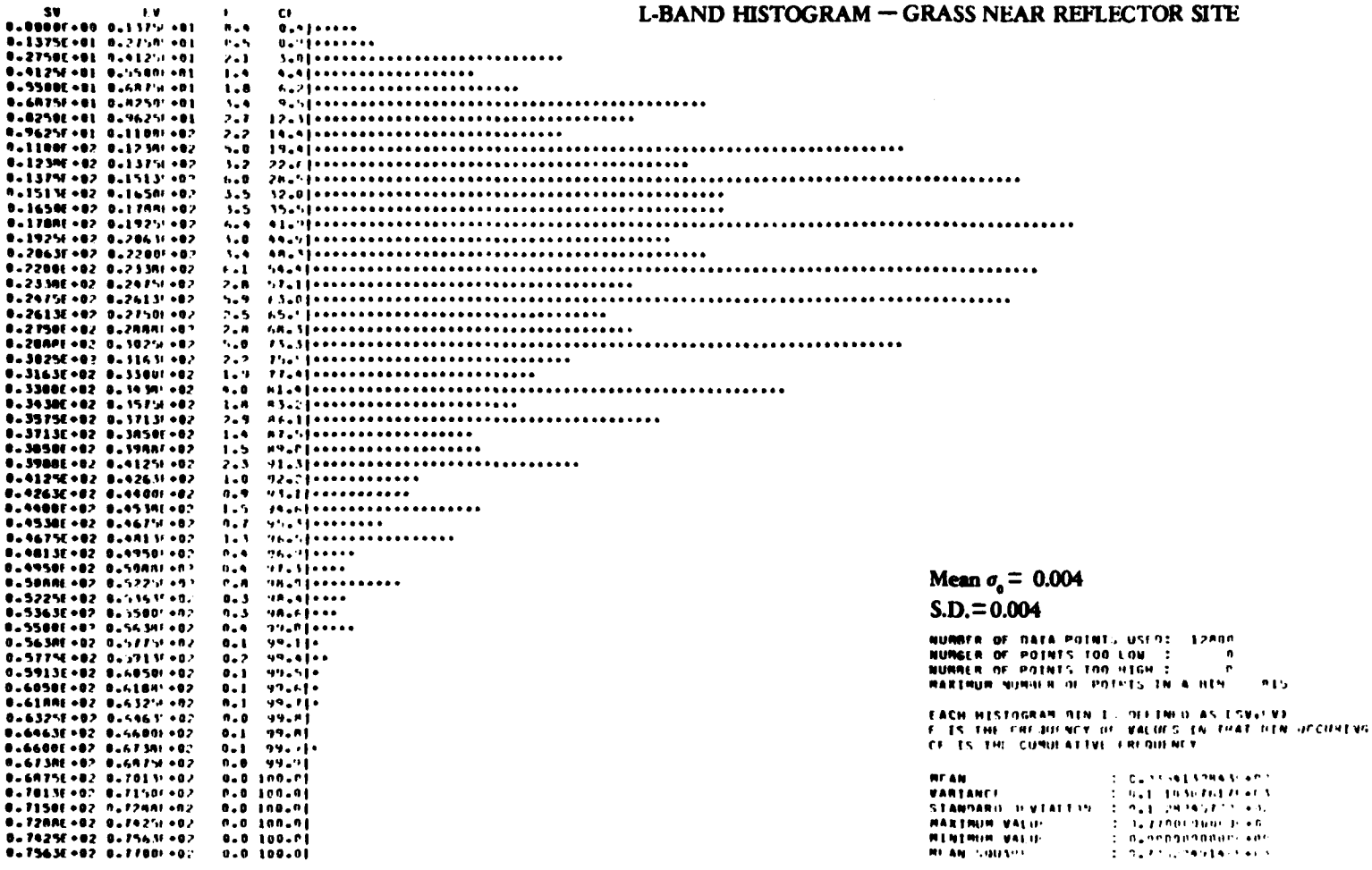

Figure 23. Example of a Histogram of Radar Cross Section

4.2 GROUND DATA

The soil samples collected during the SAR overflights were used to obtain three parameters: dielectric constant, soil moisture and soil density. Dielectric constant measurements were made using a coax cavity at L-band. Estimates of the precision of the dielectric measurements were obtained by measuring different sub-samples of the same soil sample. The standard deviation obtained was about 5 percent of the mean. Soil moisture measurements were obtained in the laboratory using samples collected at each site. A known volume of each sample was weighed, then heated at 300°F in an oven for a period of at least 8 hours. The dryed sample was then weighed. The before and after weights were used to compute moisture content by weight and by volume. Soil density measurements were obtained by weighing a known volume of each soil sample. The measured soil parameters are summarized in Table 13 for the Duke Forest test sites and in Table 14 for the Peconic River Airport test sites.

The raw surface profile measurements were digitized. Figure 24 presents an example of a digitized height profile obtained from the raw measurements. This profile was obtained from the grass field near reflector Site 3 at the Peconic River Airport. These data will be used as an example throughtout the remainder of this section. Examples of these raw measurements for each of the fields is included in the Appendix. These raw measurements were then used to calculate a set of surface descriptors.

The surface height profiles to be correlated with the observed scattering patterns are considered as statistical samples of a random process. Surface height, $h(x)$, is considered as a random variable and various statistical measures are derived. These measures will be used in attempts to correlate surface properties with observed scattering patterns. At this time only horizontally-polarized data over a very limited range of incident angles have been considered.

TABLE 13
CHARACTERISTICS OF SOIL SAMPLES FROM DUKE FOREST TEST SITES
(Density and Dielectric Constant)

Name of Sample	Wet Bulk Density	Percent Water	Dry Bulk Density	ε	tan δ
L-3 North End 0-5 cm	1.10	16.38	1.12	9.4	0.3
L-3 North 5-10 cm	Not Enough Soil Sample				
L-3 North 10-15 cm	1.33	8.76	1.38	3.7	0.14
L-3 South End 0-5 cm	1.13	9.15	1.14	4.0	0.19
L-3 South End 5-10 cm	1.12	11.88	1.14	6.6	0.30
L-3 South End 10-15 cm	1.32	5.87	1.34	3.5	0.21
L-3 South 10-15 cm	1.04	15.79	1.05	6.2	0.31
L-3 South 15-20 cm	1.11	15.62	1.13	6.2	0.28
West of L-3 South End 10-15 cm	1.36	10.12	1.42	4.7	0.18
West of L-3 North)-5 cm	0.90	19.41	0.88	7.0	---
West of L-3 North 5-10 cm	1.31	8.76	1.35	5.1	0.37
West of L-3 North 10-15 cm	1.40	10.27	1.47	5.8	0.27
West of L-3 South 0-5 cm	0.66	31.77	0.57	---	---
West of L-3 South End 5-10 cm	1.35	10.56	1.81	5.1	0.30
Duke 1 0-5 cm	1.06	18.98	1.07	8.4	0.33
Duke 1 L-3 10-15 cm	1.13	15.57	1.15	5.8	0.24
Duke 1 L-3 26.25 cm	1.13	13.12	1.15	4.4	0.19
Duke 1 L-3 South 0-5 cm	1.14	15.20	1.16	4.8	0.26
3-yr. Pines West of L-3 North End 0-5 cm	1.21	13.01	1.24	5.0	0.26
3-yr. Pines West of L-3 North End 5-10 cm	1.27	11.54	1.32	4.7	0.22
3-yr. Pines West of L-3 North End 10-15 cm	1.42	5.45	1.57	3.3	0.10
3-yr. Pines West of L-3 5-10 cm	1.20	11.50	1.23	5.7	0.30
3-yr. Pines West of L-3 10/5 cm	1.19	10.54	1.22	5.9	0.19
LS-6-L-G Area 0-5 cm	0.99	15.47	0.99	6.8	0.28
LS-6 L-G Area 10-15 km	1.18	11.88	1.21	6.1	0.27

TABLE 14
CHARACTERISTICS OF SOIL SAMPLES FROM PECONIC RIVER AIRPORT TEST SITES

Name of Sample	Wet Bulk Density	Percent Water	Dry Bulk Density	Dielectric ε	Dielectric tan δ
Field A 0-5 cm Crest	1.05	7.08	1.06	4.05	0.302
Field A 0-5 cm Trough	0.99	9.83	0.99	3.74	0.291
Field E 0-5 cm	0.98	12.84	0.97	4.05	0.302
Field E 5-10 cm	1.08	12.46	1.10	4.32	0.285
Field F 0-5 cm	0.87	17.25	0.85	3.88	0.407
Field F 5-10 cm	0.94	16.86	0.93	4.35	0.316
Field G (Corn) 0-5 cm	0.94	16.91	0.93	3.25	0.514
Field G (Between Rows) 5-10 cm	0.97	15.62	0.96	3.68	0.427
Field H 0-5 cm	1.07	10.72	1.08	4.40	0.344
Field H 5-10 cm	0.93	11.94	0.92	3.66	0.274
Field K (Short Grass) 0-5 cm	1.02	18.01	1.03	4.33	0.310
Field K (Long Grass) 0-5 cm	0.84	16.58	0.82	4.24	0.288
Field K (Short grass) 7-14 cm	0.90	17.92	0.88	3.41	0.490
Field L 0-5 cm	0.88	9.25	0.87	3.32	0.185
Field L 10-15 cm	0.97	8.93	0.97	3.35	0.189
Field M 0-5 cm	1.00	11.65	1.00	3.98	0.289
Field M 5-10 m	0.96	12.25	0.95	3.99	0.299
Field N 0-5 cm	0.90	13.67	0.88	3.81	0.279
Field N 5-10 cm	0.86	13.53	0.84	3.88	0.292
Field O 0-5 cm	1.09	10.93	1.10	3.62	0.284
Field P 0-5 cm	1.08	8.40	1.09	3.70	0.274
Field P 5-10 cm	0.97	11.85	0.97	4.01	0.267
Field Q 0-5 cm	Not Enough Soil Sample			4.22	0.288
Field Q 5-10 cm					
Field R 0-5 cm	1.06	9.00	1.07	4.07	0.273
Field R 5-10 cm	1.09	10.00	1.10	4.05	0.283
Field Z 5-10 cm	0.89	14.38	0.88	4.18	0.282
Site Z 0-5 cm	1.03	9.94	1.04	3.82	0.287
Site Z 5-10 cm	0.99	12.24	0.99	4.17	0.304
Field 3 (Cost) 0-5 cm	1.07	8.06	1.08	3.49	0.251
Field 3 (Trough) 5 cm	1.00	9.46	1.00	3.40	0.237
Reflector Array Site					
Site 1 (Large) 0-5 cm	0.83	18.29	0.80	3.89	0.396
1 (Large) 5-10 cm	0.92	15.97	0.90	3.95	0.405
2 0-5 cm	0.80	16.03	0.77	4.10	0.321
2 5-10 cm	0.89	14.67	0.87	3.86	0.274
3 (Grassy Area) Surface	0.71	14.03	0.68	3.29	0.193
3 (Reflector Array) 0-5 cm	0.75	13.21	0.73	3.69	0.246
3 (Reflector Array) 5-10 cm	1.04	12.93	1.05	3.69	0.290
3 (Grassy Area) 10-12 cm	0.99	8.39	0.99	3.40	0.125

Therefore, initial comparisions are made between the statistics of the SAR reflectivety data for several fields but at one incident angle. The next year's effort will expand the analysis to obtain correlation if possible, over a range of incident angles and for both H and V polarization.

Using the surface height profiles, additional roughness properties were calculated:

1. Spectrum of the surface height;
2. Slope Distribution;
3. Radius of Curvature; and
4. Auto-Correlation of the surface heights.

Surface height spectra are obtained by taking an FFT of the surface height profiles. An example of the spectra obtained for the height profile in Figure 24 is given as Figure 25. Additional spectra are given in the Appendix.

Surface slope information is obtained by differentiation of the surface height profiles. The histogram for the calculated slope values from the example field is given as Figure 26. Values of the mean slope for a number of the test areas are listed in Table 15.

Values for slope spectra $S_s(k)$ can also be obtained directly from the FFT of the slope function or from the spectra of the height profile data using the relationship:

$$S_s(k) = K^2 S_h(k) \tag{8}$$

where $S_h(k)$ = surface height profile spectrum
$S_s(k)$ = slope spectrum

An example of a surface slope spectra is given in Figure 27.

An additional parameter that is related to the scattering cross-section of surfaces is the radii of curvature of surface structure. The initial approach at obtaining radii of curvature statistics from

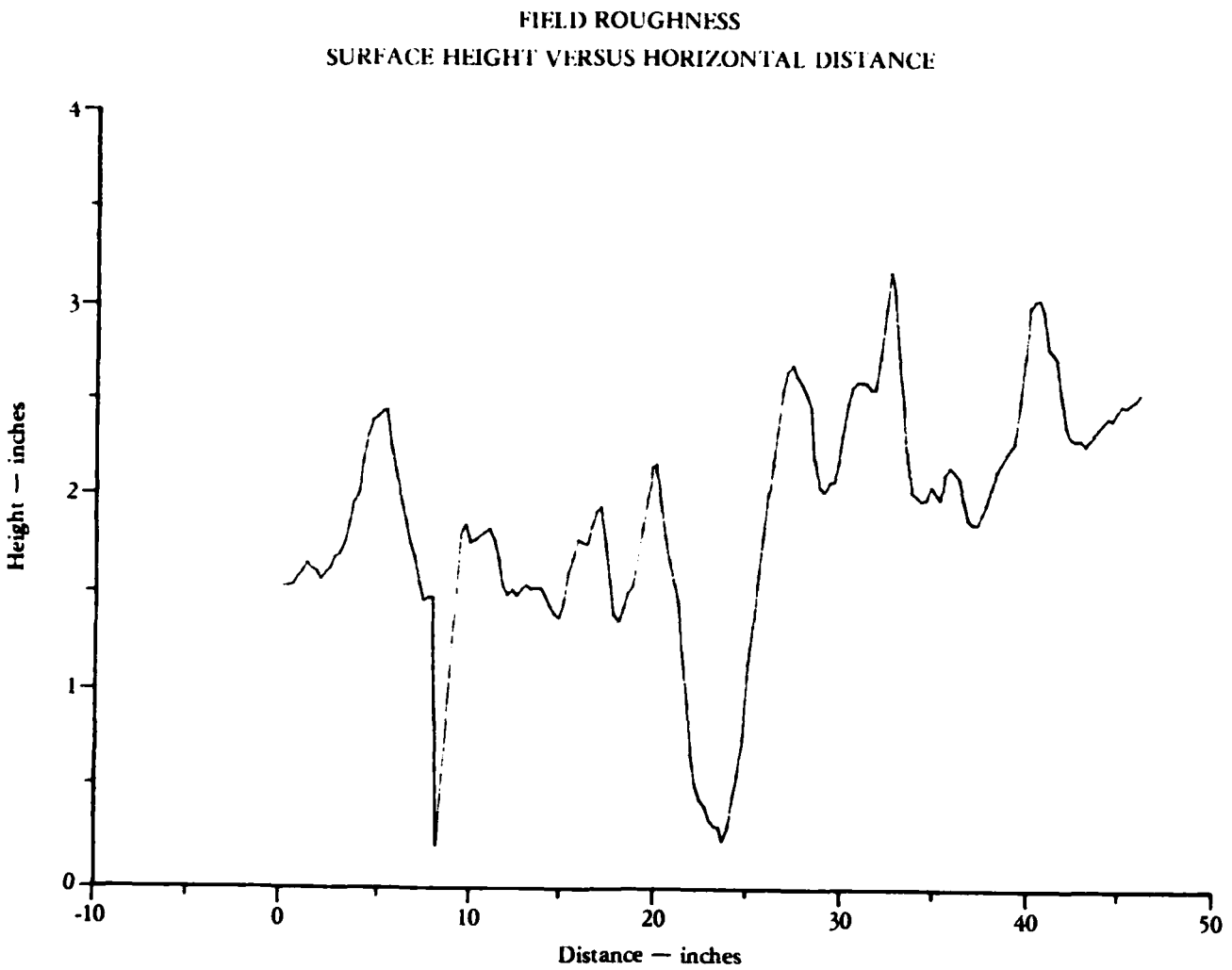

Figure 24. Example of Digitized Surface Height Profile

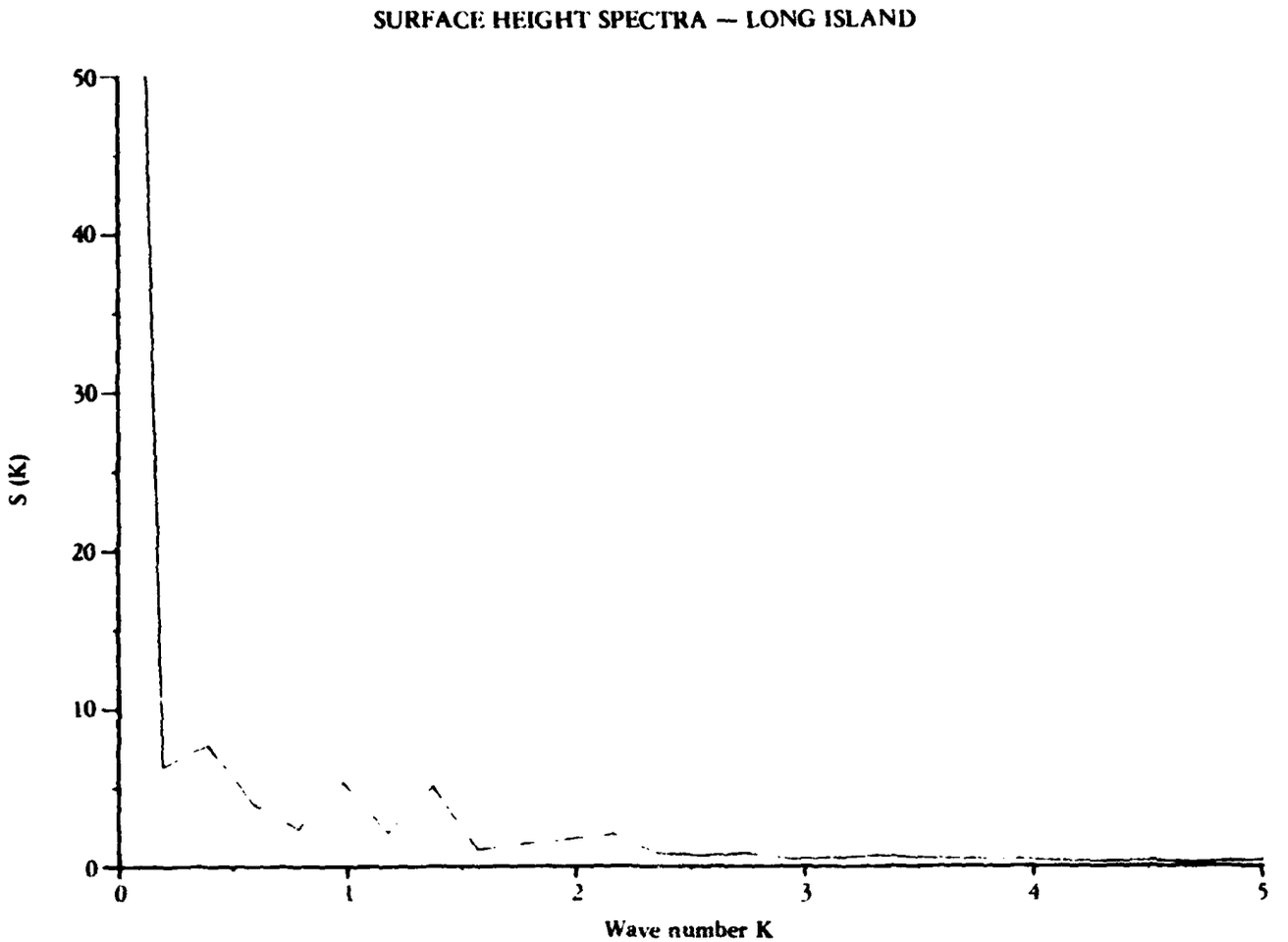

Figure 25. Example of the FFT Spectra of the Surface Height Profile

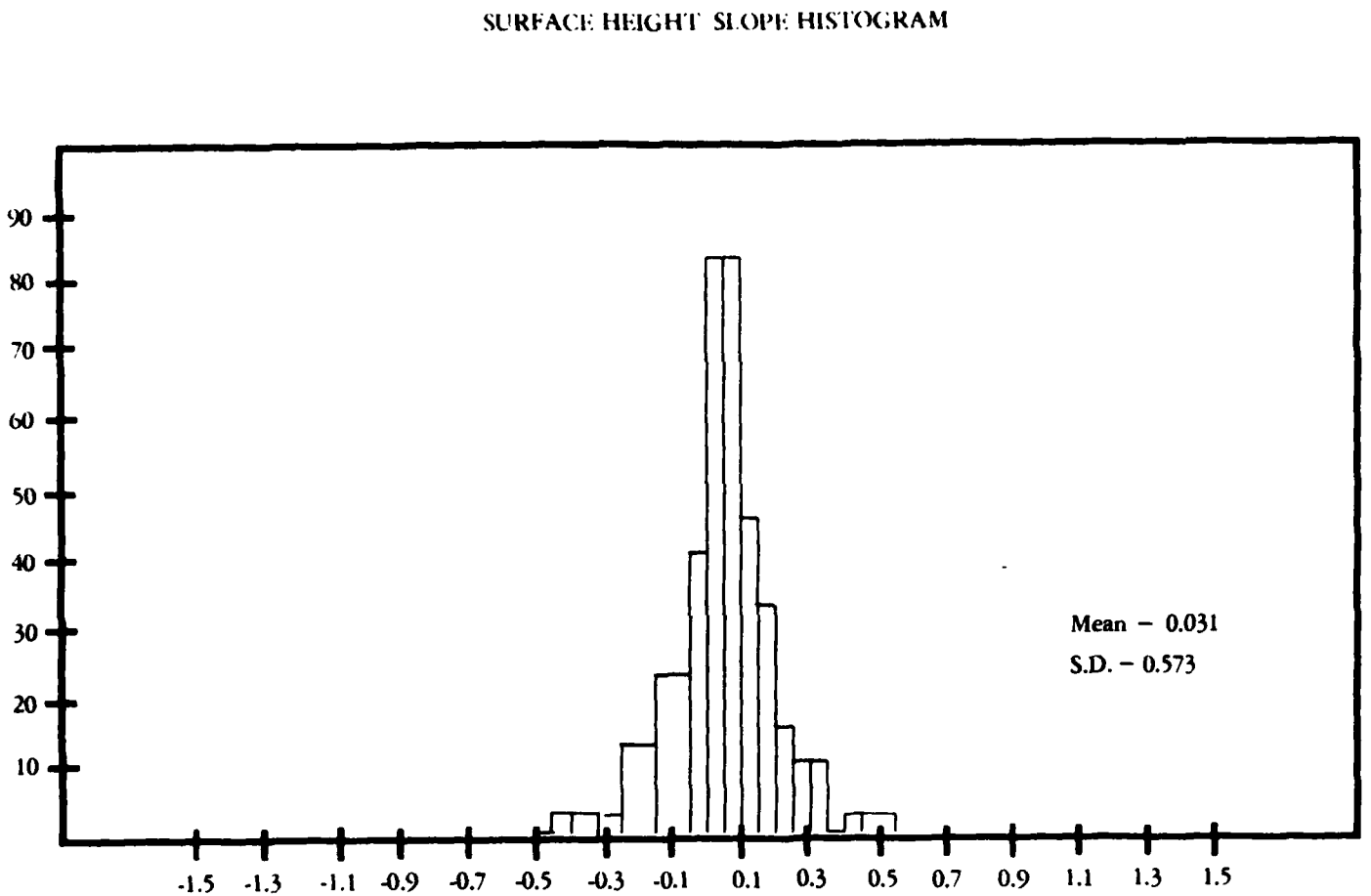

Figure 26. Example of the Histogram of Surface Slope Values

TABLE 15
VALUES OF MEAN RADIUS OF CURVATURE, MEAN SLOPE AND CORRELATION LENGTH OBTAINED FROM SEVERAL FIELDS IN THE LONG ISLAND TEST AREA

Field Designation	Mean Radius of Curvature R Inches	Mean Slope S	Correlation Length Inches
FRS-3B G	0.2×10^7	0.03	60.0
RFS3R G	0.17×10^7	0.008	47.5
F-F2 G	0.27×10^6	-0.07	45.0
RFS2 G	0.16×10^7	0.08	60.0
K Tall Grass	0.3×10^6	0.005	34.0
E Furrows EG	-0.035	-0.014	13.0
E Peak ERP	-138	-0.299	18.0
E Trough (ERT)	0.49×10^7	-0.02	--
HG Corn	0.26×10^6	0.17	--
HR Corn	-4.1	0.18	--
N Smooth	-5.5	-0.0029	40.0
3 Potatoes	0.184×10^3	-0.044	

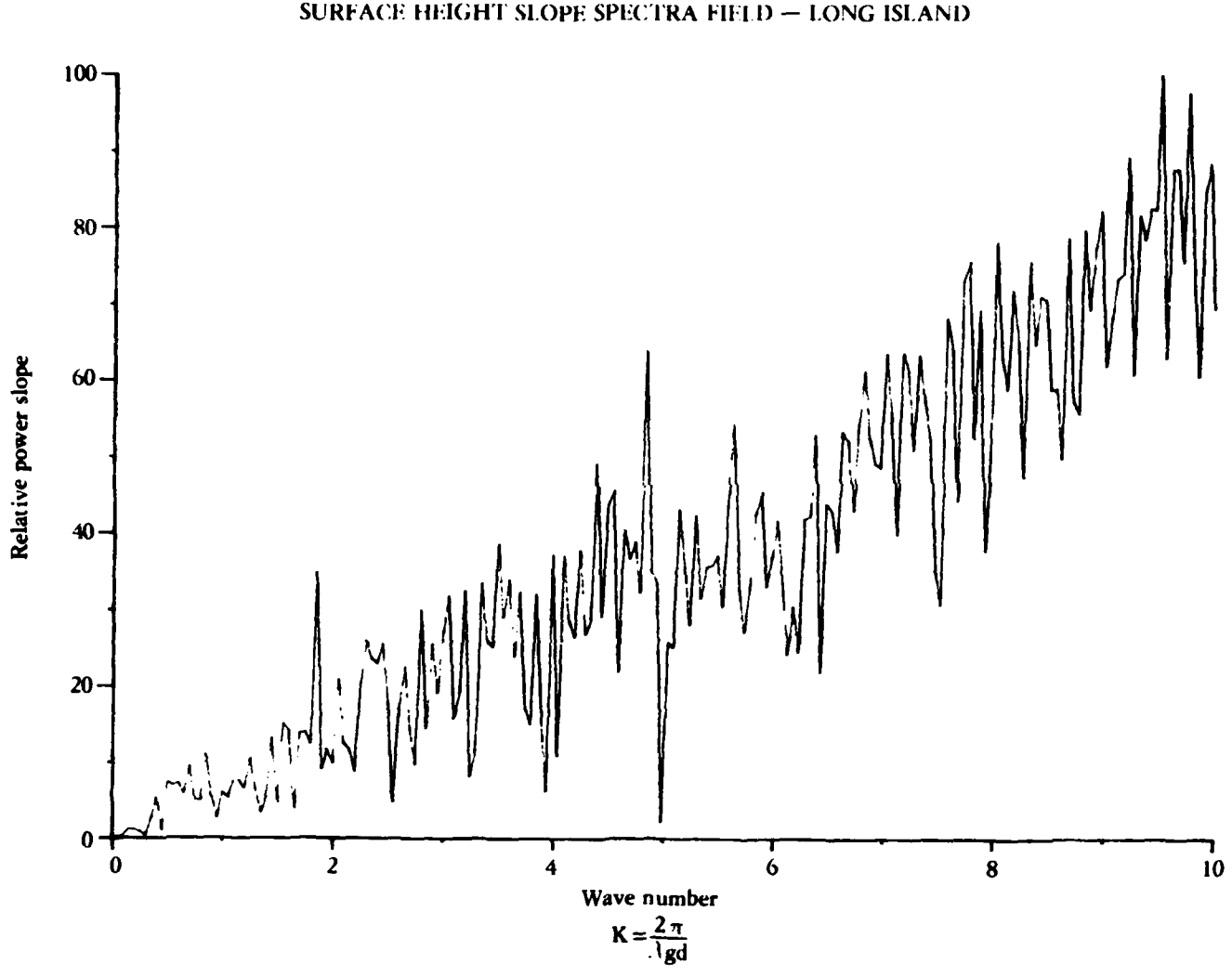

Figure 27. Example of Surface Slope Spectra

the measured surface height profile is to utilize the generated curve of slope vs. distance and calculate second derivatives. Thus, for each sample point a radius of curvature R_c is calculated using the standard relationship

$$R_c = \frac{(1 + h')^{3/2}}{h''} \tag{9}$$

where h' = surface slope [1st derivative of $h(x)$]

h'' = second derivative

Examples of mean value of radii of curvature obtained are given in Table 16 and of the histogram for the radius of curvature in Figure 28.

The autocorrelation function of the surface profile is defined as

$$\rho(x^i) = \frac{1}{h^2} - \int h(x^i)h(x - x^i)\, dx \tag{10}$$

A basic computer program performs the correlation with an example autocorrelation function given in Figure 29 and in the Appendix.

Additional histograms for both slope distributions and radii of curvature were also generated and examples of each are given in the Appendix.

TABLE 16
SCATTERING COEFFICIENTS OBTAINED FROM REFLECTOR SITE 3

Date	Incident Angle (degrees)	σ_o	σ_o (dB)
31 August	56.5	0.024	-12.9
7 September	63.9	0.004	-20.3

SURFACE HEIGHT STATISTICS
RADIUS OF CURVATURE
FIELD F2
(Values in inches)

SV	EV	F	CF
-.1700E+02	-.1639E+02	0.3	0.3
-.1639E+02	-.1579E+02	0.0	0.3
-.1579E+02	-.1518E+02	0.0	0.3
-.1518E+02	-.1457E+02	0.0	0.3
-.1457E+02	-.1396E+02	0.3	0.6
-.1396E+02	-.1336E+02	0.0	0.6
-.1336E+02	-.1275E+02	0.0	0.6
-.1275E+02	-.1214E+02	0.6	1.1
-.1214E+02	-.1154E+02	0.3	1.4
-.1154E+02	-.1093E+02	0.0	1.4
-.1093E+02	-.1032E+02	0.3	1.7
-.1032E+02	-.9714E+01	0.0	1.7
-.9714E+01	-.9107E+01	0.3	2.0
-.9107E+01	-.8500E+01	0.6	2.5
-.8500E+01	-.7893E+01	0.3	2.8
-.7893E+01	-.7286E+01	0.3	3.1
-.7286E+01	-.6679E+01	0.6	3.7
-.6679E+01	-.6071E+01	0.8	4.5
-.6071E+01	-.5464E+01	0.3	4.8
-.5464E+01	-.4857E+01	0.6	5.4
-.4857E+01	-.4250E+01	0.8	6.2
-.4250E+01	-.3643E+01	1.4	7.6
-.3643E+01	-.3036E+01	1.4	9.0
-.3036E+01	-.2429E+01	3.4	12.4
-.2429E+01	-.1821E+01	3.1	15.5
-.1821E+01	-.1214E+01	4.8	20.3
-.1214E+01	-.6071E+00	14.4	34.6
-.6071E+00	0.0000E+00	15.8	50.4
0.0000E+00	0.6071E+00	13.5	63.9
0.6071E+00	0.1214E+01	16.1	80.0
0.1214E+01	0.1821E+01	7.6	87.6
0.1821E+01	0.2429E+01	4.5	92.1
0.2429E+01	0.3036E+01	1.1	93.2
0.3036E+01	0.3643E+01	1.4	94.6
0.3643E+01	0.4250E+01	0.3	94.9
0.4250E+01	0.4857E+01	0.6	95.5
0.4857E+01	0.5464E+01	0.3	95.8
0.5464E+01	0.6071E+01	1.1	96.9
0.6071E+01	0.6679E+01	0.3	97.2
0.6679E+01	0.7286E+01	0.6	97.7
0.7286E+01	0.7893E+01	0.0	97.7
0.7893E+01	0.8500E+01	0.6	98.3
0.8500E+01	0.9107E+01	0.3	98.6
0.9107E+01	0.9714E+01	0.0	98.6
0.9714E+01	0.1032E+02	0.3	98.9
0.1032E+02	0.1093E+02	0.3	99.2
0.1093E+02	0.1154E+02	0.0	99.2
0.1154E+02	0.1214E+02	0.3	99.4
0.1214E+02	0.1275E+02	0.0	99.4
0.1275E+02	0.1336E+02	0.3	99.7
0.1336E+02	0.1396E+02	0.0	99.7
0.1396E+02	0.1457E+02	0.3	100.0
0.1457E+02	0.1518E+02	0.0	100.0
0.1518E+02	0.1579E+02	0.0	100.0
0.1579E+02	0.1639E+02	0.0	100.0
0.1639E+02	0.1700E+02	0.0	100.0

NUMBER OF DATA POINTS USED : 355
NUMBER OF POINTS TOO LOW : 6
NUMBER OF POINTS TOO HIGH : 6

MAXIMUM NUMBER OF POINTS IN A BIN : 57

EACH HISTOGRAM BIN IS DEFINED AS (SV,EV)
F IS THE FREQUENCY OF VALUES IN THAT BIN OCCURING
CF IS THE CUMULATIVE FREQUENCY

MEAN : [illegible]
VARIANCE : [illegible]
STANDARD DEVIATION : [illegible]
MAXIMUM VALUE : 0.1000000000E+04
MINIMUM VALUE : [illegible]
MEAN SQUARE : [illegible]

Figure 28. Example of Histogram of Radii of Curvature Values

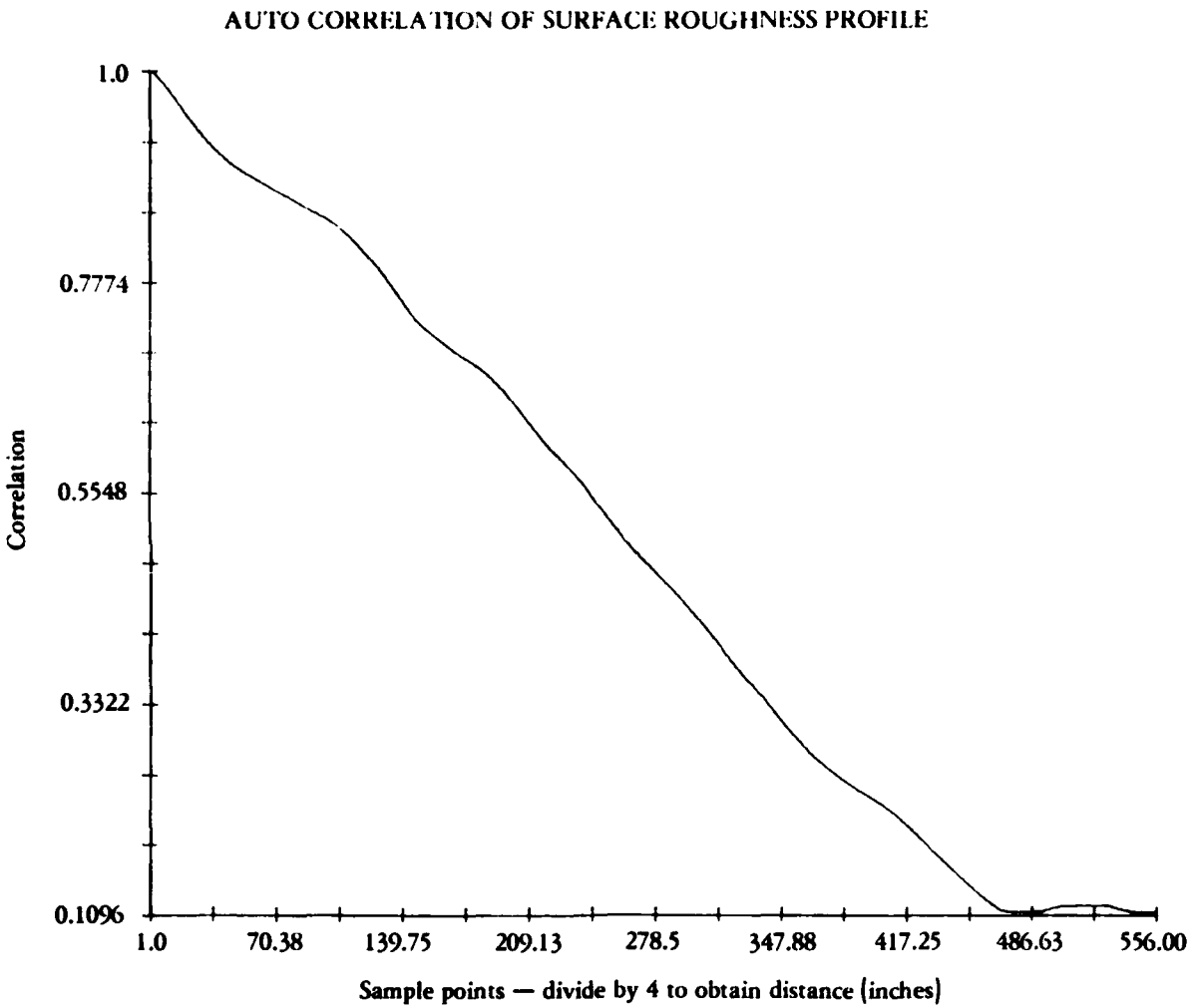

Figure 29. Example of An Auto Correlation Surface Roughness Profile

5
DATA ANALYSIS

Descriptions of backscatter from terrain and ocean are required by both the microwave remote sensing researcher, particularly those utilizing SAR imagery and by the radar system design engineers. It is interesting to point out that for the remote sensor scientist backscatter forms the desired signal. And by contrast, for the engineers designing detection radars surface scattering or clutter becomes the noise competing with desired signals. The important radar parameters for which backscatter characteristics will vary include wavelength, aspect angle, polarization and resolution. There is a very large set of terrain types and conditions that are encountered. These range from rough to smooth surfaces, wet to dry conditions and bare surfaces and vegetated areas.

Descriptions of the radar sensor parameters can be quantified; however, quantifying the terrain scattering surfaces has proven to be very difficult. Several measures have been used to describe terrain. For example, a measure of surface roughness, dielectric constant, density and moisture content, height and density of vegetation and others. Qualitative descriptions such as photographs, soil type, vegetation type are also used to classify terrains.

During the past 30 years or so, various researchers have studied the scattering characteristics of terrain. An extensive research effort conducted by Peake (1960) during the late 1950's to 1965 provided the first systematic approach to the study of scattering properties. This work consisted of analysis and measurement of the angular response of scattering from various terrain types and surfaces. Also, the dependency on wavelength was considered for both horizontal and vertical polarization. Subsequent work from the mid 1960's expanded on the analysis with many publications appearing. An excellent summary is given in Beckmann and Spizzichino (1963). A more

recent compilation of scattering theories is given in a two volume series by Ishimaru (1978). Also, an excellent summary giving results from a number of scattering measurement programs is given by Long (1983). And a summary of recent work on the electromagnetic interaction problem is given by Ulaby, et al. (1981 and 1982).

All of this effort on electromagnetic scattering has, in one way or another, attempted to relate a scattering model to parameters describing various surfaces. Radar systems engineers have developed models to describe the radar clutter environment. Clutter models have been developed using results obtained from the various measurements and analysis described. Several researchers have reported on the development of clutter models such as, for example Greenstein, et al. (1969).

The availability of data from calibrated synthetic aperture radar (SAR) systems has provided an additional source of scattering data. Also, the SAR has been used in remote sensing collection demonstration programs to obtain data from very large areal areas and from remote locations (MIZEX 1983-84). The calibrated SAR has also been utilized in the study of clutter characteristics (Larson, et al., 1981).

5.1 SCATTERING MODELS

An objective of this program is to utilize the measured clutter data in scattering models in order to improve the capability of predicting scattering properties. Analysis during the first year has been directed toward the selection of models to describe scattering in terms of the surface properties of the various test fields using an example of a statistical method of describing the measured distributions of the backscatter coefficients. For the initial analysis, data has been selected from several test sites in the Long Island area. The results obtained from analysis during the first year are described in this section.

Results from analysis of the surface measurement data indicate that most of the test sites satisfy the slightly rough or rough surface criteria for 23 cm wavelength data. A number of semi-empirical models for the scattering cross-section from rough surfaces have been proposed (Ruck 1970). Several of these models include incidence angle, wavelength and some measure of surface roughness properties as input parameters. One of the models listed by Ruck, proposed by Spetner and Katz (1960), has been selected as a candidate for use in relating surface properties to the measured scattering pattern. The model is given as

$$\sigma = \frac{K_7}{\lambda_o^2} e^{-\tan^2 \theta_i / 2S_o^2} \qquad (\lambda_o < \lambda_z) \qquad (11a)$$

$$\sigma = \frac{1}{\lambda_o^6} K_8 e^{-(\tan^2 \theta_i)\lambda_o / 2S_o^2 \lambda_z} + K_9 \qquad (\lambda_o > \lambda_z) \qquad (11b)$$

where, K_7, K_8, K_9 are constants defined in the reference in terms of the surface roughness properties

λ_o - wavelength

λ_z - upper limit on slope spectrum

S_o^2 - mean-square slope of surface

Barrick and Peake (1967) have derived a scattering model for a slightly rough surface given as

$$\sigma_{pq} = 4\pi K_o^4 h^2 \cos^4 \theta_i \, \alpha_{pq}^2 \, W(-2k \sin \sigma_i, 0) \qquad (12)$$

where, for backscatter

k_o - wave number

h^2 - rms surface height

α_{pq} - scattering matrix elements for p, q polarization

W - surface height power spectrum

(13)

For situations where very rough surface conditions are applicable, the Barrick (1968) specular point model will be applied. The form of this model is given as

$$\sigma = \pi \sec^4\gamma \, \rho(s) \, R(o)^2 \tag{14}$$

where γ - local angle of incidence

$\rho(s)$ - slope probability density function

R(o) - Fresnel coefficient, normal incidence

Selection of the candidate models described is tentative and is based on the use of surface descriptions that can be obtained from emperical data. It is anticipated that, during the next year effort models will be modified to best fit the data available. Also, other models will be investigated for applicability such as that developed recently by Winebrenner and Ishimaru (1985).

Although, thus far only data obtained at one incidence angle have been used in the analysis, a comparison of σ_o values of different angles from one site near the reflector array has been made. This site is a grass area near reflector site 3 that is included on both the 31 August and 7 September data. The values of σ_o obtained are given in Table 16, both for horizontal polarization. Two σ_o values obtained 7 days apart for the same location are seen to differ by 7.4 dB. Field roughness data indicated that the field was slightly rough for the L-band wavelength of 23 cm. Using the Barrick (1967) model for slightly rough surfaces, given in Eq. (12), a ratio of σ_o values for the two measurements was obtained.

TABLE 17
IG STATISTICS FOR A VARIETY OF TERRAIN SAMPLES

IG STATISTICS FOR A VARIETY OF TERRAIN SAMPLES

TERRAIN	PIXELS	MEAN	STD DEV	APLHA	MU	LAMBDA
Field E1	1x1	2011	2203	-246	2257	1965
Field E1	3x3	2655	6433	241	2413	1827
Field E2	1x1	2320	2237	-365	2684	3009
Field E2	3x3	3017	5965	301	2715	2488
Field F1	1x1	452	459	-64	516	528
Field F1	3x3	564	915	568	507	566
Field F2	1x1	417	420	-61	478	485
Field F2	3x3	566	1266	81	482	347
Field G1	1x1	1768	1808	-249	2017	1979
Field G1	3x3	2133	3219	87	2046	2404
Field G2	1x1	1521	1622	-194	1715	1577
Field G2	3x3	2162	6701	147	2015	1473
Grass	1x1	289	309	-42	331	313
Grass	3x3	289	167	-14	304	1292
Forest 3	1x1	1764	1832	-233	1997	1862
Forest 3	3x3	2818	5387	69	2749	2368
Cluttr 1	1x1	326	323	-41	367	342
Cluttr 1	3x3	323	169	-33	356	1526
Cluttr 2	1x1	299	306	-33	333	294
Cluttr 2	3x3	296	161	-58	354	1732
Forest 2	1x1	1505	1595	-190	1695	1539
Forest 2	3x3	2572	5483	169	2403	1453
Forest 1	1x1	1167	1276	-139	1306	1114
Forest 1	3x3	2159	5294	86	2073	1111

Ground truth records showed that the area was very wet during the time of data collection on 31 August, due to heavy rain the preceeding morning. Although dielectric constant measurements were not made on 31 August, the fact that the field was saturated would put the real part of the dielectric constant over 10 with a very large loss tangent. Using these estimated values and the measured dielectric constant values obtained on 7 September to calculate values for α_{hh}, a value for the σ ratio of about 7 dB is obtained. Note that there is a 7.4 degree difference in incidence angle for the two data sets.

Additional calibration data points will be obtained during the next year's effort to refine the calibration and to extend the calibration to include the North Carolina data and to the Mountain data of 7 September.

5.2 SAR DATA CHARACTERIZATION

Since the attributes which characterize most of the earth's natural surfaces (such as terrain, water, or ice) are essentially random in nature, it is necessary to describe the scattering from such surfaces in terms of statistical parameters. The ideas to be suggested and examined in this section proceed somewhat in the reverse of the usual treatments. That is, we hypothesize that there is at least one probability distribution in terms of which surface scattering can be well described. We further expect that the parameters of such a distribution can be used to separate not only types of surfaces but also incidence angles (and perhaps polarizations) for which a particular surface is examined.

The distribution suggested for this role is the inverse Gaussian (IG) distribution. This distribution has been around since the days of Schroedinger (1915) who used it in the study of first passage time in Brownian motion. Tweedie (1957) proposed the inverse Gaussian

name because of the inverse relationship which exists between the cumulant generating function of the first passage time distribution and that of the Gaussian distribution. Excellent discussions of this distribution in terms of its history, its properties, and some of its applications are given by Folks and Chhikara (1978) and by Cheng and Amin (1981).

Tweedie suggests at least four forms for the IG density function. The one which we shall adopt for our purposes is given by

$$f(x;\ \alpha,\ \mu,\ \lambda) = \left(\frac{\lambda}{2\pi(\bar{x} - \alpha)^3}\right)^{1/2} \exp\left(-\frac{\lambda(x - \alpha - \mu)^2}{2\mu^2(\bar{x} - \alpha)}\right) \tag{15}$$

where μ is the mean of the population, x is equal to the square-root of one-half the mean, i.e., $(\mu/2)^{1/2}$, and λ is defined as

$$\lambda = \frac{\mu^3}{S^2} \tag{16}$$

where S is the standard deviation of population.

One observes immediately that the density function depends upon the three parameters: α, μ, and λ. It is proposed that, in the space of these three parameters, points corresponding to samples from different terrain types will be well separated. And not only will points for different terrain types be quite distinct, but also different regions of the three-parameter space will characterize different surface types. The reasons for believing that these ideas hold some validity is that they have been partially tested on SAR ice data with promising results (Maffett, 1979). Eventually we wish to test the fit of the IG distribution to the cumulative histograms for various terrain samples by some standard nonparametric test such as, for example, a Komologoroff-Smirnov test (see, for example, Folks and Chhikara, 1978 or Conover, 1980).

Our reasons for choosing the approach outlined above and for choosing, in particular, the IG distribution are based on the long-standing and rather successful application of the log-normal distribution to describe clutter data of various sorts. It is planned to compare calculated IG fits with log-normal fits for the same data samples. We believe that the IG distribution will offer an improvement over the log-normal because of its tail behavior. The tail of the IG distribution goes more quickly to zero than does the tail of the log-normal distribution. This fact should be advantageous in describing terrain (or other earth surface) data since there are no infinite values of clutter RCS. There exists exact sampling distribution theory for the IG distribution and it is a reasonably easy distribution to work with. These facts make the IG distribution an attractive candidate to describe skewed terrain data.

SAR images used in this research are recorded and processed to give data which are proportional to square root of relative power. Since it may be desirable to examine resolution cells of different sizes, each datum of a sample is squared before any analysis is carried out. In this way, resolution cell size may be varied and the results normalized to the resolution cell area. The result is normalized radar cross-section (NRCS), "σ." One problem to be investigated is the effect of resolution cell size on the distribution from which the sample has been drawn.

The chosen sample is now used to find estimates (α, μ, and λ) for the parameters α, μ, and λ of an IG distribution. The estimates used are maximum liklihood (ML) ones given by Cheng and Amin (1981) and are numerically straightforward. Their formulas require an iteration, but in actual practice (and especially for small samples) it is almost never necessary to go beyond α_0. The estimates α, u, and λ are calculated as:

$$\hat{\alpha}_0 = x_1 - (2s^2 \log n)^{-1}(\bar{x} - x_1)^3 \tag{17}$$

$$\hat{\alpha}_{m+1} = \alpha_m + \left[\frac{3}{n} \sum_{i=1}^{n} \frac{1}{x_i - \alpha_m} + \lambda_m \left\{ \frac{1}{\mu_m^2} - \frac{1}{n} \sum_{i=1}^{n} \frac{1}{(x_i - \alpha_m)^2} \right\} \right] \left\{ \frac{3}{\mu_m \lambda_m} + \frac{12}{\lambda_m^2} \right\} m = 0, 1, \ldots \tag{18}$$

$$\hat{\mu}_m = \bar{x} - \alpha_m; \; m = 1, 2 \ldots \tag{19}$$

$$\hat{\lambda}_m = \left(\frac{1}{n} \sum_{i-1}^{n} \frac{1}{x_i - \alpha_m} - \frac{1}{\mu_m} \right)^{-1}, \quad m = 0, 1, 2, \ldots \tag{20}$$

where x_1 is the smallest datum of the sample and $\bar{x}$ and s are the sample mean and standard deviation, respectively.

To illustrate the nature of these parameters, an example will be presented. A small sample ($n = 256$ points) from a SAR image of a grassy field was selected. Each datum is squared and considered individually; that is to say, each squared datum is proportional to the power returned from a resolution cell of dimensions 1.5 m by 1.44 m. In this example only, the datum is <u>not</u> divided by the resolution cell area. The smallest squared datum had a value 4, the largest had a value 37636. The mean was 5639.918 and the standard deviation 5651.794. Using the above formulas, we find the ML estimates for α, μ, and λ to be -1159.568, 6799.486, and 8658.059, respectively. Only the first step of the iteration was used since the second step α was identical with the first. Figure 30 presents a histogram of the data and the IG density resulting from the above parameter estimates. The fit seems quite reasonable considering the small sample size.

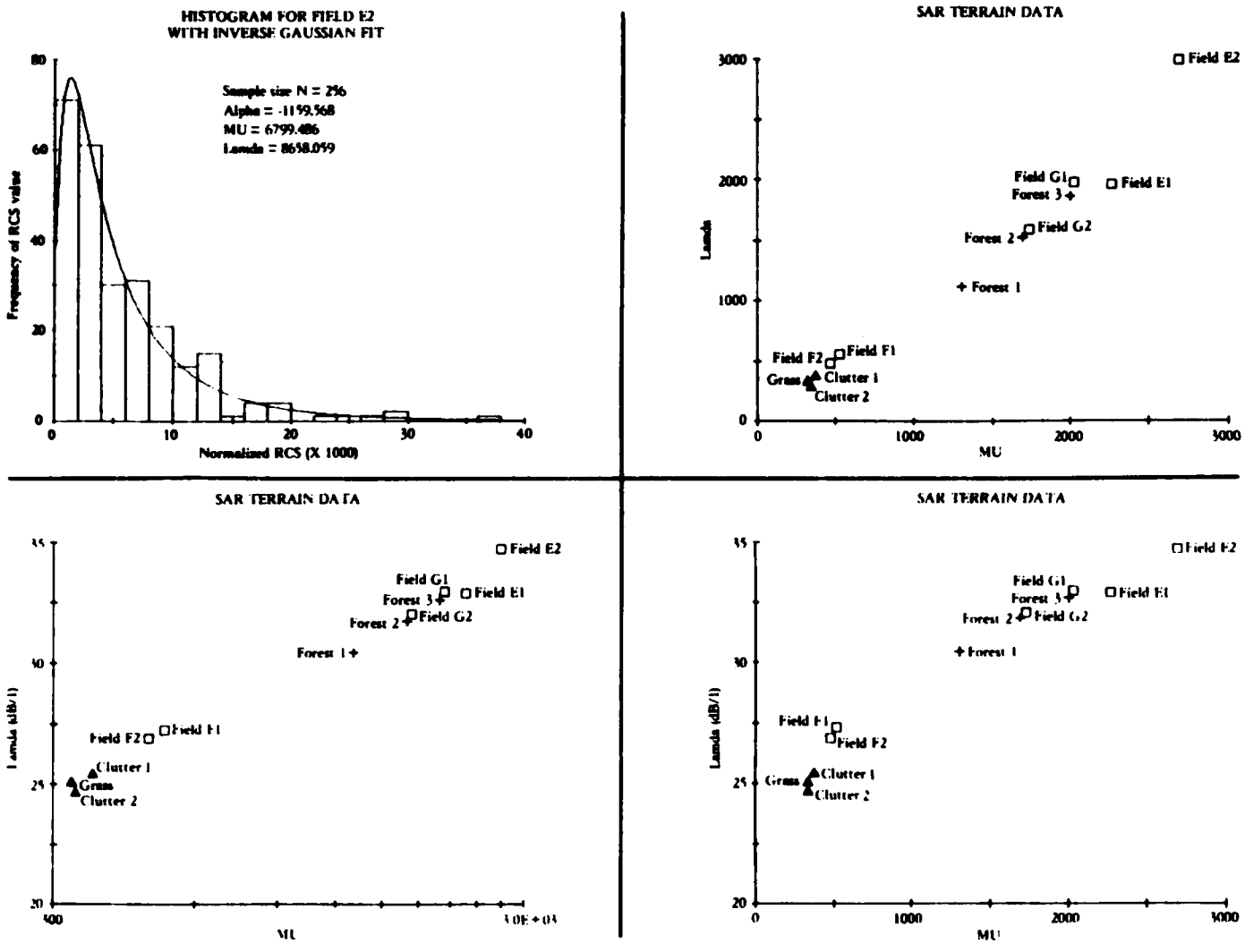

Figure 30. Characterization of SAR Data using the Inverse Gaussian Distribution

5.3 EXAMPLE

A preliminary examination of the IG distribution inputs (α, μ, and λ) from 12 extracts from SAR images has been started. These extracts are comprised of samples from 3 grass-clutter areas, 6 field areas, and 3 forest areas. The digital output from each of these areas has been described above. In the processing to be discussed here, the data have not been converted to σ_0 by dividing sums of squares pixel outputs by appropriate areas. If various sampling methods are to be compared, this normalization should be carried out.

Samples of sizes ranging from 900 to 12800 pixels have been processed so as to vary the effective resolution by grouping various sized sets of pixels (for example, 1 x 1, 3 x 3, and so on). Estimates for the IG parameters α, μ, and λ have been computed for each of the various samples. Table 17 summarizes these results as well as the means and standard deviations of the samples. To some degree, the α, μ, and λ parameter values duplicate some of the information supplied by the mean and standard deviation. For example, consider Field F1 compared with Forest 3. The means and standard deviations, as well as the μ values compare favorably. The α and λ values, however, even though similar, are distinct enough to separate these two scenes. μ and λ are only partially interpretable as location and scale parameters since (if α is taken to be zero for the moment), although the mean of the IG distribution is μ, its variance is the cube of μ divided by λ.

It is noted that the α parameter is a redundant; however, it serves as a location parameter which allows a negative range of variable values. It may be useful later in the study to examine the question of resolution size. The behavior of μ and λ by will be examined looking at a plot of λ versus μ for the 1 x 1 pixel case. The graphs given in Figure 30 show linear-linear, log-linear, and log-log plots. We can see that the log-log plots separate the 12

scenes somewhat and yet significantly groups certain fields. At the lower left portion of this graph, Clutter 1, and Clutter 2, and other grass scenes are grouped. These scenes are all quite similar in that they all are characterized by fairly "smooth" surfaces. Next come Fields F1 and F2 which are also smooth, yet not as smooth as the grass areas.

Towards the upper right portion of the graph are the rougher scenes. First, the Forests 1, 2, and 3, which are all very similar in type, mainly deciduous in nature. Fields E1, E2, G1, and G2 are all of very rough surfaces, the first two being plowed fields, the latter two being corn fields.

Thus, using the IG characterization parameters μ and λ suggests that the variation from lower left to upper right represents a variation from very smooth to very rough scene chartacteristics. The linear-linear and the log-log plots show that the progression from lower left to upper right closely approximates a straight line making a 45° angle with the axes. At the moment no firm explanation for this behavior has been determined, but it is hypothesized that it may be connected with the phenomena of surface roughness and/or slope distribution. So it is very possible that this behavior will also depend upon the resolution question mentioned earlier (that is, the grouping of pixel sets).

5.4 FUTURE WORK

The results presented in this report represent a summary of the first year effort of the analysis of SAR generated L-band clutter data (see Figure 1 and Table 1). Efforts during the next year of this program will focus on the analysis of this data as described in this report. In addition, emphasis will be given to the determination of relationships between the empirical scattering data and the measured characteristics of the scattering surfaces. An expanded

AD-A165 916 CALIBRATED L-BAND TERRAIN MEASUREMENTS AND ANALYSIS PROGRAM. (U) ENVIRONMENTAL RESEARCH INST OF MICHIGAN ANN ARBOR R W LARSON ET AL. FEB 86 ERIM-174200-5-P 2/2

UNCLASSIFIED RADC-TR-85-266 F19628-84-C-0081 F/G 8/6 NL

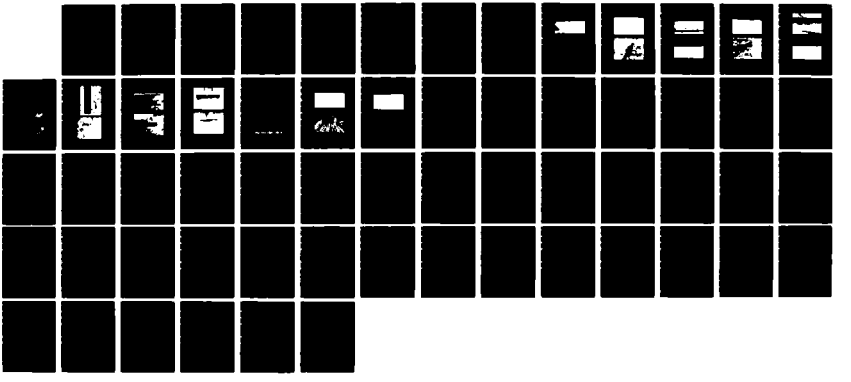

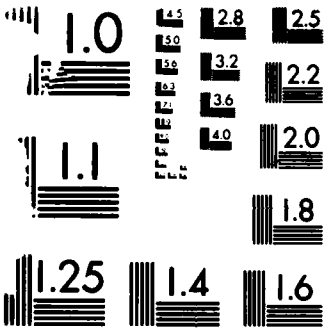

data set, to include effects of incidence angle and polarization, will be utilized during next year's effort.

Additional calibration relationships will be generated using SAR data from both the Long Island and North Carolina reflector arrays. Calibration signal generator values, which are recorded on each data pass, will be used to normalize calibration relationships in order to improve accuracy.

Analysis of the measured data describing the surface properties will also be continued during the next year. The ground measurement data that has not been considered during the first year effort will be reduced. Parameters describing the slope, radiis of curvative and correlation lengths will be determined, for the remaining ground data. Techniques described in this report will be utilized, in addition, analysis to determine improved data reduction methods will be carried out.

Determinate and statistical descriptions of the ground profile parameters will be developed. The emphasis will be directed toward the determination of surface descriptors which correlate with the IG or other parameters derived to discribe the scattering data. Consideration will be given to the size of the data set and resulting statistics. Additional data samples may be required. The deterministic and statistical parameters required for use in the several candidate rough surface scattering models selected will be calculated. These models will be used to determine the ability to describe the measured angular scattering response. Also, results will be compared with available published values of scattering coefficients.

SAR data from the test sites will be used in obtaining additional parameter values for the IG distribution. Values obtained for the parameter triplets (i.e., μ, λ, α) will be analyzed to determine distinct characteristics, properties or trends as a function of properties of the scattering surfaces. Additional data sets to be

used will include measured values over a range of incidence angles for a number of the test sites. The first analysis will be confined to horizontal polarization data. After this initial analysis is completed, vertical polarization data from the same test sites will be analyzed following an identical procedure. The total data set will then be analyzed to determine characteristics that are distinct between horizontal and vertical SAR clutter from the test fields.

There are two separate ideas involved in the estimation of the parameters that will be investigated using the Inverse Gaussian. First, that the parameter triplets (α, μ, λ) will be different for distinct terrain types. It is hypothesized that triplets should be distinct for distinct incidence and polarization views of the same terrain scene. Second, that the the distribution best fitting the data is the IG distribution. The first can be accepted or rejected on the basis of plots of parameter triplets for a wide variety of terrain data which is available at ERIM.

The second idea is more difficult. One would like to bring the log-normal distribution into play in the examination of these terrain data. A triplet of parameters can also be used to define an appropriately fitting log-normal distribution. It has been shown for ice data that in many cases the fitting IG and log-normal densities cannot be visually distinguished from each other. However, in that case, the IG triplets seemed to offer wider separation for different ice types than the log-normal triplets. To make a final choice between the IG and log-normal, one would like to formulate a test based on a ratio of maximum liklihoods for these two distributions. However, at present there does not exist a table of critical values for such a test involving these two distributions. And to establish such a table will require some sort of Monte Carlo procedure.

It is planned to examine goodness of fit of both the IG and log-normal distributions to histograms based on various samples, using

the Kolmogoroff-Smirnov test. The analysis and tabular data necessary to carry out this test at an arbitrary significance level already exist in the statistical literature.

The surface height, slope and radius of curvature distributions will be used in a statistical analysis similar to that described above for the scattering data. The goal of this part of the analysis will be to determine correlation between surface and scattering statistics within the limitation of the data sample points available. If it can be demonstrated that surface profile data can be related to scattering characteristics a semi-empirical model may result for use in SAR image simulations and detector.

6
RECOMMENDATIONS

The present program, which will be completed at the end of FY 1986, was intended to serve as an initial effort in collecting and analyzing calibrated L-band SAR terrain measurements. This effort was limited in nature because only a small set of SAR data were utilized. This limited SAR data set contained a sampling of the various categories of terrain types which may be considered. Future research efforts in this area should be focused in two areas: data collection and data analysis.

Future data collection efforts should be of three types: (1) SAR data; (2) scatterometer data; and (3) ground measurements. Future SAR data collections would utilize the ERIM X-, C- and L-band SAR system. Efforts are currently underway to install this system into a U.S. Navy owned and operated P-3 aircraft (Shuchman, et al., 1984). As was accomplished during the present program, SAR data of different terrain types could be collected on a target of opportunity basis during test flights or other SAR data collection programs.

We also recommend that ground-based L-band scatterometer measurements of various terrain types be collected. Although these measurements can not be used to determine the statistical distribution of L-band clutter data, this type of data would be useful in evaluating L-band scattering models. This data type is much more easily collected than airborne SAR data and can be used to help verify the scattering models. Scatterometer data would be collected coincident with the SAR data collections described above and the ground measurements discussed below. In addition, scatterometers and ground measurements could be collected separately from the SAR missions.

Finally, a ground measurements program coincident with both SAR and scatterometer data collections is recommended. The ground measurements to be collected include dielectric measurements of surface

materials, soil moisture, soil density and surface roughness measurements.

For analysis of the calibrated L-band terrain measurements, we recommend that research be conducted in three separate areas:

1. Further evaluation of the statistical distribution of L-band terrain data and the correlation to ground measurements;
2. Further evaluation of L-band clutter/scattering models; and
3. Evaluation of the utility of L-band SAR image simulation models.

In the statistical analysis of the L-band clutter data, efforts would focus on the extraction of radar backscatter signatures from both L-band SAR and scatterometer data sets. These signatures would then be correlated with the surface roughness and other scattering statistics. Finally, we could continue evaluation of the statistical distributions of the L-band clutter data.

Using the L-band terrain measurements and surface scattering statistics, various scattering models would be further evaluated for agreement between the model predictions and empirical data.

As a final task, we recommend that the utility of a SAR image simulation model being developed at ERIM be evaluated. An airborne SAR terrain image simulation model is currently being developed at ERIM as part of an effort being sponsored by the U.S. Army. Under the recommended future effort, we would concentrate on the L-band portion of this model. The model would be upgraded using the L-band terrain measurements obtained during the recommended program as well as using the results of the backscatter model evaluation. The imaging model would be evaluated utilizing SAR imagery available at ERIM. Finally, a point target simulation model which has been developed at ERIM could be incorporated into the terrain model.

APPENDIX
EXAMPLES OF GROUND MEASUREMENT DATA

This appendix presents results from ground measurements made during the North Carolina and Long Island SAR data flights. Figures A-1 to A-12 includes photographs of sites in the Long Island area selected for initial analysis. Examples of measured surface height variation after digitization of the raw data are given as Figures A-13 through A-24; histograms of calibrated σ values from example fields are given in Figures A-25 through A-30.

Examples of results obtained from reduction of the surface roughness records are given as Figures A-30 through A-49. These include derived examples of the following parameters

Histograms of surface slope values	A-30 through A-32
Spectra of surface slopes	A-33 through A-37
Spectra of surface height	A-38 through A-42
Histograms of surface height	A-43
Histograms of surface slope	A-44
Histograms of radius of curvature	A-45 through A-46
Autocorrelation of surface roughness	A-47 through A-49

Radar data from grass fields in the reflector test array sites, Peconic River Airport and from fields E, F and G have been used in the initial statistical analysis reported in Section 5. Examples of ground data from these areas are included in this appendix.

In addition to the ground data included in this appendix, surface roughness measuremets are available from other fields listed in Table 7 for the North Carolina sites and Table 10 for the Long Island sites. Also, photographs showing these sites are available, as are tape recordings of observations made during the 7 September 1984 data collection at Peconic River Airport.

Surface roughness measurements were made at the Long Island test sites during the period 27 August to 6 September 1984. All soil

samples were collected on 7 September 1984 during the data collection period between 1200 to 1700 hours EST. Surface roughness measurements were made of the North Carolina site during the period 5 April to 10 April. Also soil samples were obtained on 8 and 9 April coincident with the SAR data collection times.

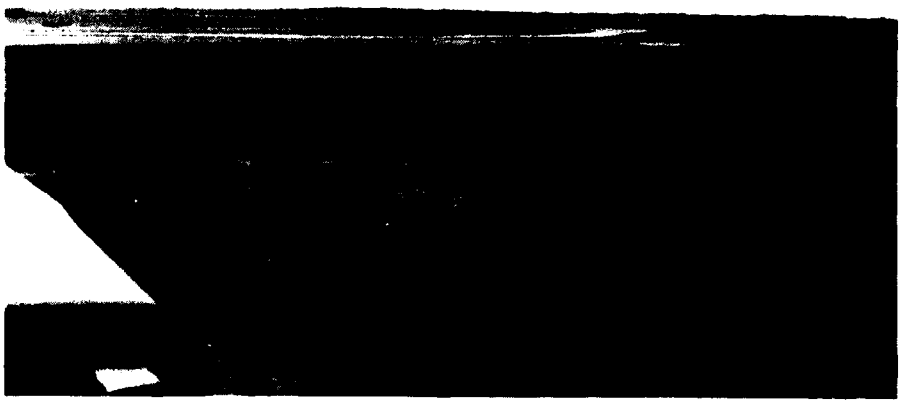

(a)

(b)

Figure A-1. a) Ground Photograph of Grass Between Reflector Area 1 and 2. Peconic River Airport, L. I.
b) Photograph of 48" Square Reflectors - Array 1 Peconic River Airport, L. I.

(a)

(b)

Figure A-2. Ground Photographs of Potato Field Near Peconic River Airport, Designated Field 3
a) Top Photo General View of Field Looking West
b) Close Up Photograph Showing Row Spacing of 2'10" and Peak to Trough Distance of 8"

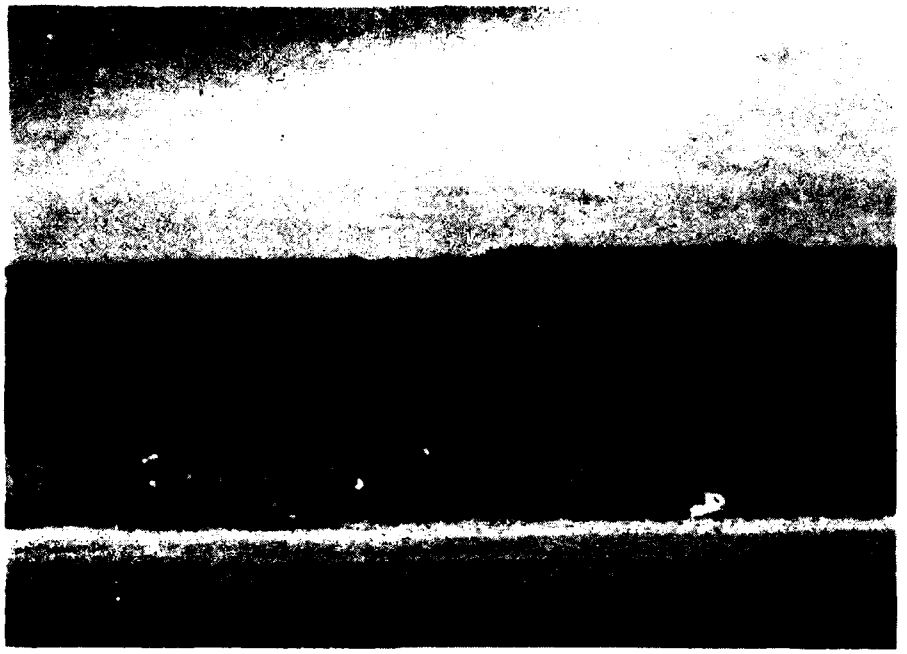

(a)

(b)

Figure A-3. Photographs of Two Smooth Fields Northwest of Peconic River Airport.
a) Smooth Bare Field Designated Field N
b) Grass Field Designated Field A

(a)

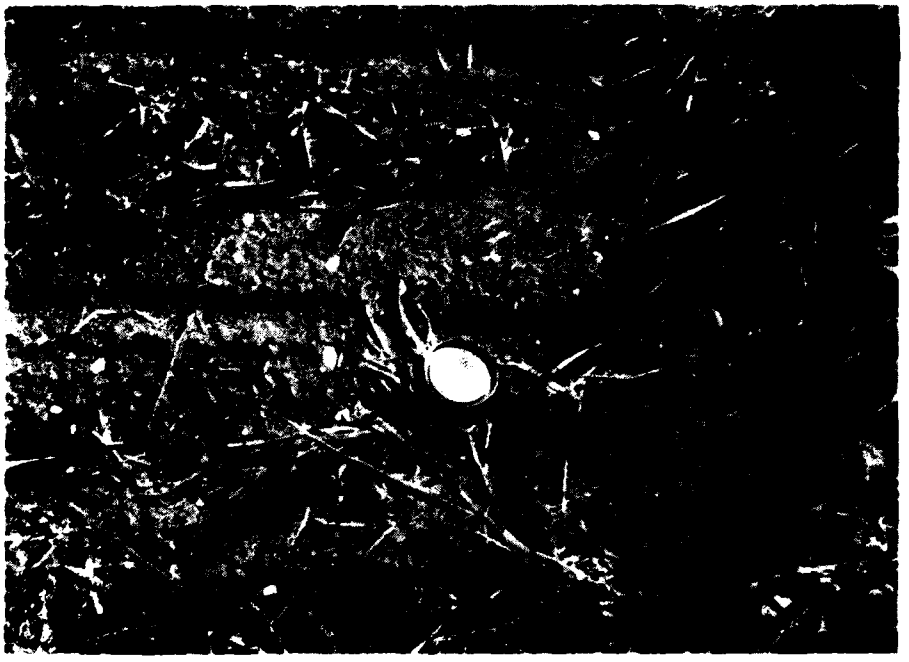

(b)

Figure A-4. Photographs of Field C Located North of Peconic River Airport on Sound Avenue
a) View Looking South From Sound Avenue
b) Close Up With Lens Cap to Show Roughness Scale

(a)

(b)

Figure A-5. Photographs of Potato Field E Located South of Field C
a) Close Up View of Roughness Board, Width of Chart Paper is 12 inches
b) View Looking Southwest

(a)

(b)

Photographs of Grass Field Designated Field F Located East of Field E and South of Field C
(a) General View of Grass Field E
(b) View of Roughness Board on Field E

(a) (b)

Figure A-7. Photographs of Corn Field Designated Field G; East of Field F
a) View of Corn Stalks to Show Height, Person Shown Is 6 Feet Tall
b) View of Roughness Board in Field G

(a)

(b)

Figure A-8. Photographs of Field of Cut Corn Designated Field H, East of Field G
a) View of Field H Looking Southeast
b) View Showing Roughness Board

(a)

(b)

Figure A-9. Photographs of Two Grass Fields Located North of Peconic River Airport, East of Landing Road
a) Field Designated I, Roughness Board Included on Photo
b) Field Designated K Roughness Board Included on Photo

(b)

Figure A-10. Photograph of Field With 6 to 8 Foot Tall Pines Sparsely Planted in Tall Grass. This Field is Designated Field L and is Very Similar to Field L-2 of the North Carolina [illegible] of Agriculture

(a)

(b)

Figure A-11. Photographs of Smooth Bare Field Located Northeast of Peconic River Airport on Middle Country Road. Upper Photo Shows View Looking West and Lower Photo Shows Close-up with Roughness Board. Peak to Trough 2 inches, Horizontal Peak to Peak Distance is 4 Inches. This Field is Designated P

(a)

Figure A-12. Photograph Showing Smooth Grass Field Designated Q, Located West of Field P. Photo Taken Looking North From Middle Country Road

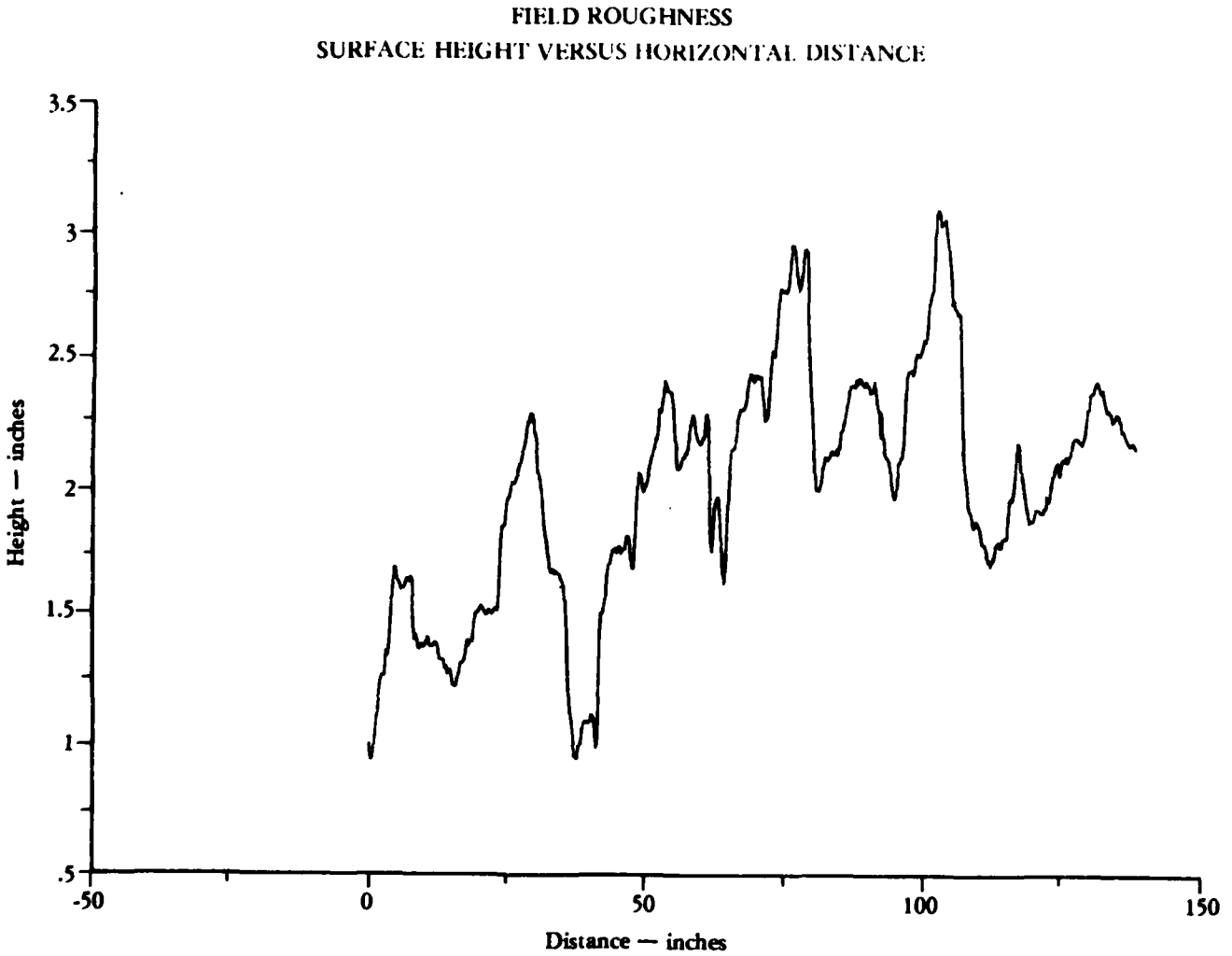

Figure A-13. Graphs Included on Figure A-13 Thru A-24 Give Digitized Values of Measured Data. Surface Roughness Plot From Field Grass Designated RFS2 Near Reflector Site 2, Peconic River Airport

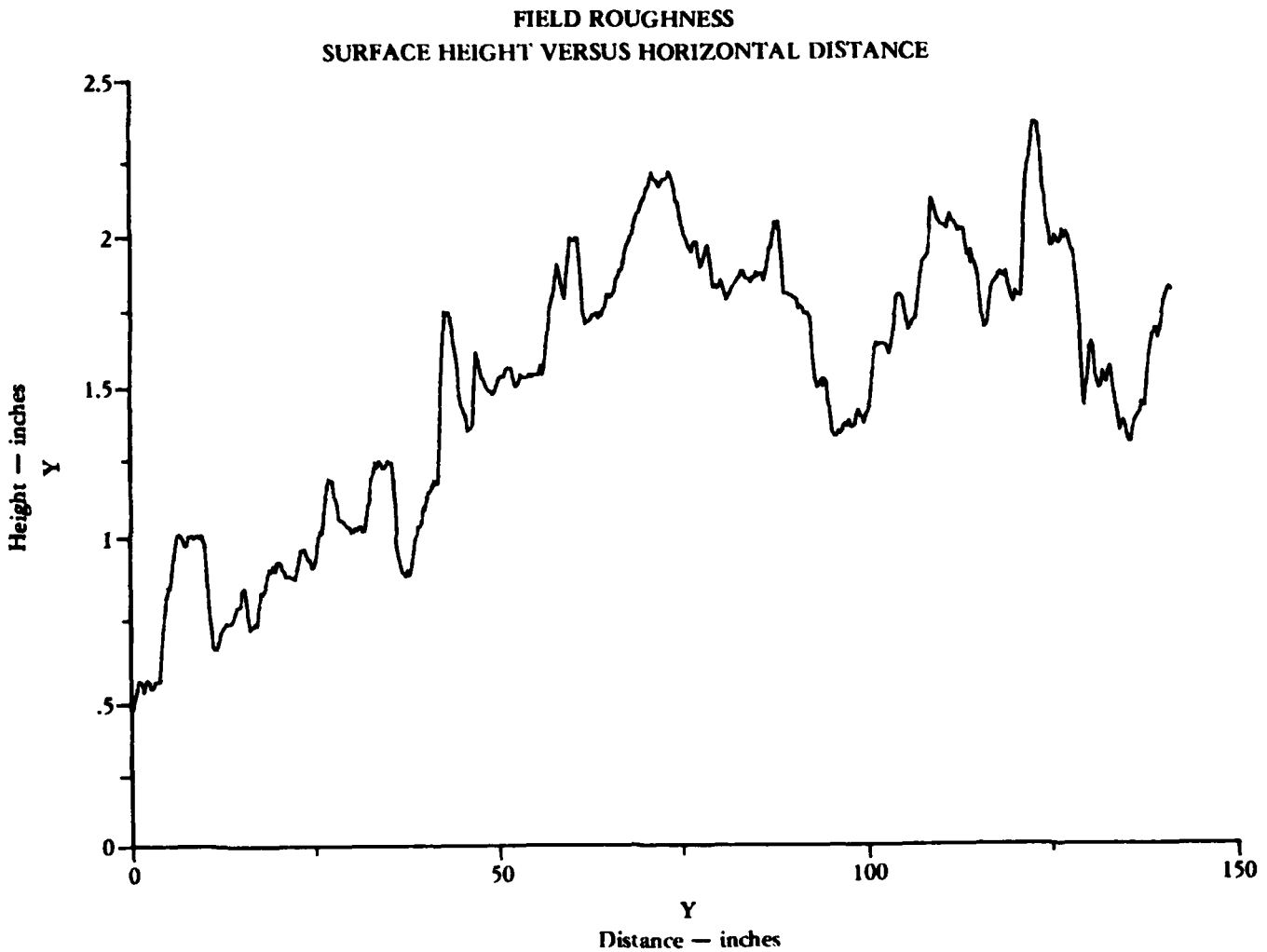

Figure A-14. Second Roughness Plot of Grass Field Site 2 Near Reflector Site 2, Peconic River Airport

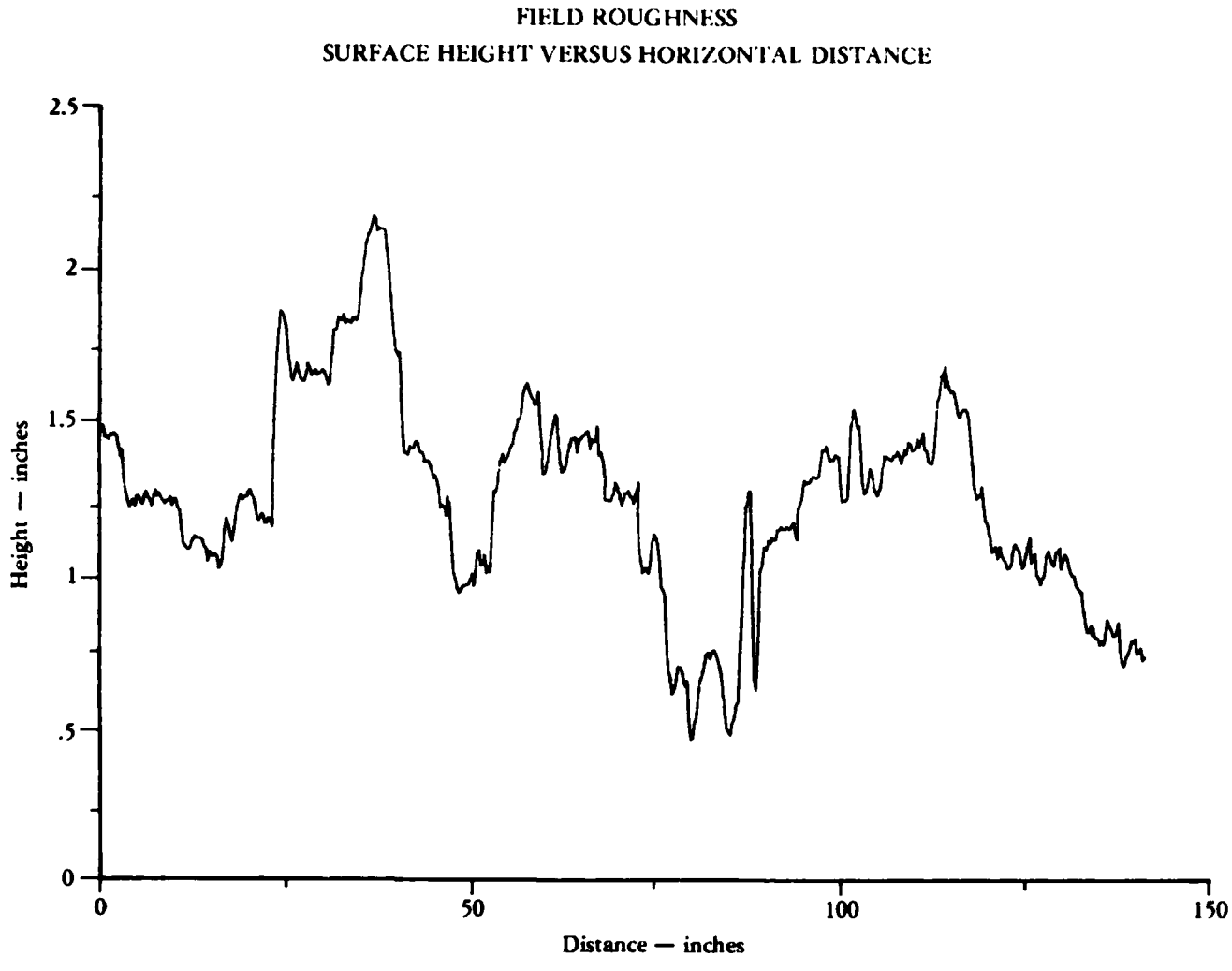

Figure A-15. Roughness Plot of Grass Near Reflector Site 3, Peconic River Airport

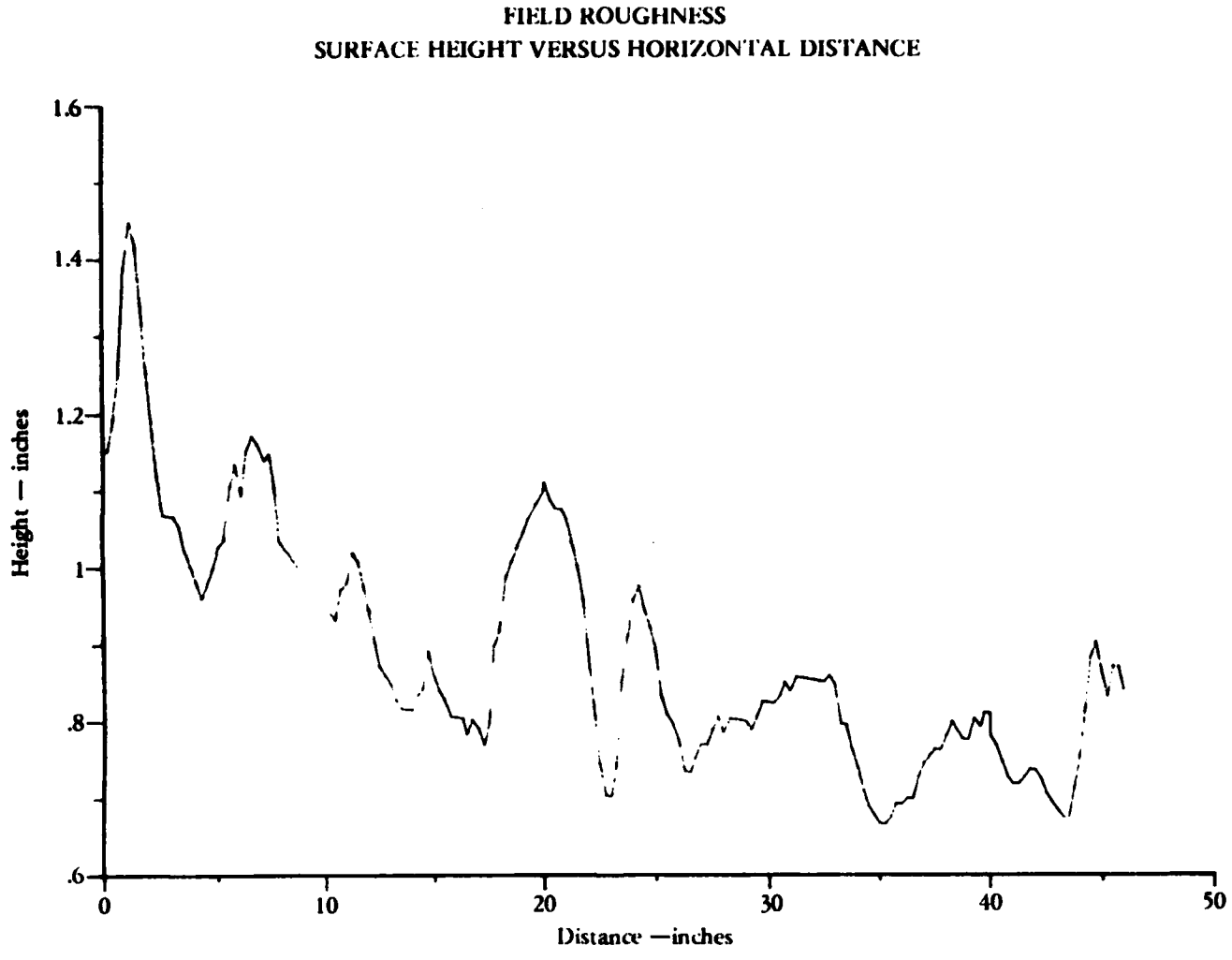

Figure A-16. Field ERT From Field Designated E, Located North of Peconic River Airport - Roughness Along Peak of Furrows

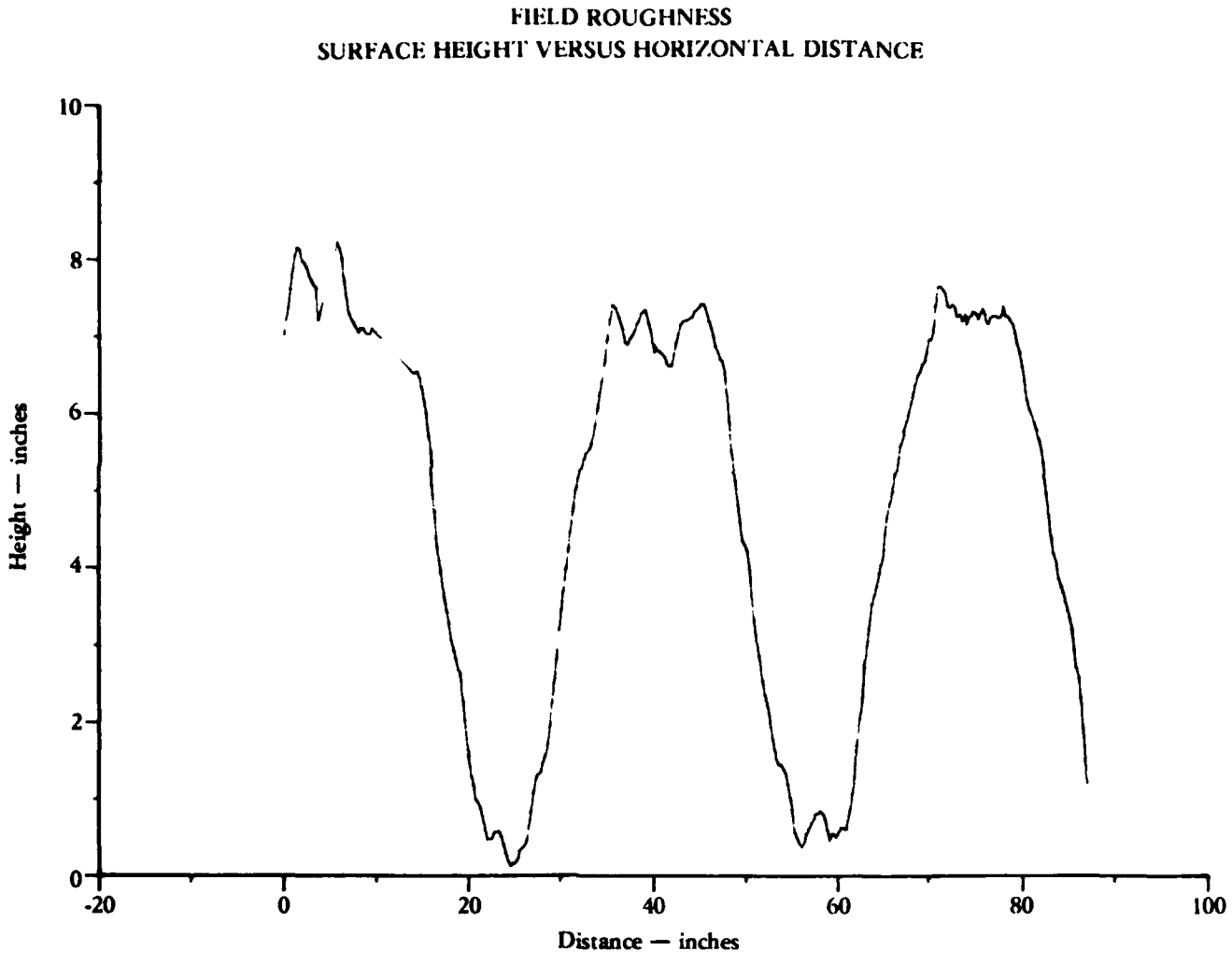

Figure A-17. Field EG From Field Designated E, Roughness Normal to Furrows

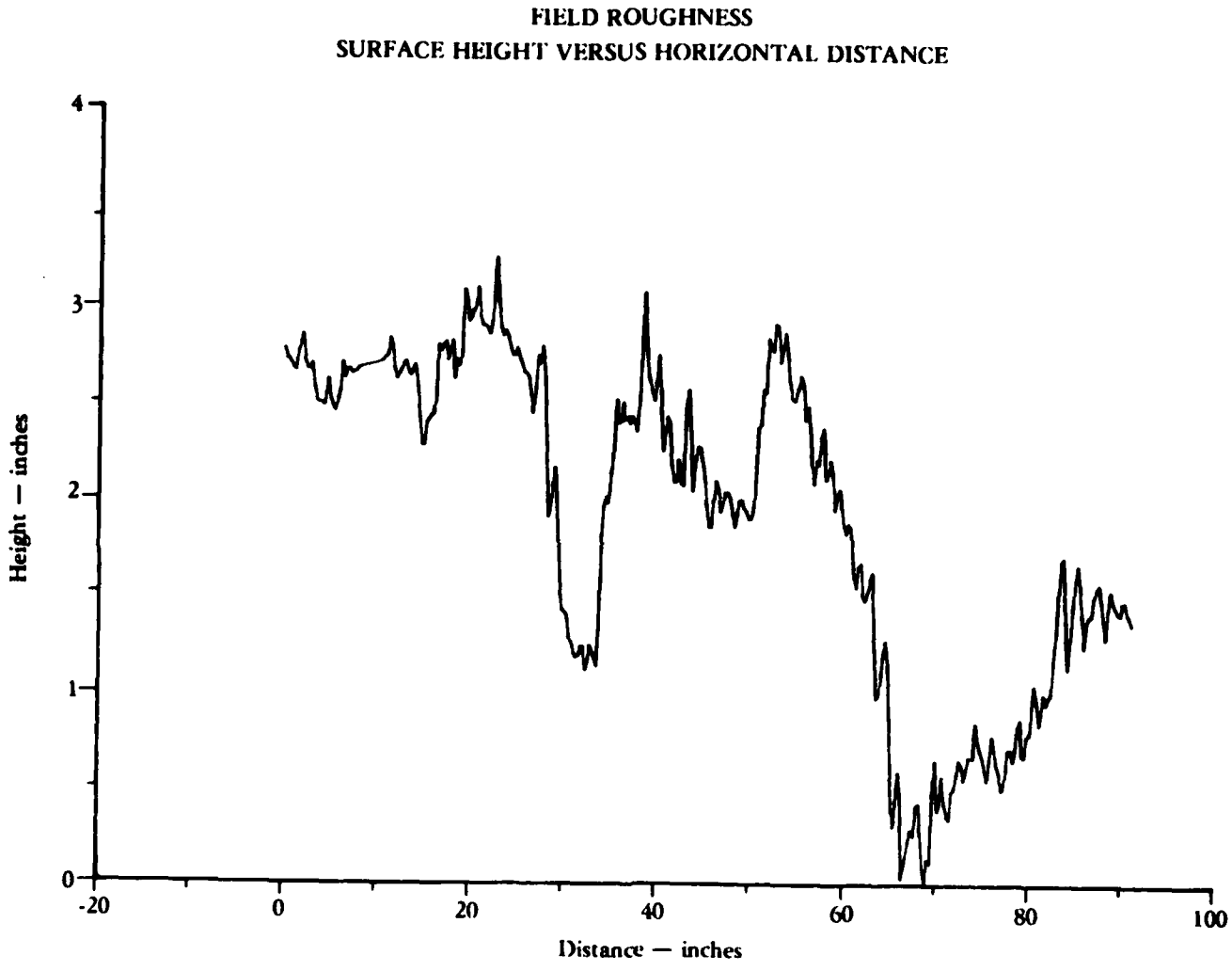

Figure A-18. Roughness Plot From Grass Field Designated F, North of Peconic River Airport

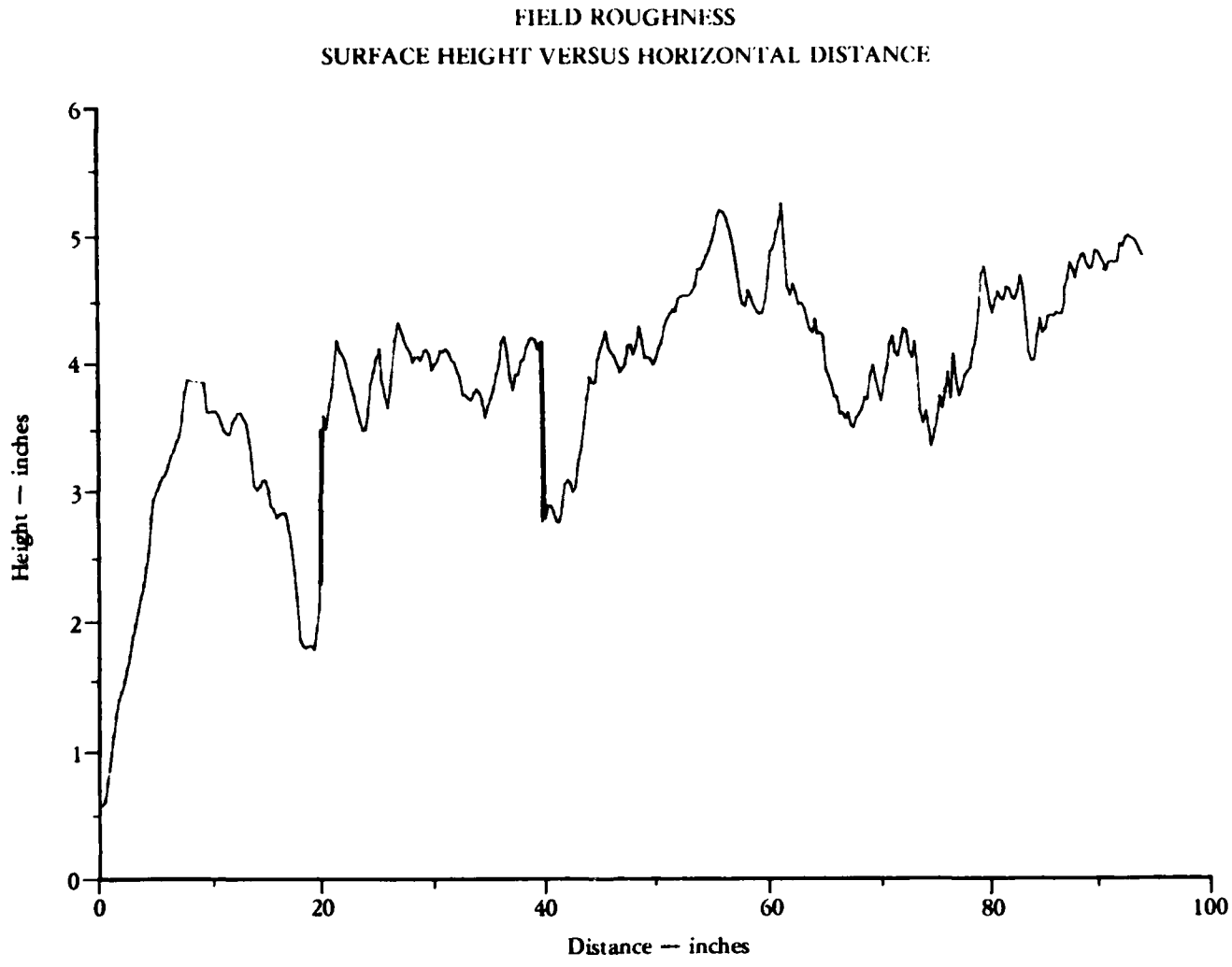

Figure A-19. Roughness Plot From Cut Corn Field Designated Field H, East of Field F

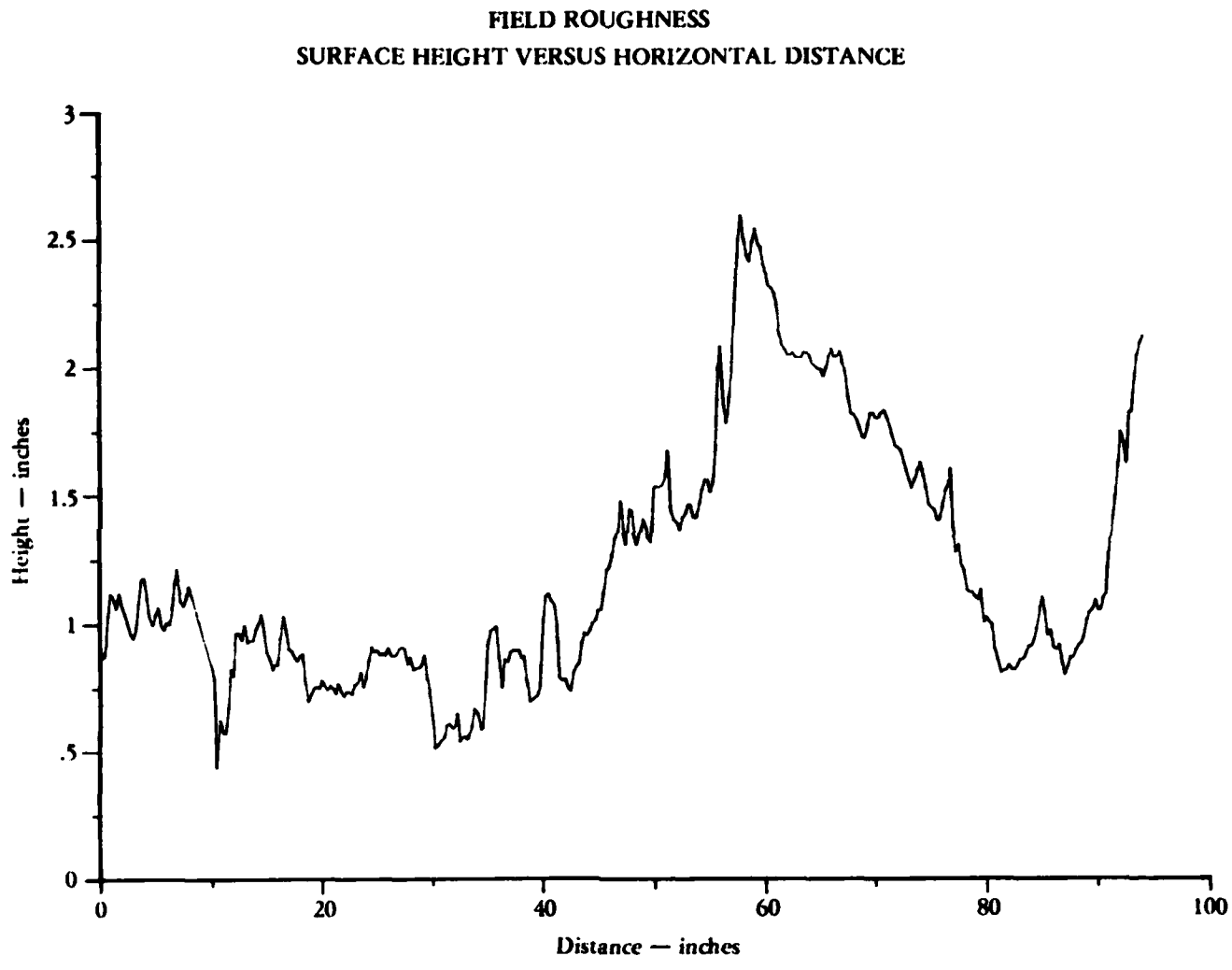

Figure A-20. Second Roughness Plot From Field H, East of Field E

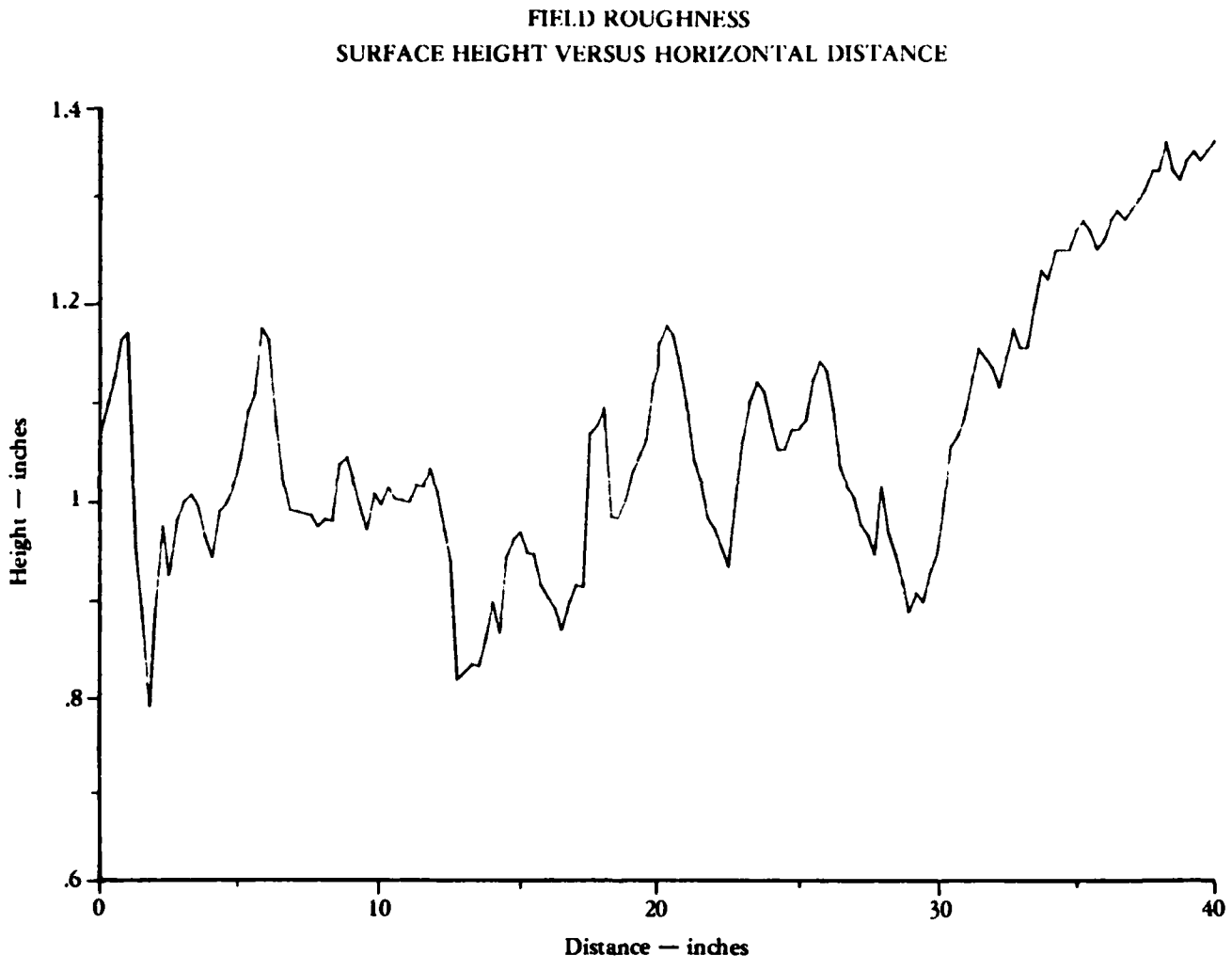

Figure A-21. Plot From Smooth Field Designated Field M, West of Peconic River Airport - Roughness Measurement Taken Along East-West Line

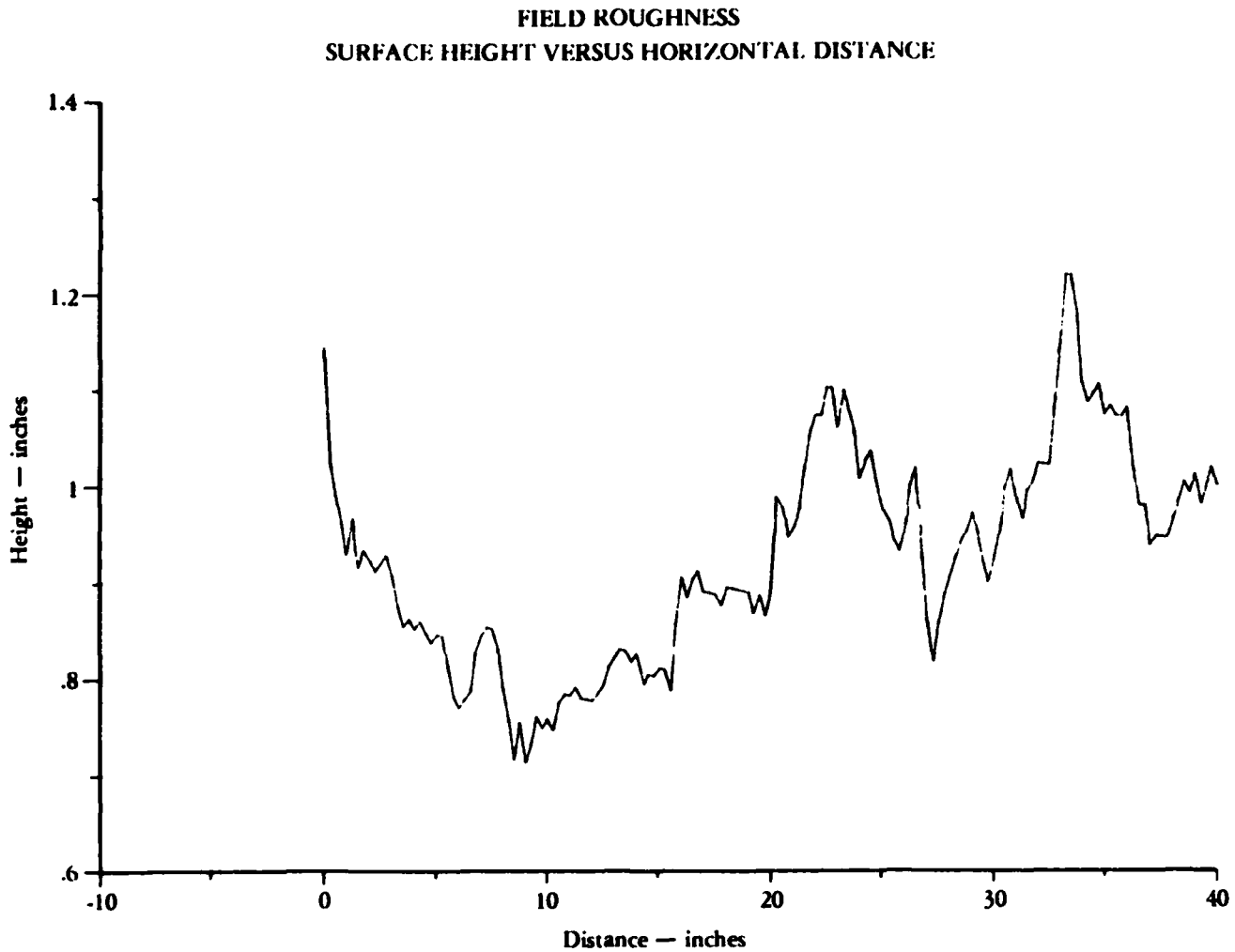

Figure A-22. Roughness Plot From Smooth Field M, Along North-South Line

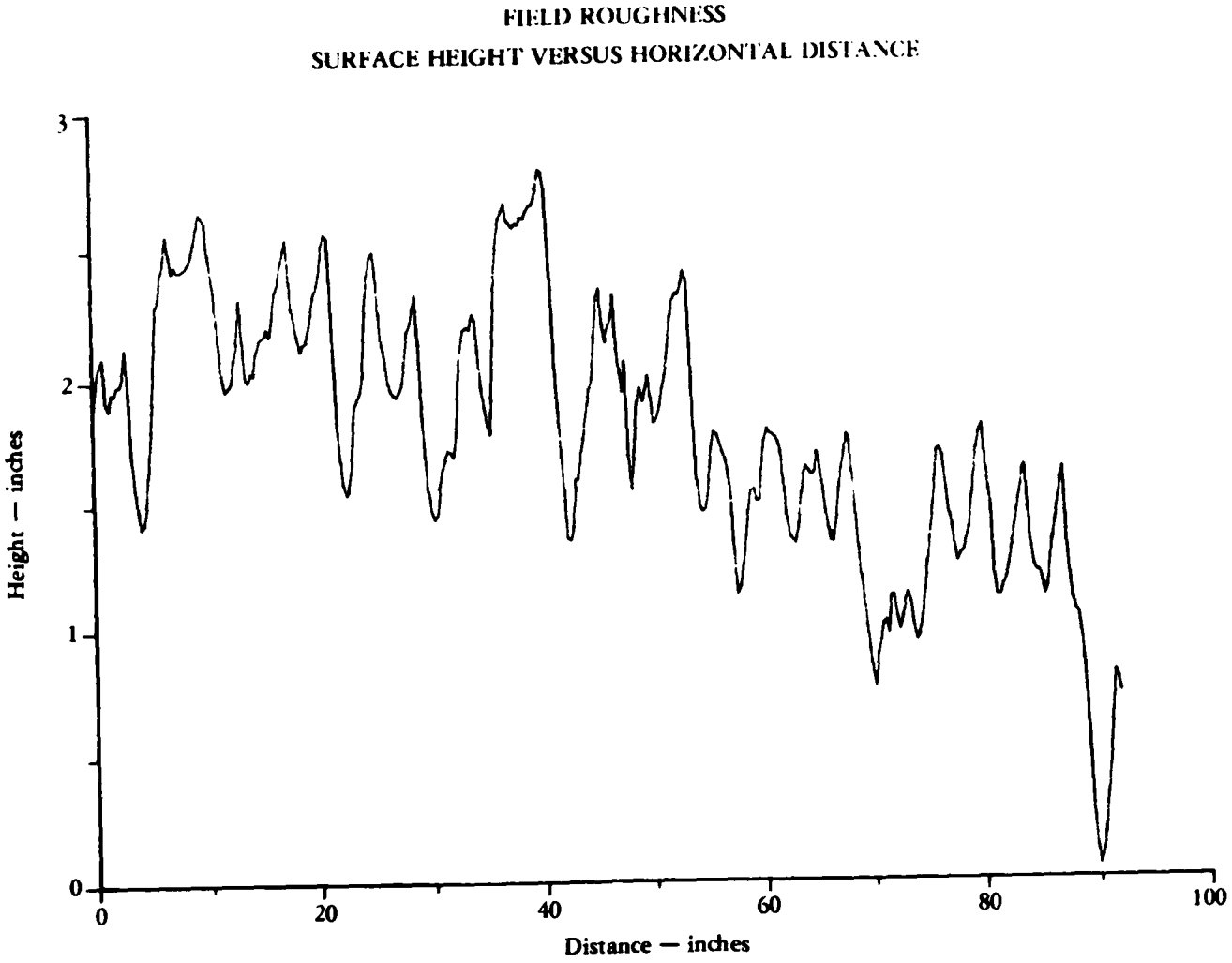

Figure A-23. Roughness Plot From Smooth Field Designated N, East of Peconic River Airport on Middle Country Road

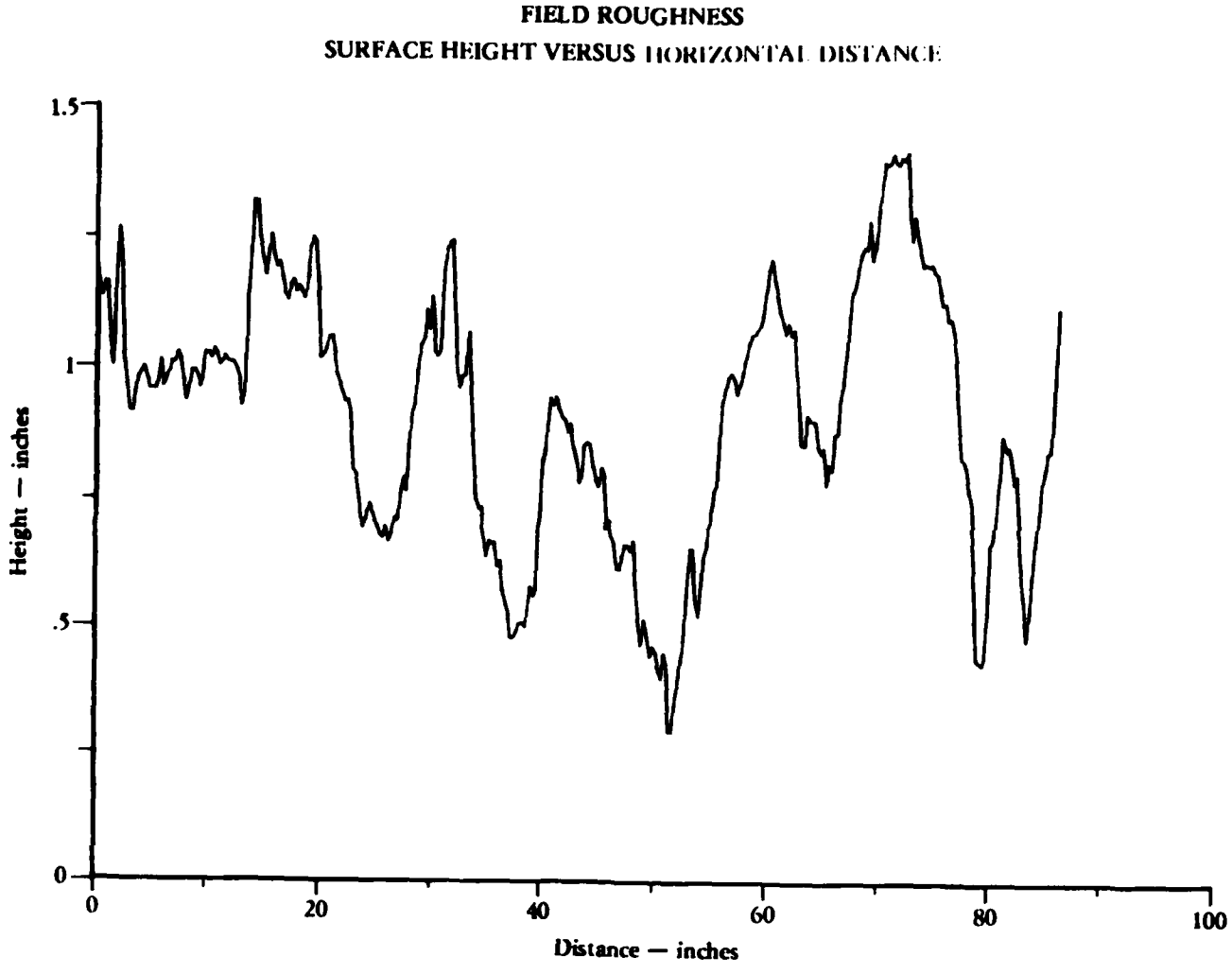

Figure A-24. Roughness Plot From Grass Field Designated K, North of Peconic River Airport Near VOR Location

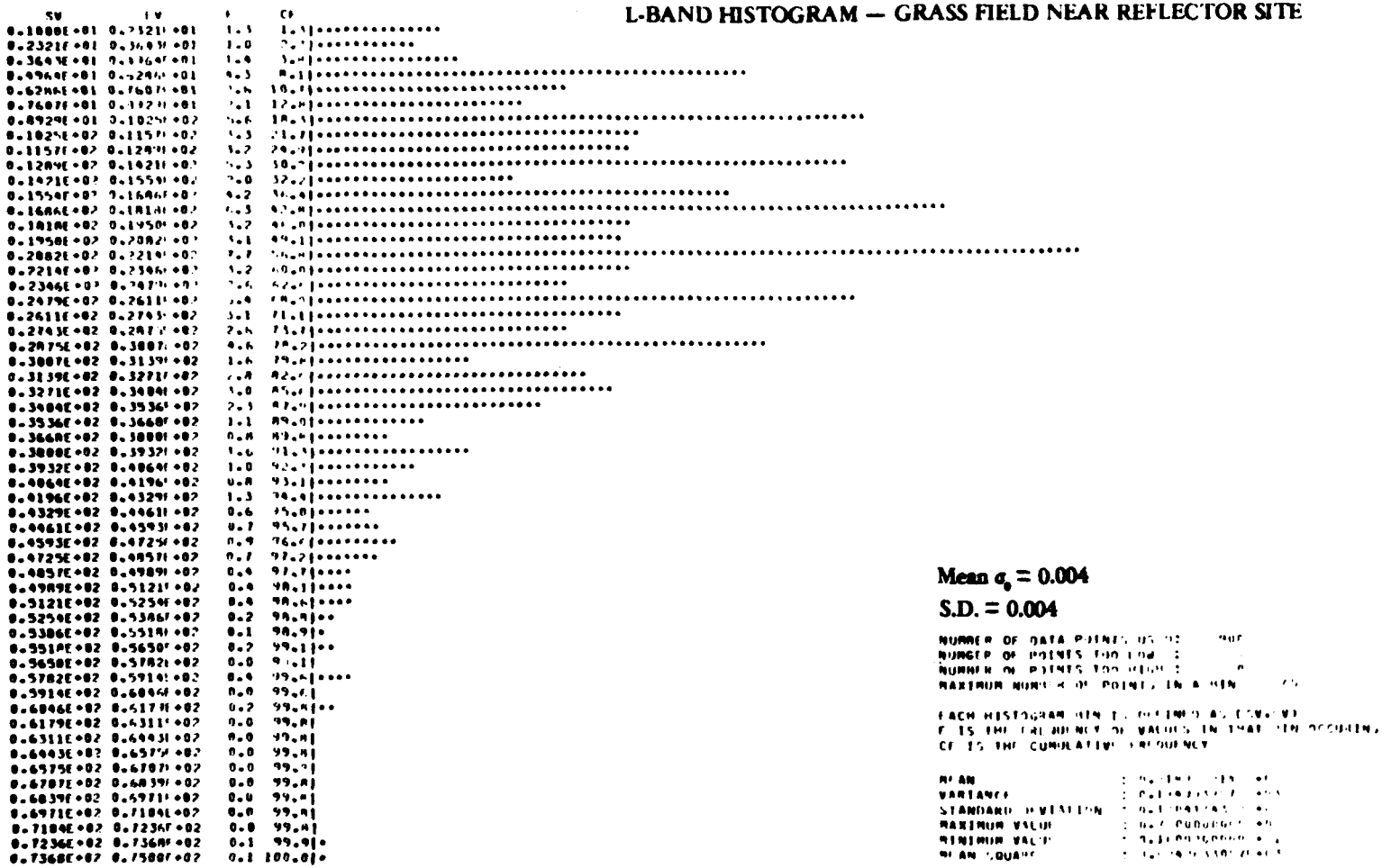

Figure A-25. L-band Histograms of Calibrated σ_O Values From Test Fields

Figure A-26. L-band Histograms of Calibrated σ_O Values From Test Fields

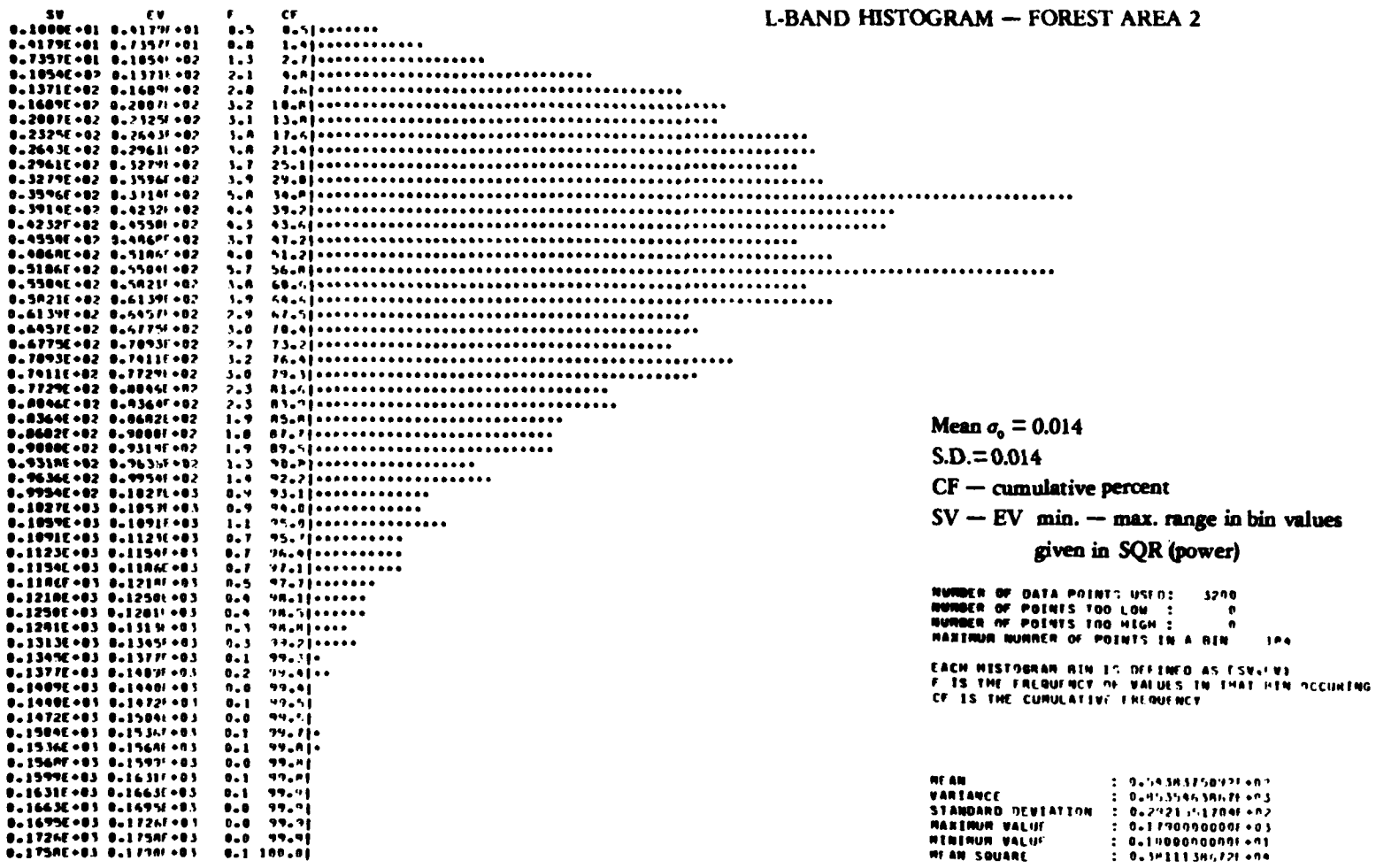

Figure A-27. L-band Histograms of Calibrated σ_0 Values From Test Fields

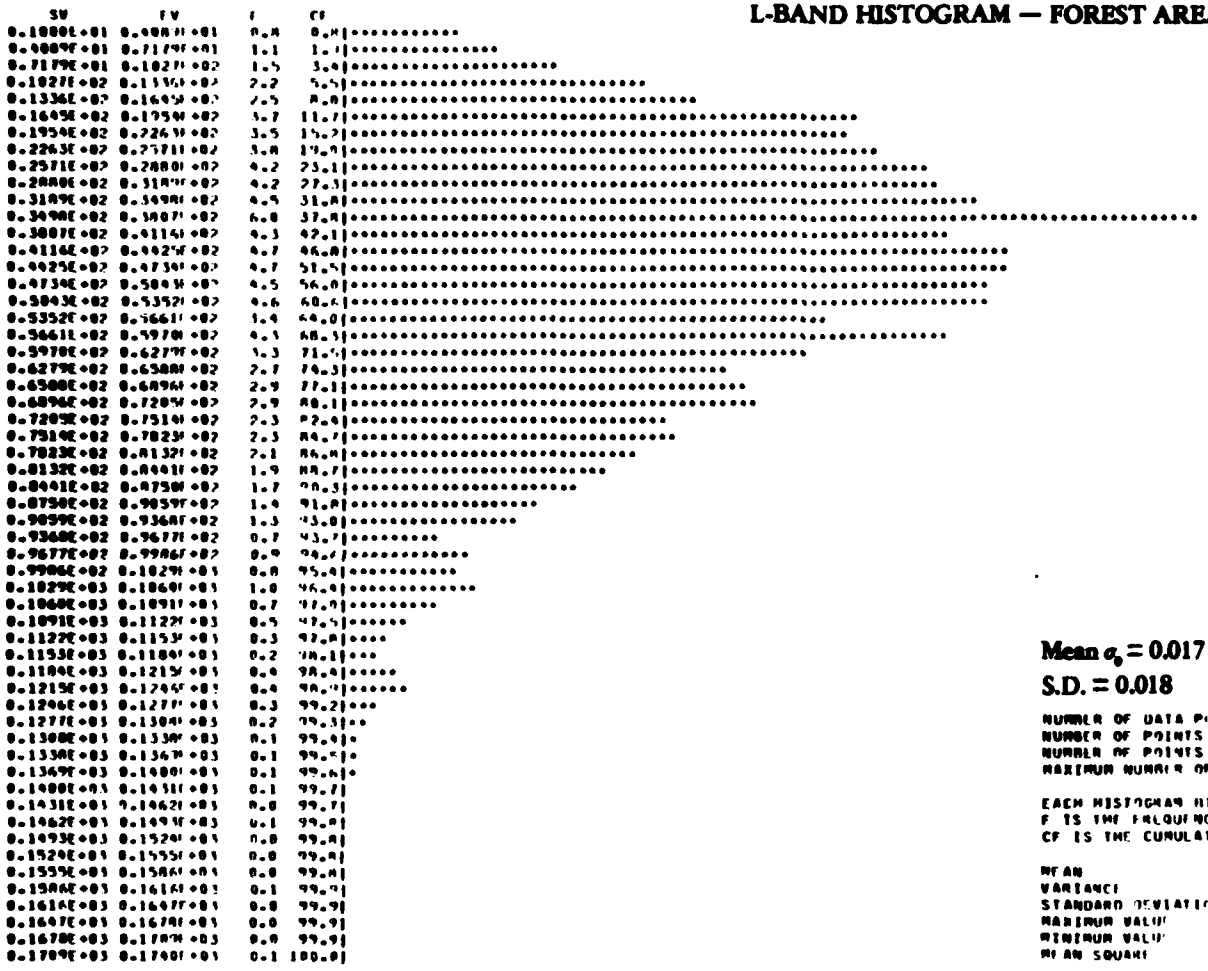

Figure A-28. L-band Histograms of Calibrated σ_o Values From Test Fields

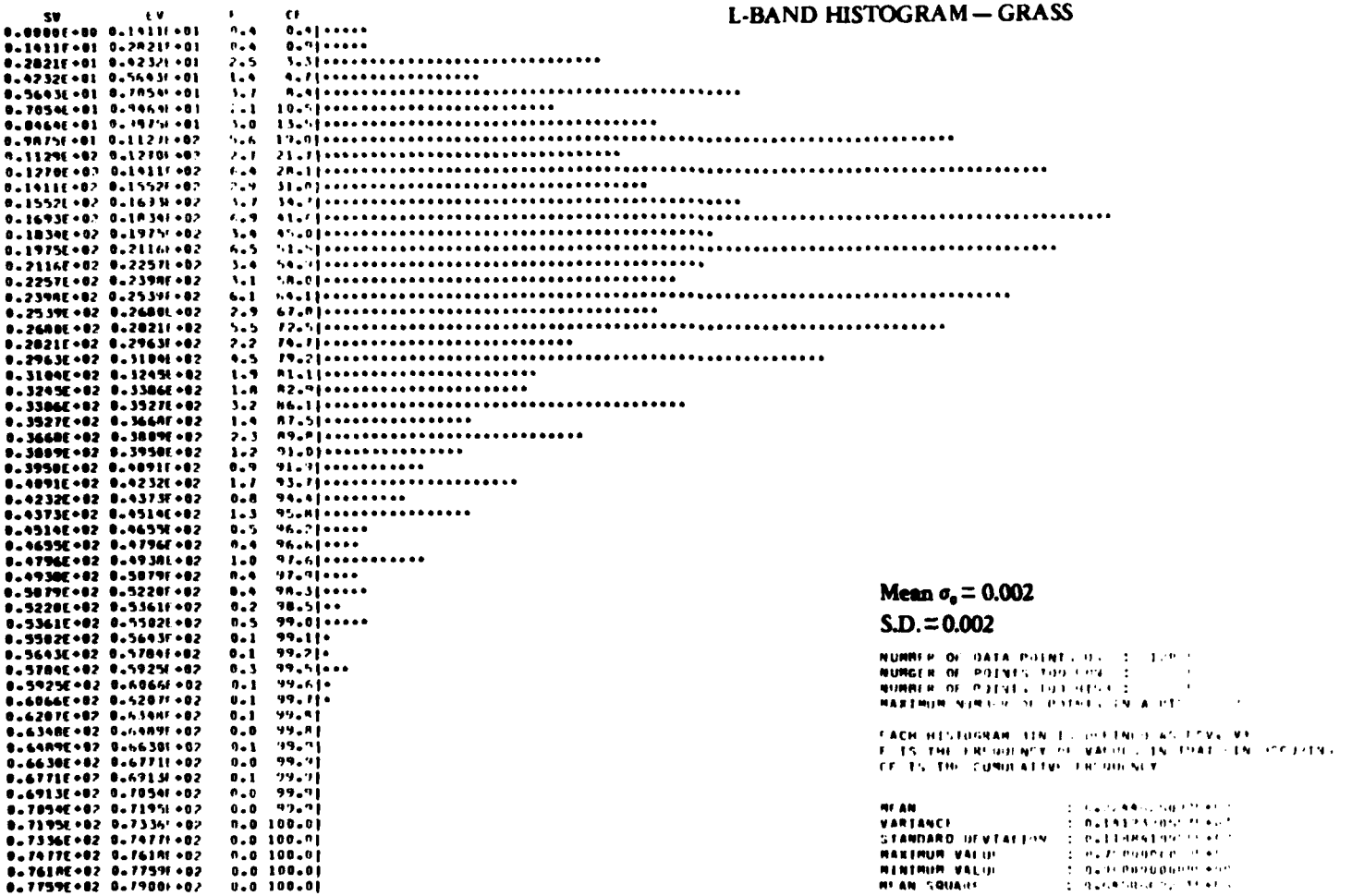

Figure A-29. L-band Histograms of Calibrated σ_0 Values From Test Fields

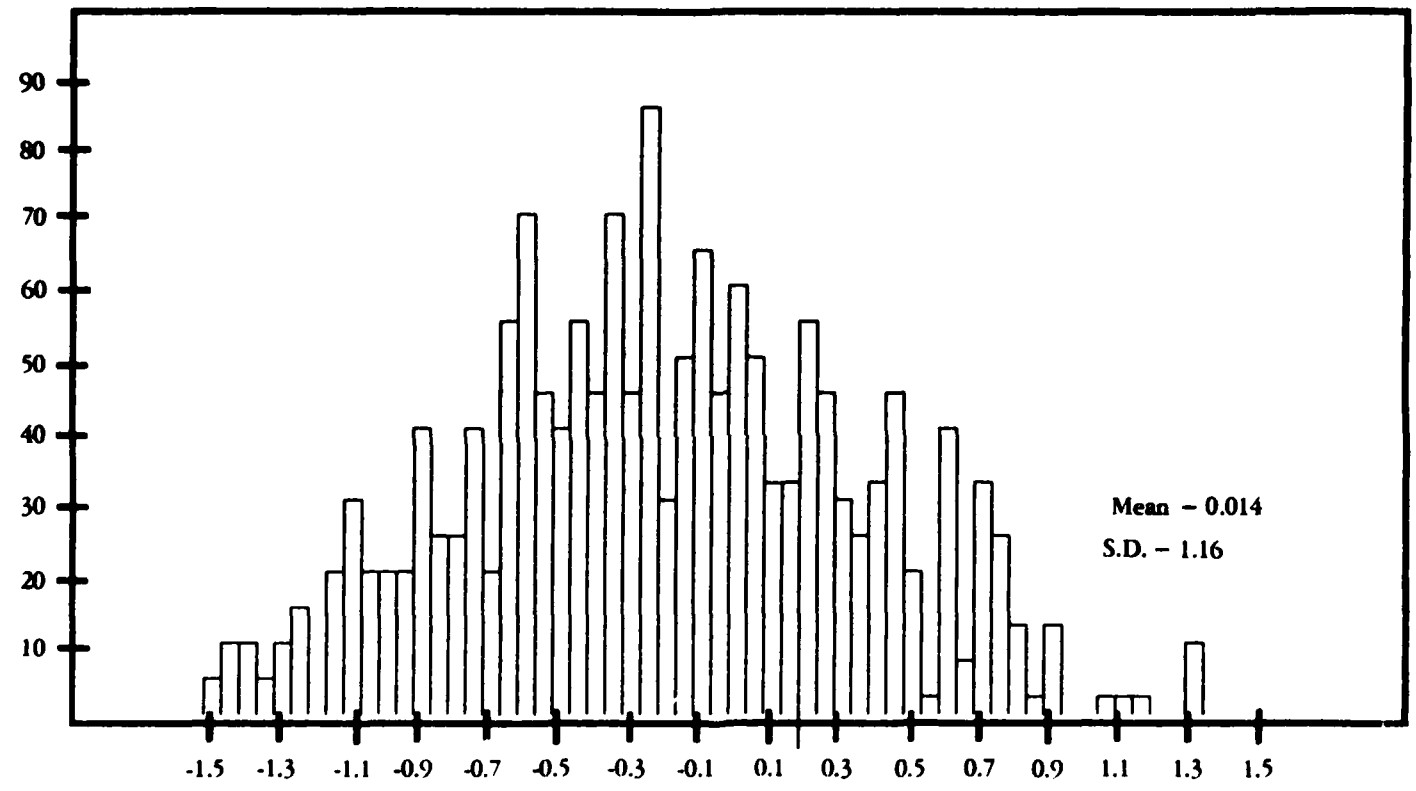

Figure A-30. Histogram of Surface Slope Field EG - Potatoe Field E, North of Peconic River Airport

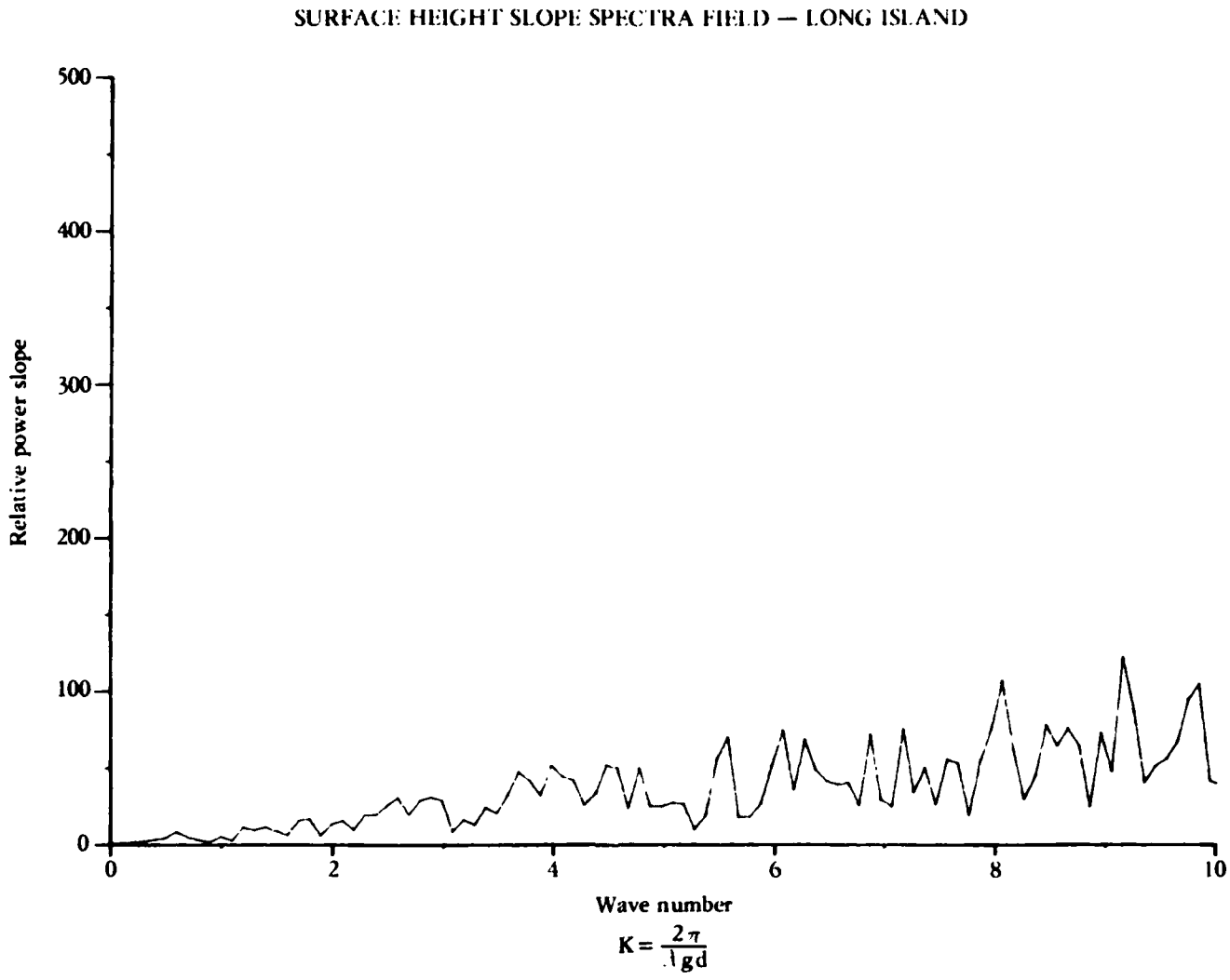

Figure A-33. Field H - Cut Corn, North of Peconic River Airport

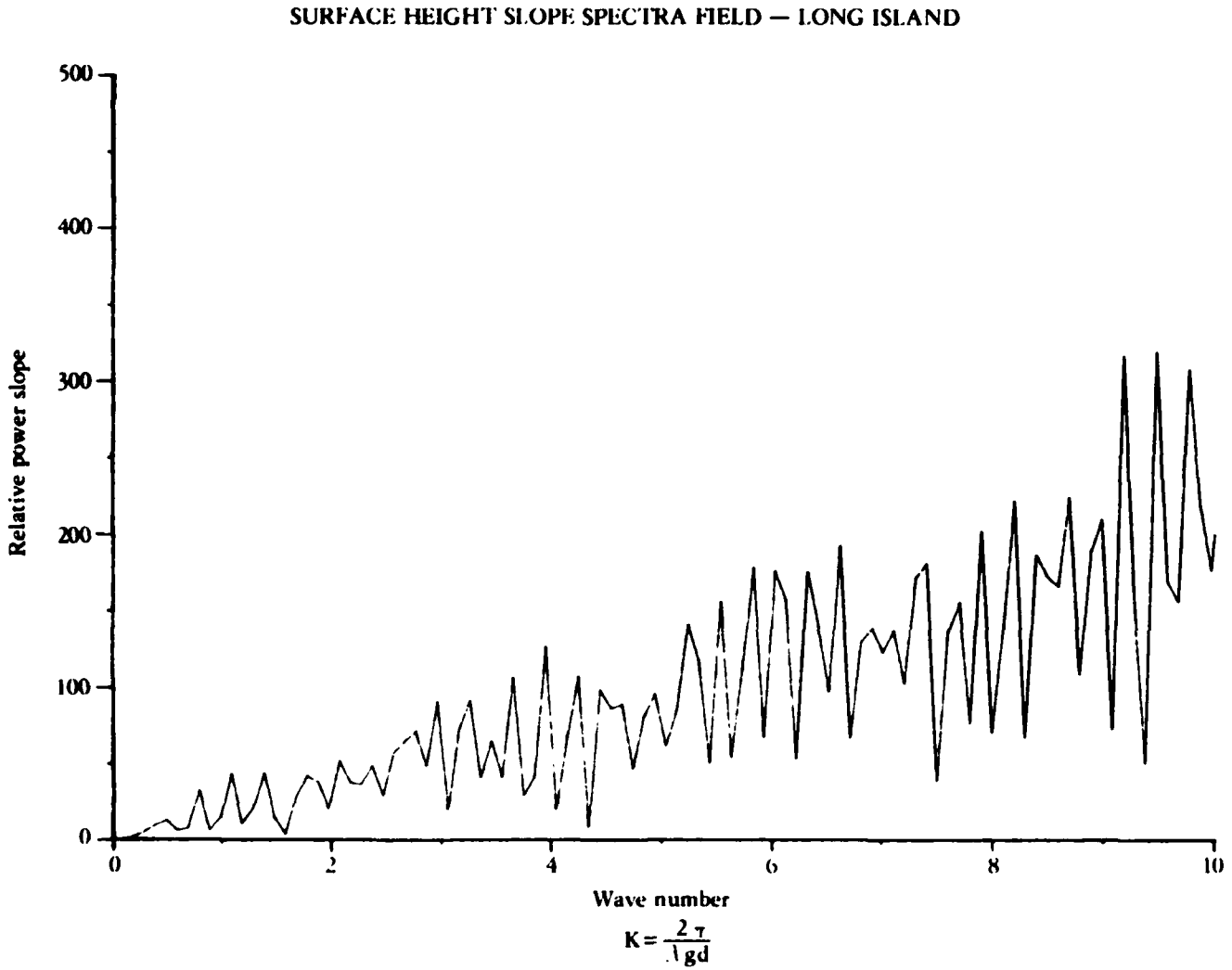

Figure A-34. Field H - Cut Corn, North of Peconic River Airport

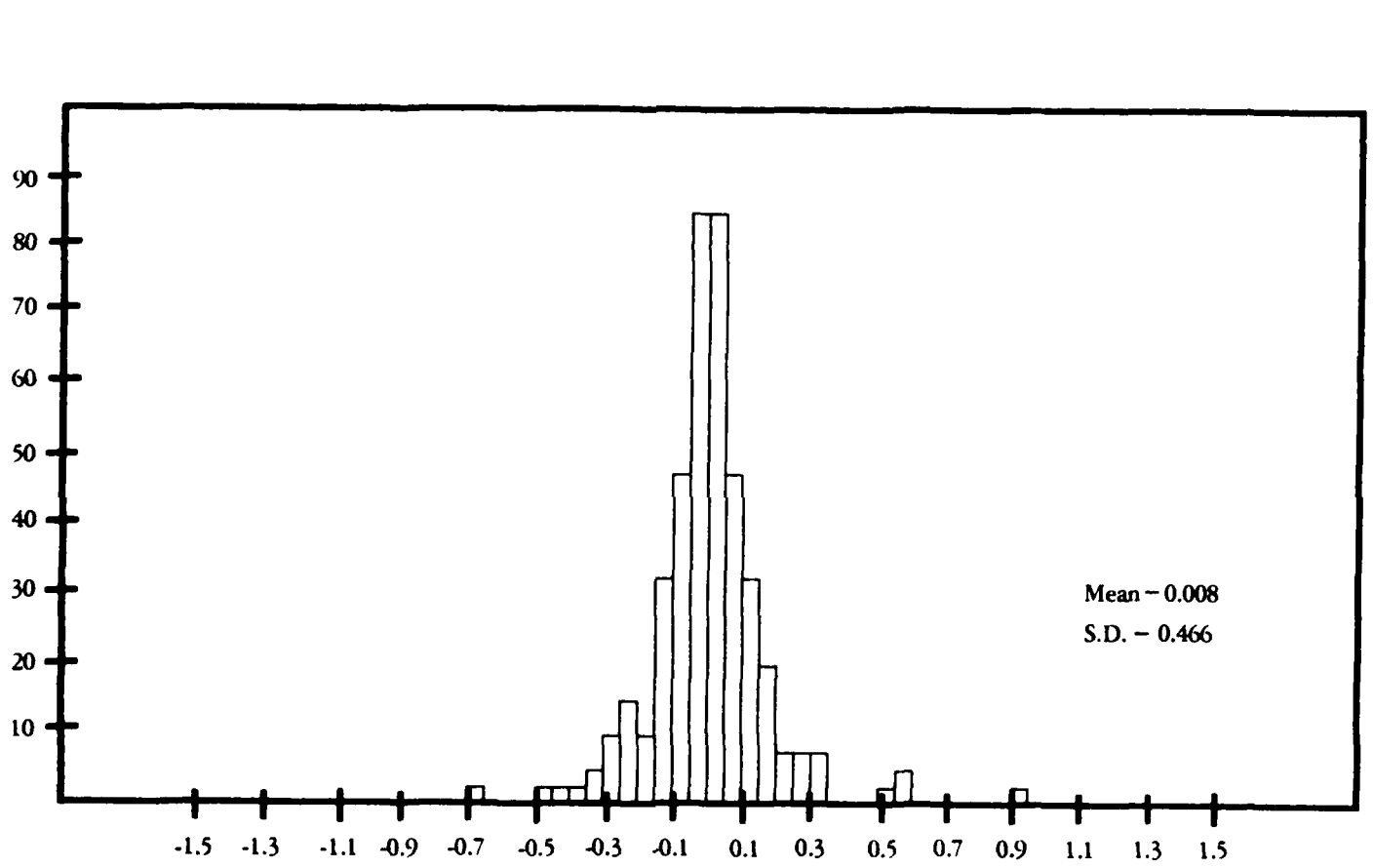

Figure A-31. Reflector Field RFS3R Grass Field Near Reflector Site 3, Peconic River Airport

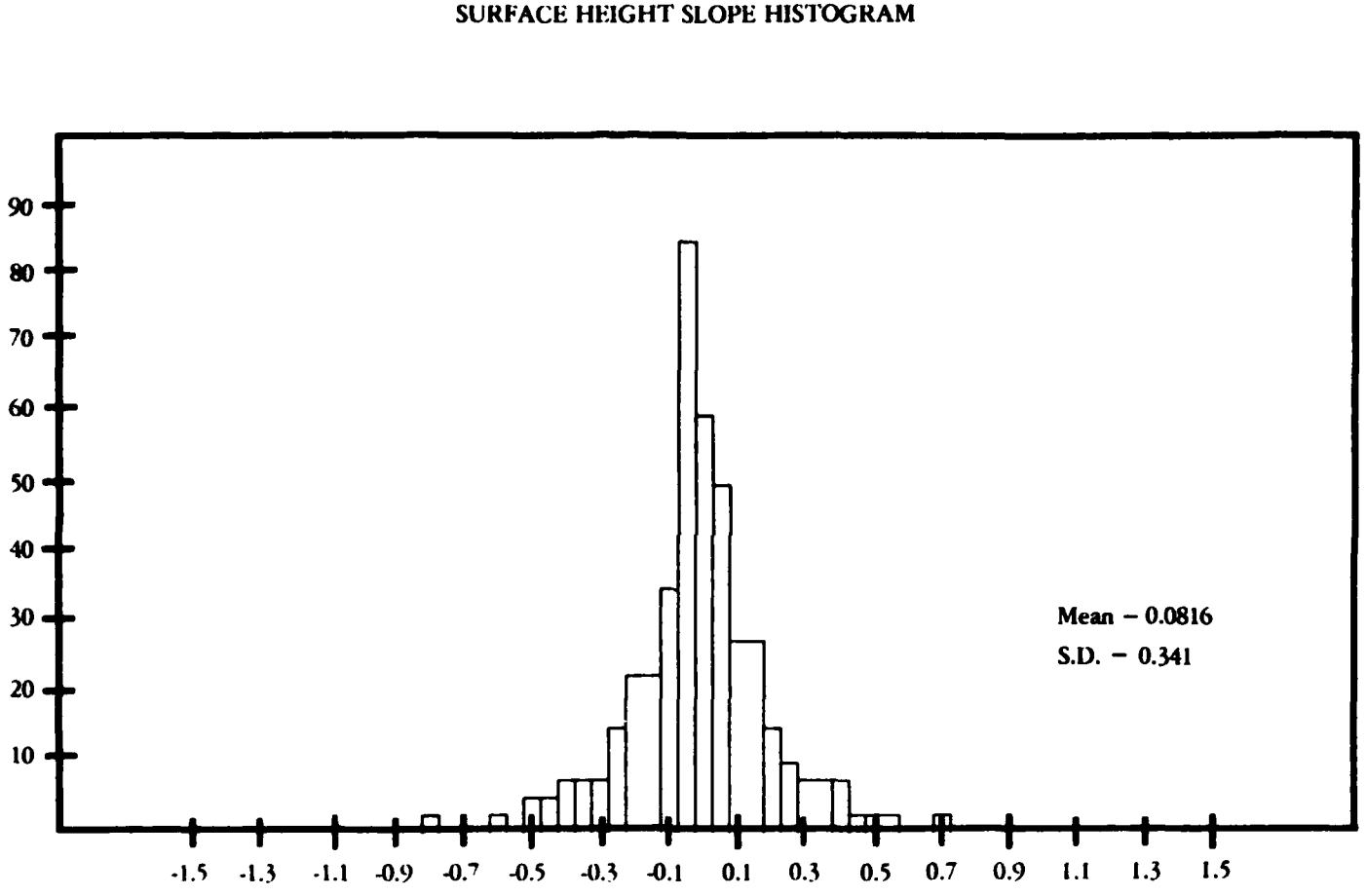

Figure A-32. Reflector Field RFS2 Grass Field Near Reflector Site 2, Peconic River Airport

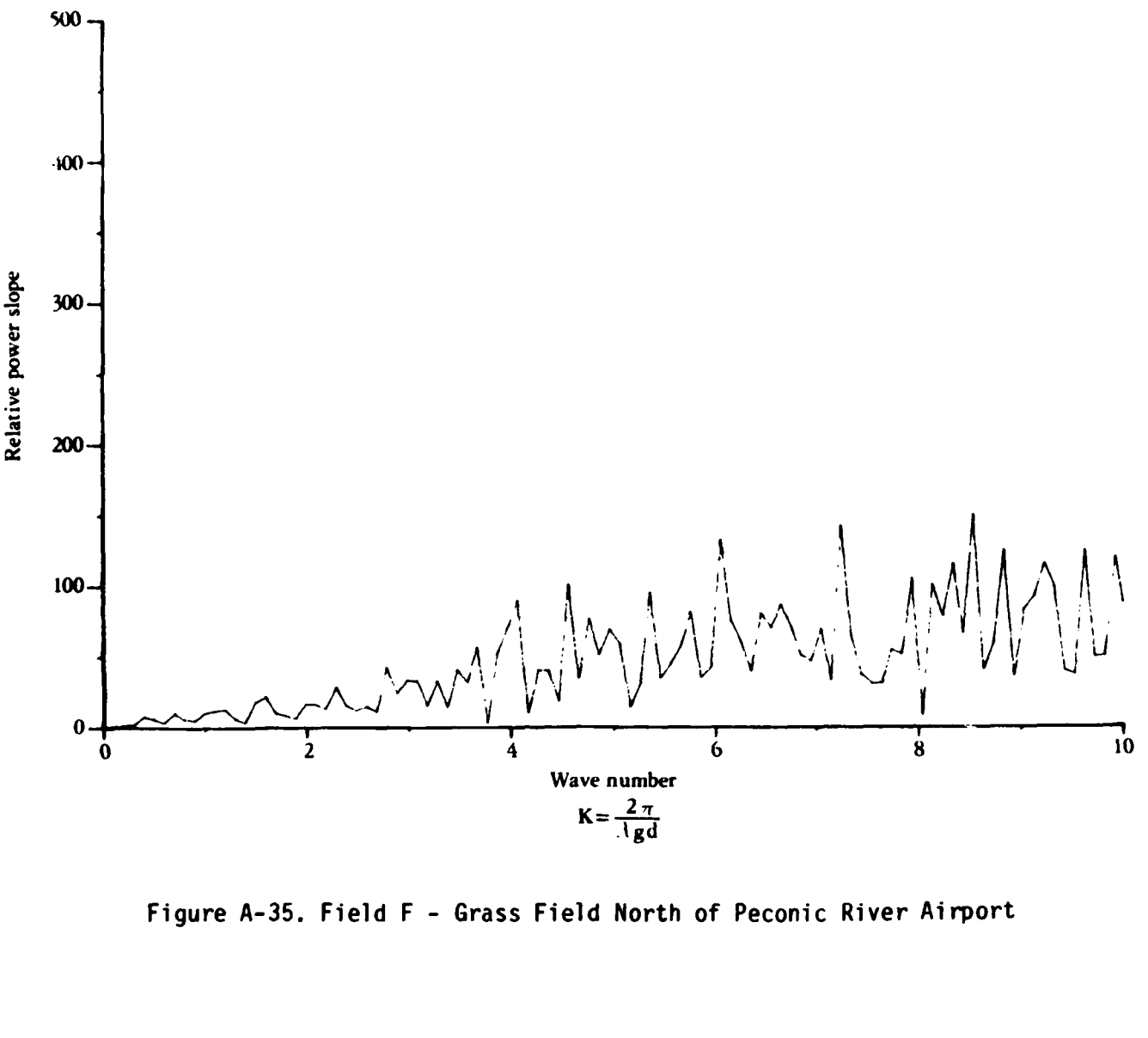

Figure A-35. Field F - Grass Field North of Peconic River Airport

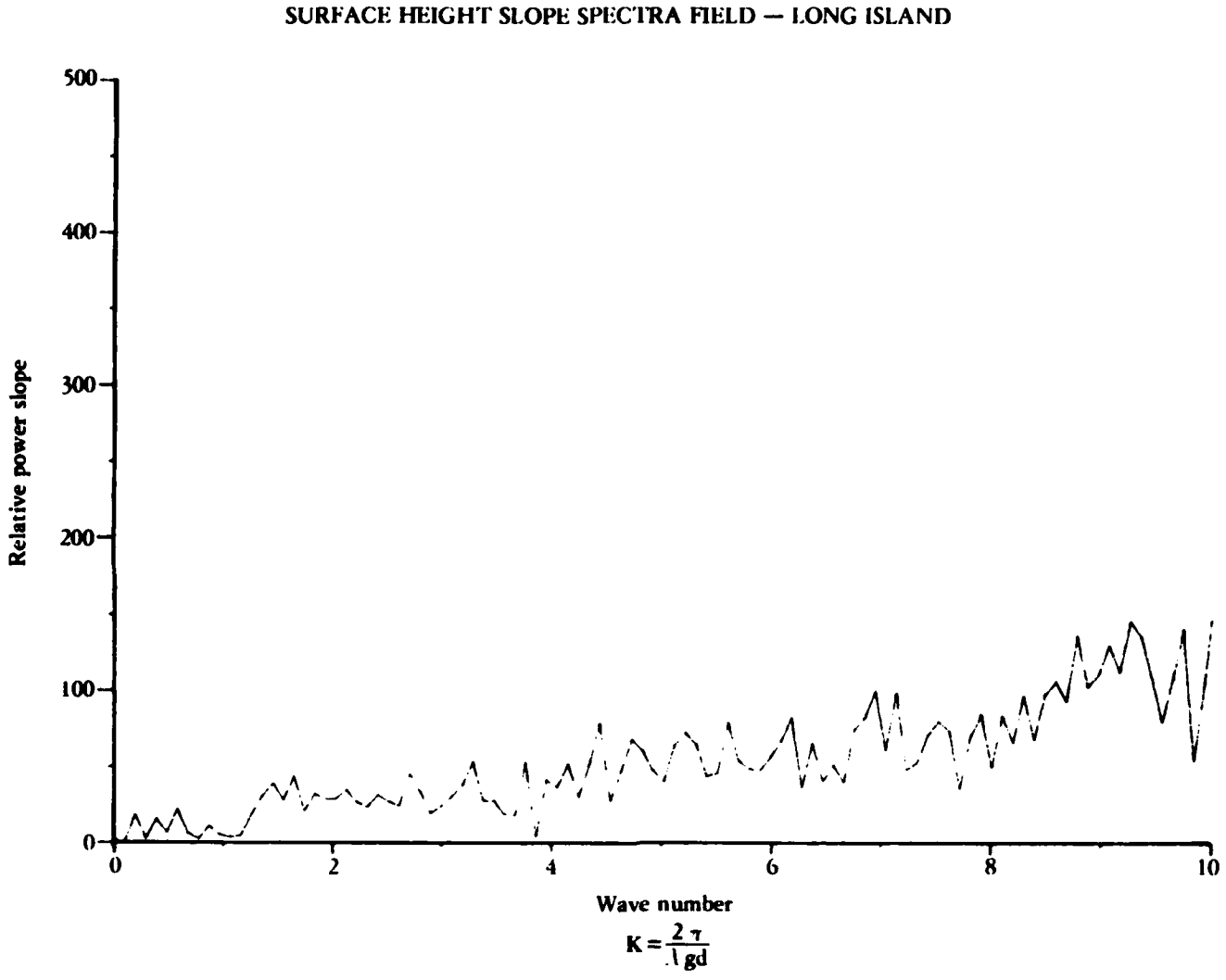

Figure A-36. Field E - Potato Field North of Peconic River Airport

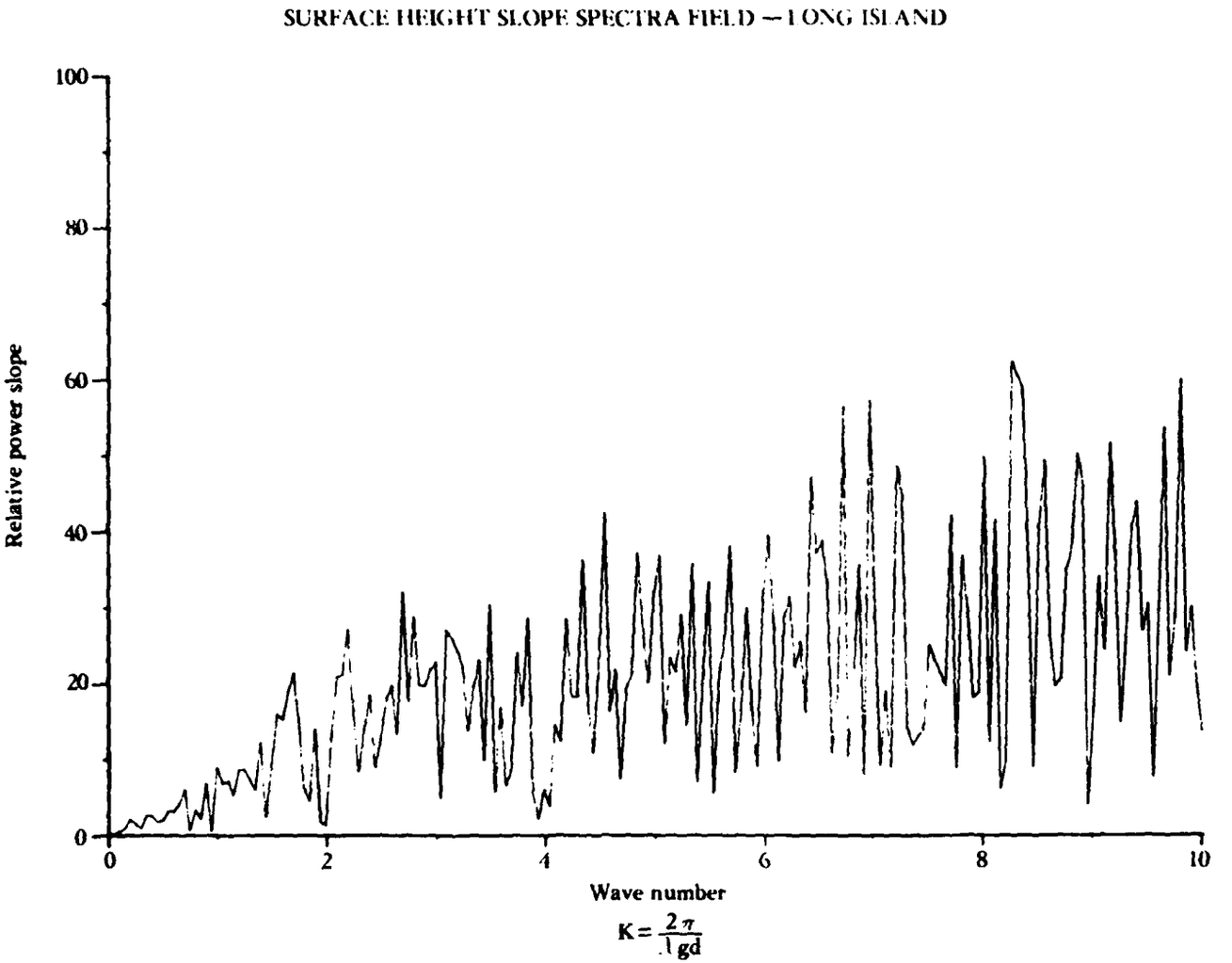

Figure A-37. Field RFS3, Grass Field Near Reflector Site 3, Peconic River Airport

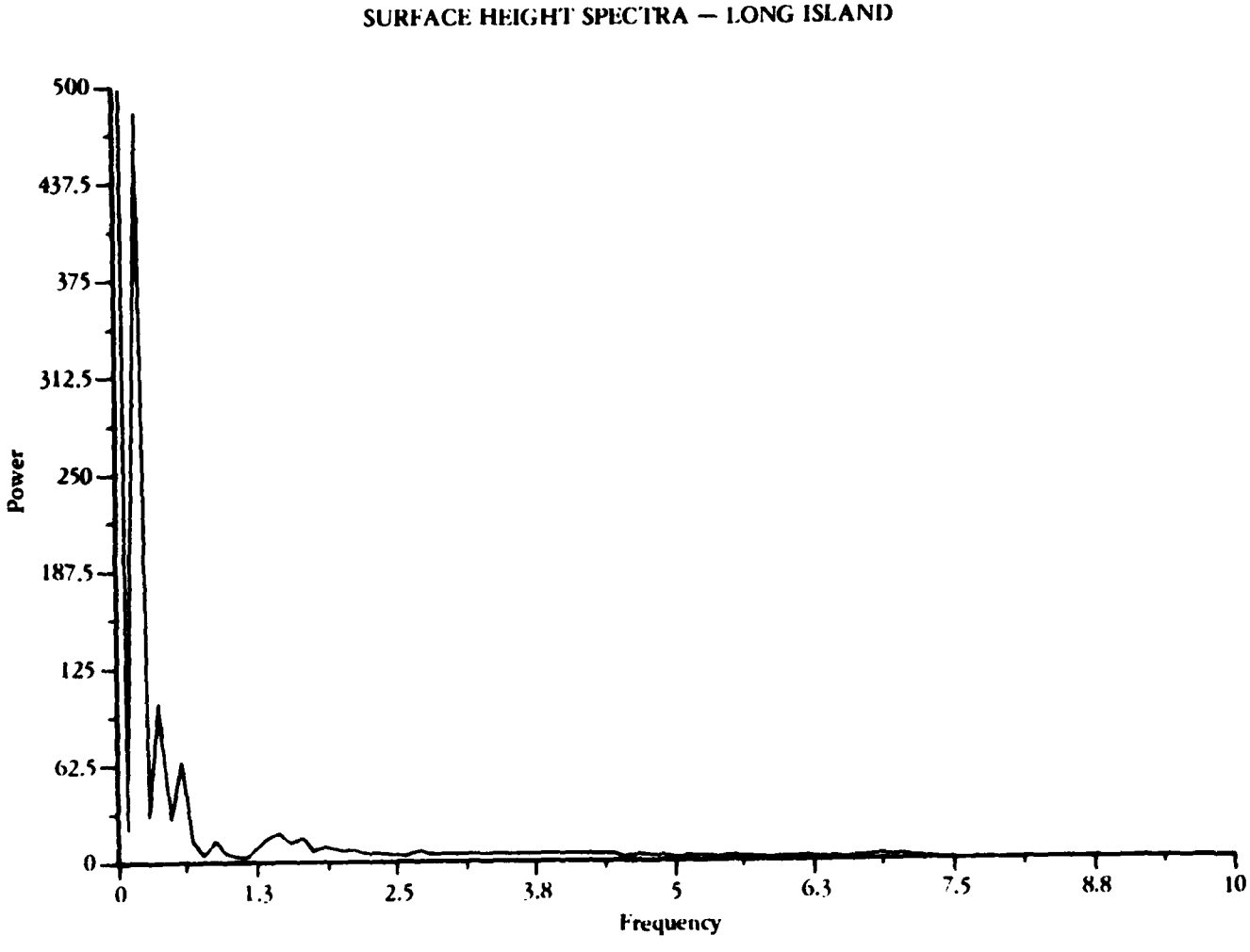

Figure A-38. Field E - Potato Field North of Peconic River Airport

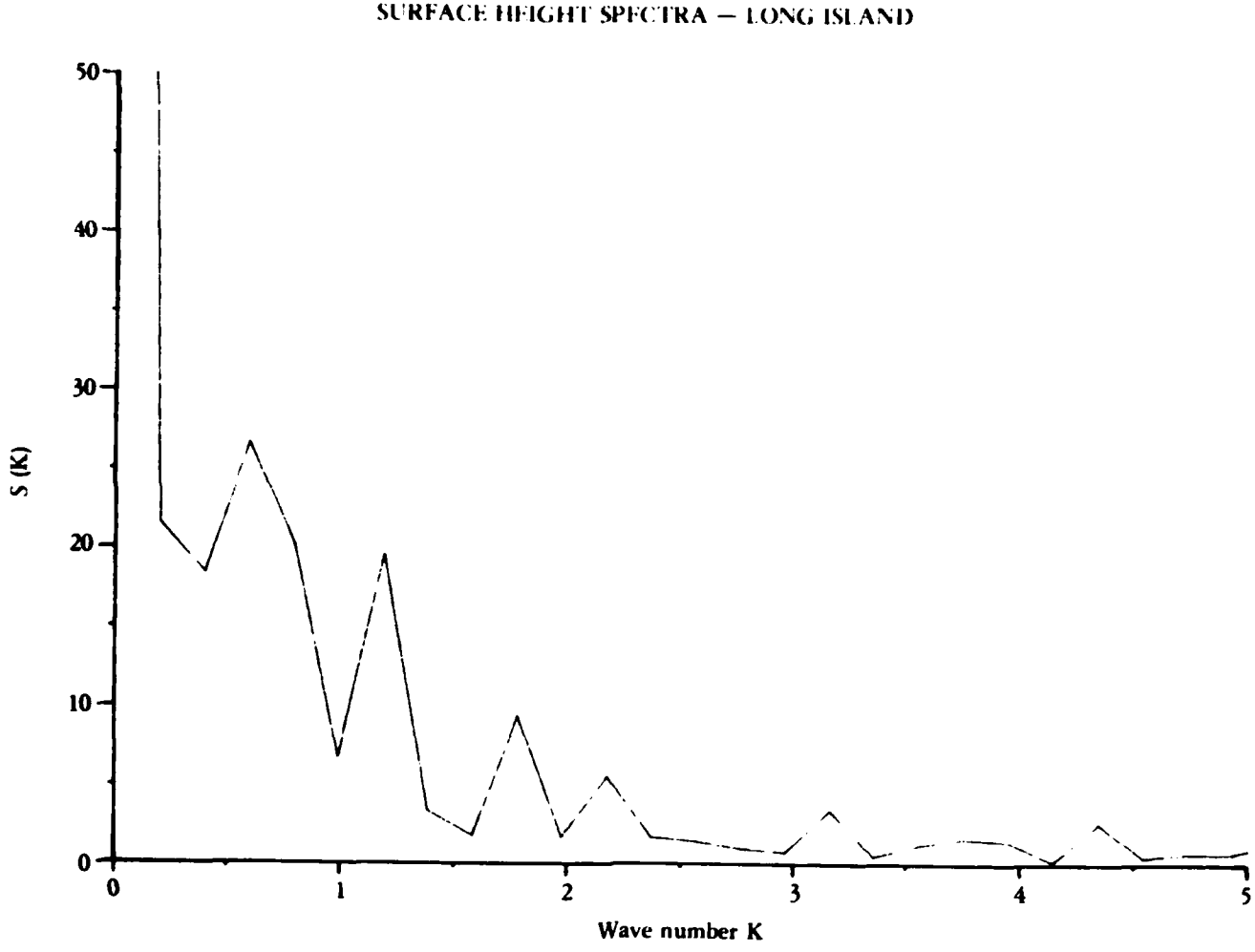

Figure A-39. Field E - Potato Field North of Peconic River Airport, Along Peak of Furrows

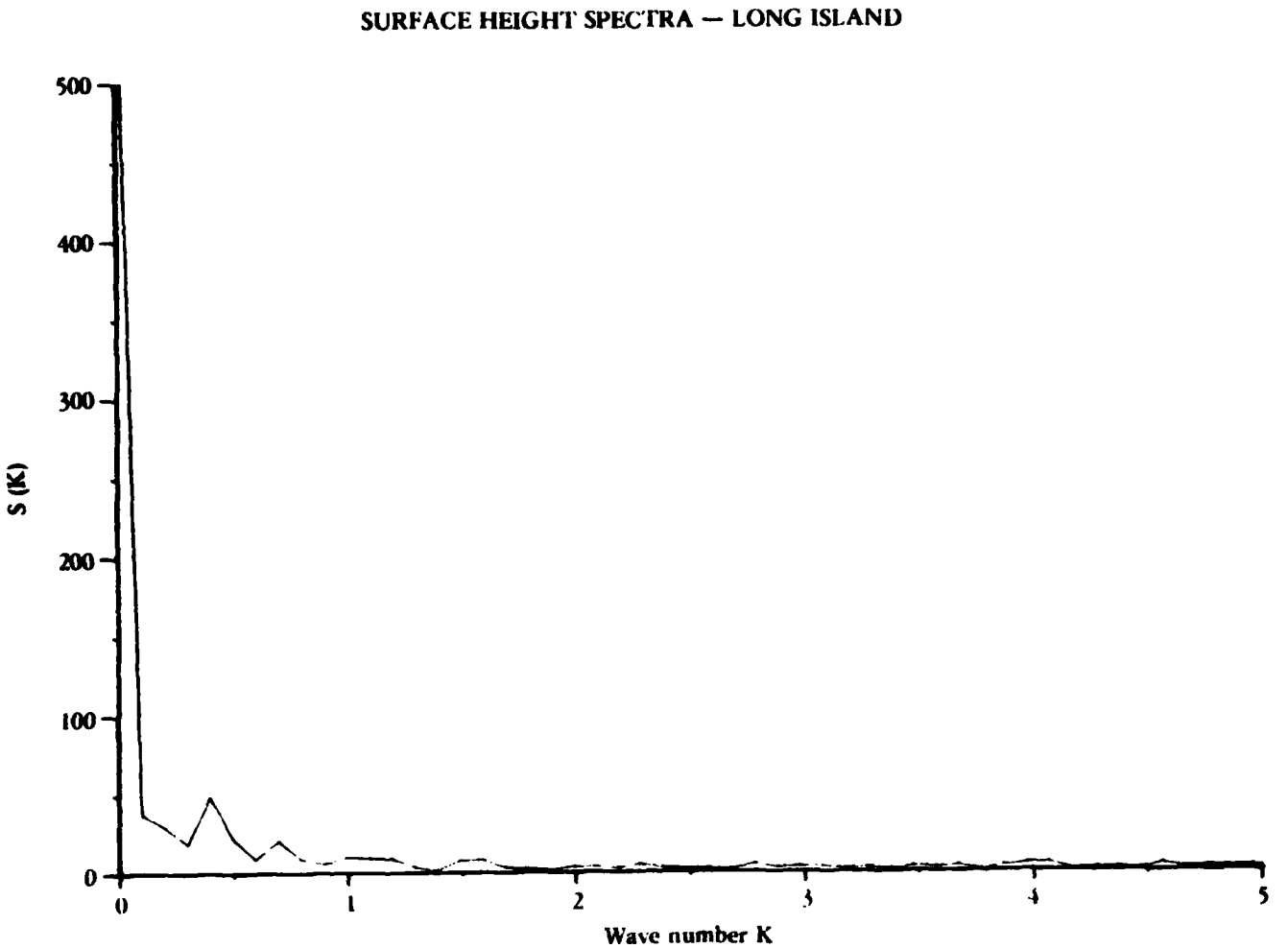

Figure A-40. Field F - Grass Field North of Peconic River Airport

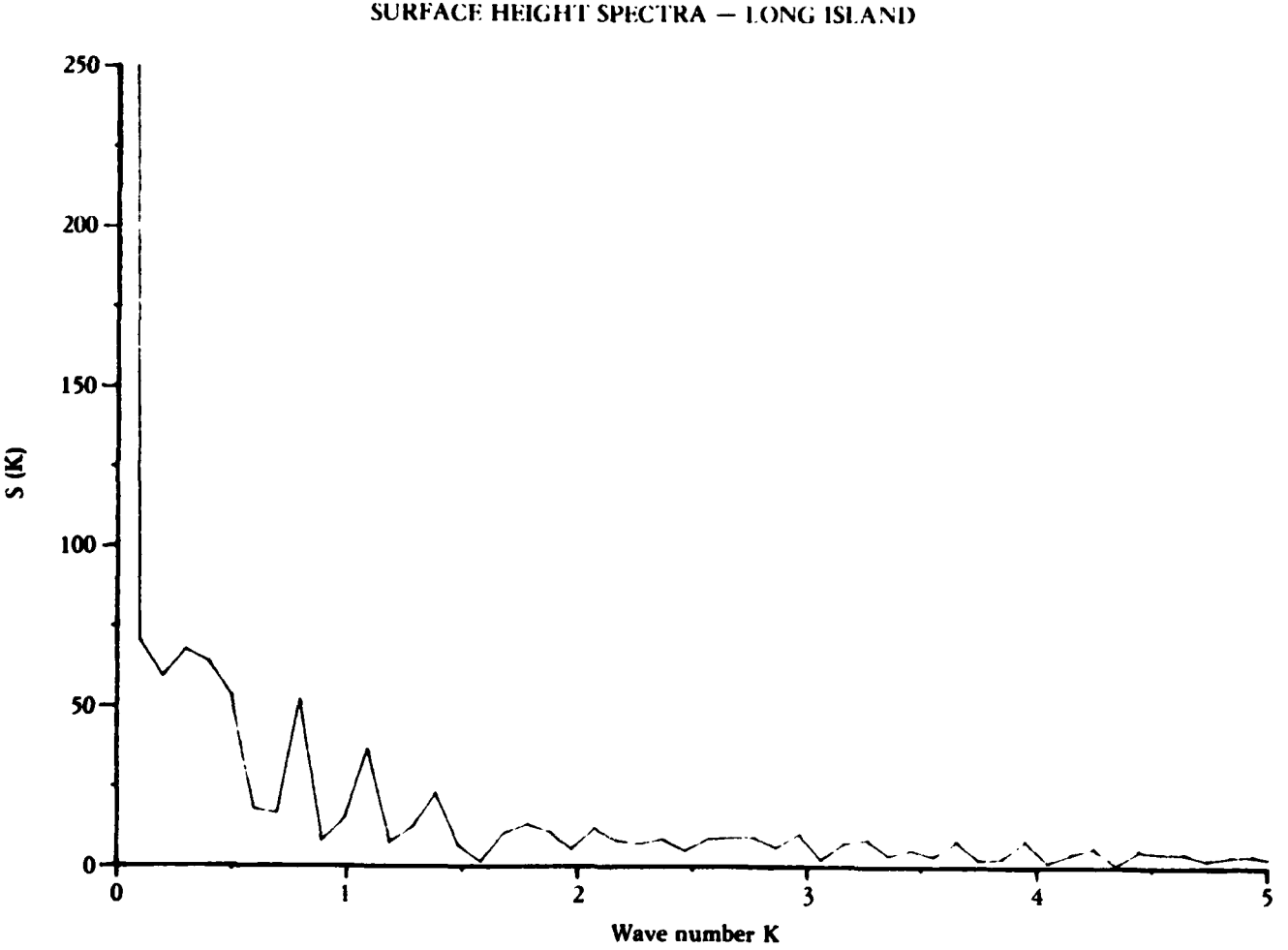

Figure A-41. Field H - Cut Corn, North of Peconic River Airport - E-W Line

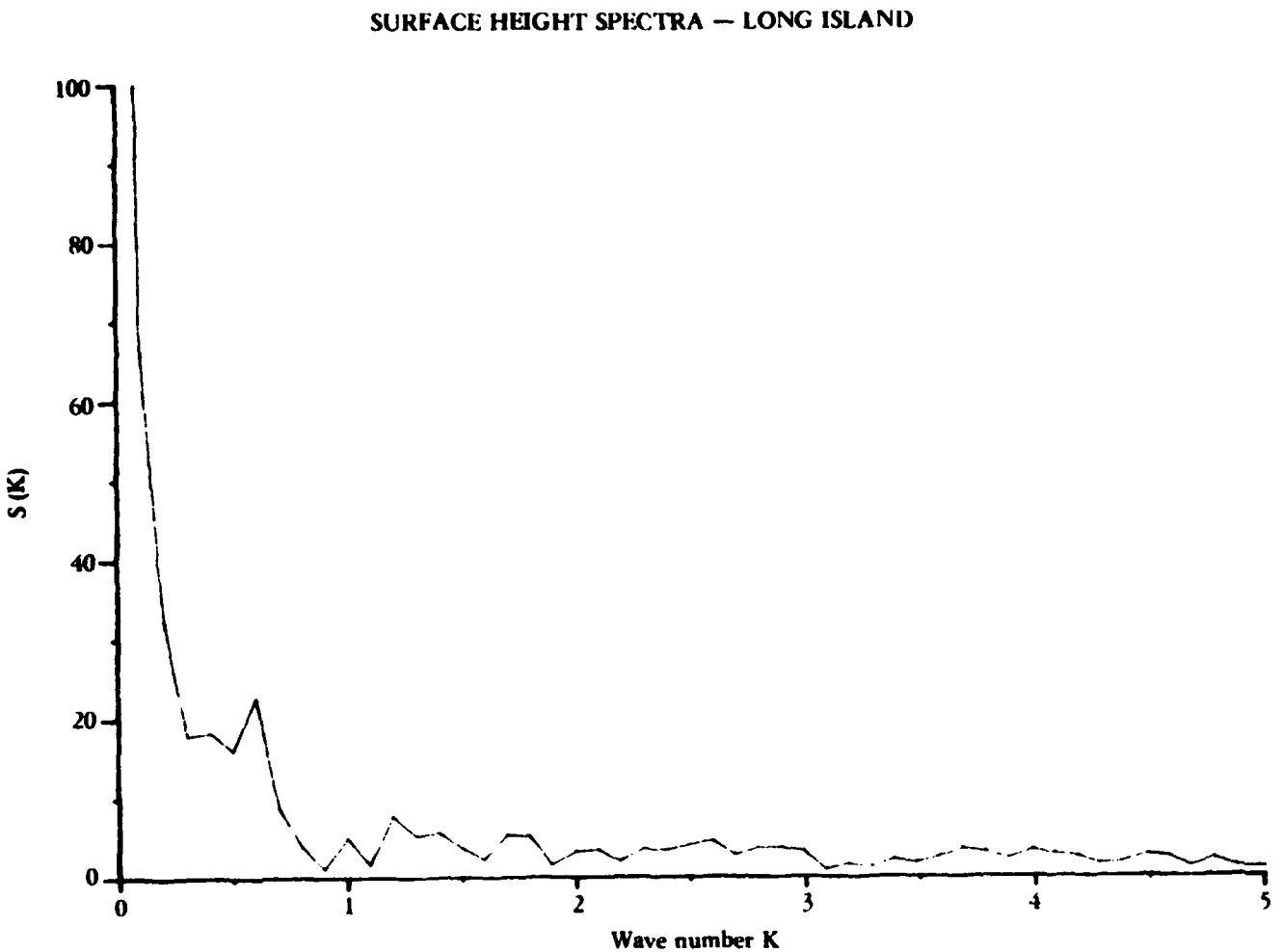

Figure A-42. Field H - Cut Corn, North of Peconic River Airport - N-S Line

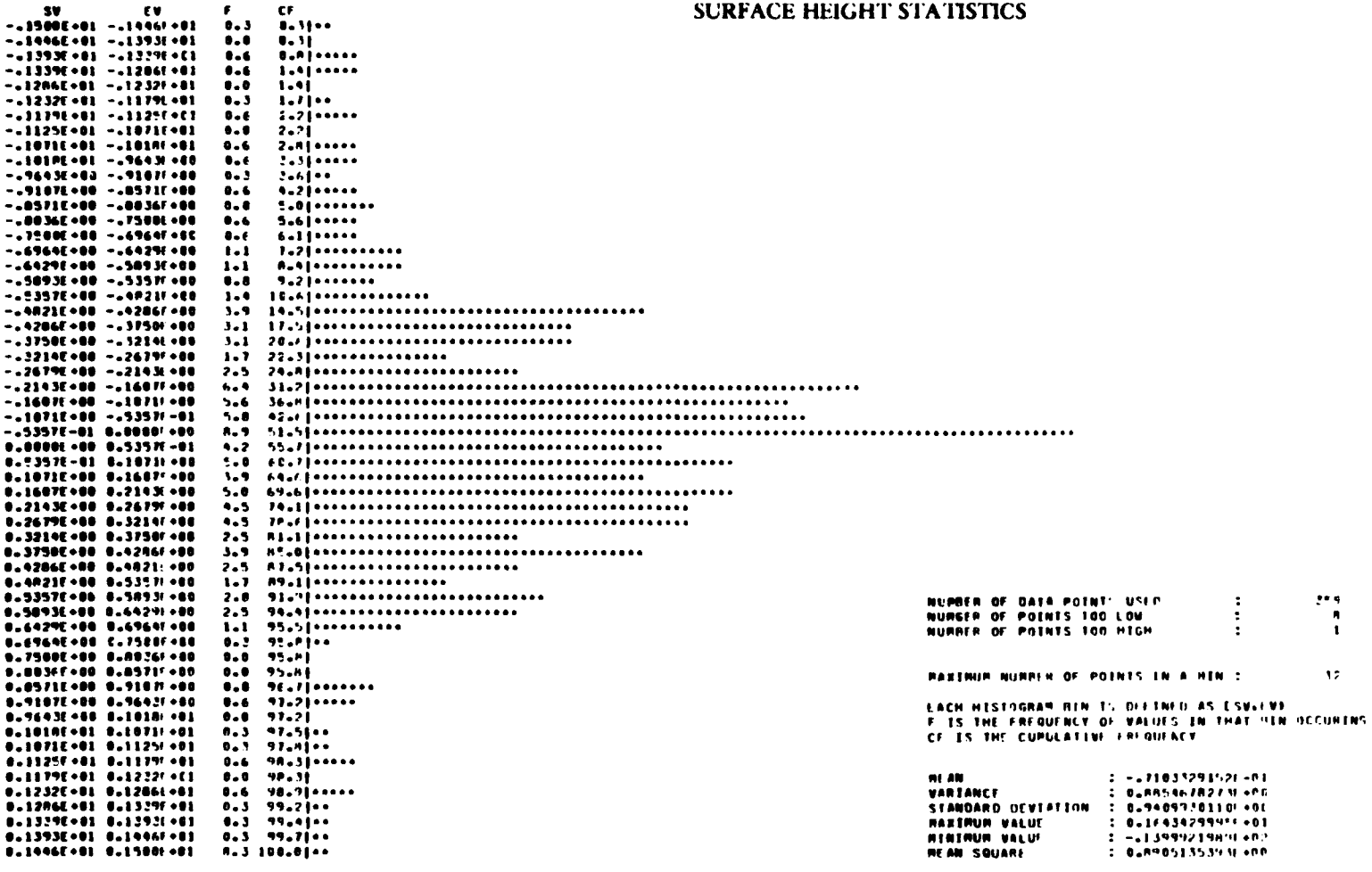

Figure A-43. Histogram of Surface Height - Grass Field F, Height Values Given In Inches

Figure A-44. Histogram of Surface Slope - Field E, Along Peak of Furrows

SURFACE HEIGHT STATISTICS
RADIUS OF CURVATURE
FIELD E — PEAK OF FURROW
(Values in inches)

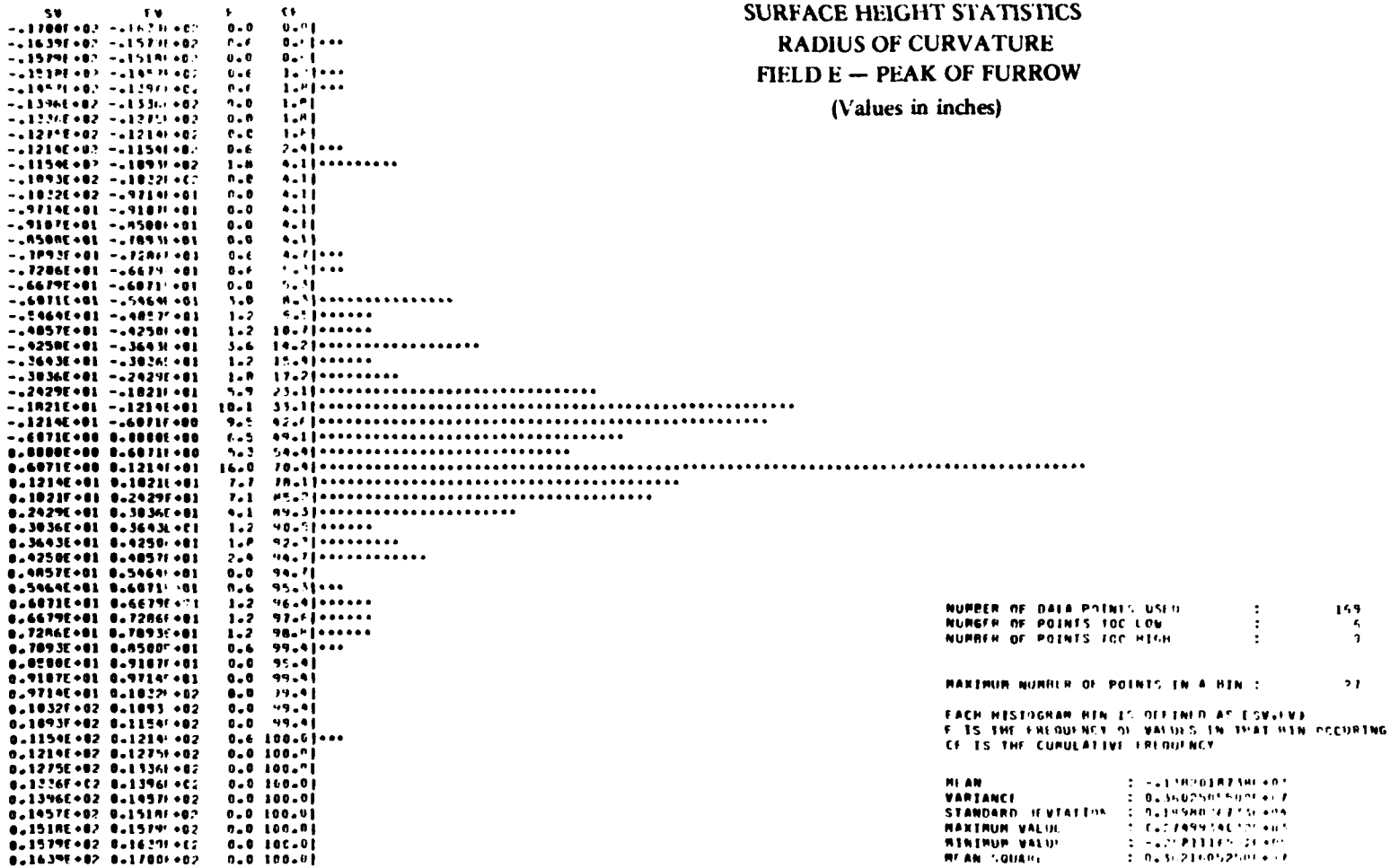

SV	EV	F	CF	
-.1780E+02	-.1639E+02	0.0	0.0	|
-.1639E+02	-.1579E+02	0.6	0.6	|***
-.1579E+02	-.1519E+02	0.0	0.6	|
-.1519E+02	-.1459E+02	0.6	1.3	|***
-.1459E+02	-.1396E+02	0.6	1.9	|***
-.1396E+02	-.1336E+02	0.0	1.9	|
-.1336E+02	-.1275E+02	0.0	1.9	|
-.1275E+02	-.1214E+02	0.0	1.9	|
-.1214E+02	-.1154E+02	0.6	2.6	|***
-.1154E+02	-.1093E+02	1.9	4.5	|*********
-.1093E+02	-.1032E+02	0.0	4.5	|
-.1032E+02	-.9714E+01	0.0	4.5	|
-.9714E+01	-.9107E+01	0.0	4.5	|
-.9107E+01	-.8500E+01	0.0	4.5	|
-.8500E+01	-.7893E+01	0.0	4.5	|
-.7893E+01	-.7286E+01	0.6	5.2	|***
-.7286E+01	-.6679E+01	0.6	5.8	|***
-.6679E+01	-.6071E+01	0.0	5.8	|
-.6071E+01	-.5464E+01	1.9	7.7	|**********
-.5464E+01	-.4857E+01	1.2	9.0	|******
-.4857E+01	-.4250E+01	1.2	10.2	|******
-.4250E+01	-.3643E+01	3.6	13.8	|******************
-.3643E+01	-.3036E+01	1.2	15.0	|******
-.3036E+01	-.2429E+01	1.8	17.2	|*********
-.2429E+01	-.1821E+01	5.9	23.1	|******************************
-.1821E+01	-.1214E+01	10.1	33.3	|**
-.1214E+01	-.6071E+00	9.5	42.8	|**
-.6071E+00	0.0000E+00	6.5	49.3	|**********************************
0.0000E+00	0.6071E+00	5.3	54.6	|***************************
0.6071E+00	0.1214E+01	16.0	70.6	|**
0.1214E+01	0.1821E+01	7.7	78.3	|**************************************
0.1821E+01	0.2429E+01	7.1	85.3	|***********************************
0.2429E+01	0.3036E+01	4.1	89.5	|*********************
0.3036E+01	0.3643E+01	1.2	90.8	|******
0.3643E+01	0.4250E+01	1.8	92.7	|*********
0.4250E+01	0.4857E+01	2.4	94.7	|************
0.4857E+01	0.5464E+01	0.0	94.7	|
0.5464E+01	0.6071E+01	0.6	95.4	|***
0.6071E+01	0.6679E+01	1.2	96.6	|******
0.6679E+01	0.7286E+01	1.2	97.8	|******
0.7286E+01	0.7893E+01	1.2	98.4	|******
0.7893E+01	0.8500E+01	0.6	99.0	|***
0.8500E+01	0.9107E+01	0.0	99.0	|
0.9107E+01	0.9714E+01	0.0	99.0	|
0.9714E+01	0.1032E+02	0.0	99.0	|
0.1032E+02	0.1093E+02	0.0	99.0	|
0.1093E+02	0.1154E+02	0.0	99.0	|
0.1154E+02	0.1214E+02	0.6	100.0	|***
0.1214E+02	0.1275E+02	0.0	100.0	|
0.1275E+02	0.1336E+02	0.0	100.0	|
0.1336E+02	0.1396E+02	0.0	100.0	|
0.1396E+02	0.1457E+02	0.0	100.0	|
0.1457E+02	0.1518E+02	0.0	100.0	|
0.1518E+02	0.1579E+02	0.0	100.0	|
0.1579E+02	0.1639E+02	0.0	100.0	|
0.1639E+02	0.1700E+02	0.0	100.0	|

NUMBER OF DATA POINTS USED : 169
NUMBER OF POINTS TOO LOW : 6
NUMBER OF POINTS TOO HIGH : 3

MAXIMUM NUMBER OF POINTS IN A BIN : 27

EACH HISTOGRAM BIN IS DEFINED AS (SV,EV)
F IS THE FREQUENCY OF VALUES IN THAT BIN OCCURING
CF IS THE CUMULATIVE FREQUENCY

MEAN : -.1[illegible]E+01
VARIANCE : 0.[illegible]E+02
STANDARD DEVIATION : 0.[illegible]E+01
MAXIMUM VALUE : 0.[illegible]E+01
MINIMUM VALUE : -.2[illegible]E+01
MEAN SQUARE : 0.[illegible]E+02

Figure A-45. Histogram of Surface Radius of Curvature, Field E, Along Peak of Furrows - Radius Values Given In Inches

SURFACE HEIGHT STATISTICS
RADIUS OF CURVATURE
FIELD E1 — TROUGH OF FURROW
(Values in inches)

SV	EV	F	CF
-.1780E+02	-.1639E+02	0.0	0.0 |
-.1639E+02	-.1579E+02	0.7	0.7 |******
-.1579E+02	-.1518E+02	0.0	0.7 |
-.1518E+02	-.1457E+02	0.0	0.7 |
-.1457E+02	-.1396E+02	0.0	0.7 |
-.1396E+02	-.1336E+02	0.0	0.7 |
-.1336E+02	-.1275E+02	0.7	1.4 |******
-.1275E+02	-.1214E+02	0.0	1.4 |
-.1214E+02	-.1154E+02	0.0	1.4 |
-.1154E+02	-.1093E+02	0.7	2.0 |****
-.1093E+02	-.1032E+02	0.0	2.0 |
-.1032E+02	-.9714E+01	0.7	2.7 |******
-.9714E+01	-.9107E+01	1.4	4.1 |************
-.9107E+01	-.8500E+01	0.0	4.1 |
-.8500E+01	-.7893E+01	2.0	6.1 |******************
-.7893E+01	-.7286E+01	2.7	8.8 |************************
-.7286E+01	-.6679E+01	2.0	10.8 |******************
-.6679E+01	-.6071E+01	2.7	13.5 |************************
-.6071E+01	-.5464E+01	2.7	16.2 |************************
-.5464E+01	-.4857E+01	0.7	16.9 |******
-.4857E+01	-.4250E+01	0.0	16.9 |
-.4250E+01	-.3643E+01	1.4	18.2 |************
-.3643E+01	-.3036E+01	3.4	21.6 |******************************
-.3036E+01	-.2429E+01	5.4	27.0 |**
-.2429E+01	-.1821E+01	8.8	35.8 |**
-.1821E+01	-.1214E+01	4.7	40.5 |**
-.1214E+01	-.6071E+00	6.1	46.6 |**
-.6071E+00	0.0000E+00	1.4	48.0 |************
0.0000E+00	0.6071E+00	0.7	48.6 |******
0.6071E+00	0.1214E+01	4.7	53.4 |**
0.1214E+01	0.1821E+01	8.1	61.5 |**
0.1821E+01	0.2429E+01	6.8	68.2 |**
0.2429E+01	0.3036E+01	4.1	72.3 |**************************************
0.3036E+01	0.3643E+01	2.7	75.0 |**************************
0.3643E+01	0.4250E+01	1.4	76.4 |************
0.4250E+01	0.4857E+01	1.4	77.7 |************
0.4857E+01	0.5464E+01	1.4	79.1 |************
0.5464E+01	0.6071E+01	4.1	83.1 |**************************************
0.6071E+01	0.6679E+01	7.4	90.5 |**
0.6679E+01	0.7286E+01	5.4	95.9 |**
0.7286E+01	0.7893E+01	0.7	96.6 |******
0.7893E+01	0.8500E+01	2.0	98.6 |******************
0.8500E+01	0.9107E+01	0.0	98.6 |
0.9107E+01	0.9714E+01	0.0	98.6 |
0.9714E+01	0.1032E+02	0.0	98.6 |
0.1032E+02	0.1093E+02	0.7	99.3 |******
0.1093E+02	0.1154E+02	0.0	99.3 |
0.1154E+02	0.1214E+02	0.0	99.3 |
0.1214E+02	0.1275E+02	0.0	99.3 |
0.1275E+02	0.1336E+02	0.0	99.3 |
0.1336E+02	0.1396E+02	0.7	100.0 |******
0.1396E+02	0.1457E+02	0.0	100.0 |
0.1457E+02	0.1518E+02	0.0	100.0 |
0.1518E+02	0.1579E+02	0.0	100.0 |
0.1579E+02	0.1639E+02	0.0	100.0 |
0.1639E+02	0.1700E+02	0.0	100.0 |

NUMBER OF DATA POINTS USED	:	104
NUMBER OF POINTS TOO LOW	:	11
NUMBER OF POINTS TOO HIGH	:	29
MAXIMUM NUMBER OF POINTS IN A BIN	:	11

EACH HISTOGRAM BIN IS DEFINED AS (SV , EV)
F IS THE FREQUENCY OF VALUES IN THAT BIN FALLING
CF IS THE CUMULATIVE FREQUENCY

MEAN	:	0.4918966500E+02
VARIANCE	:	0.4676873820E+01
STANDARD DEVIATION	:	0.2162252600E+00
MAXIMUM VALUE	:	0.1800000000E+02
MINIMUM VALUE	:	-.1869929040E+01
MEAN SQUARE	:	0.2418961912E+04

Figure A-46. Histogram of Surface Radius of Curvature

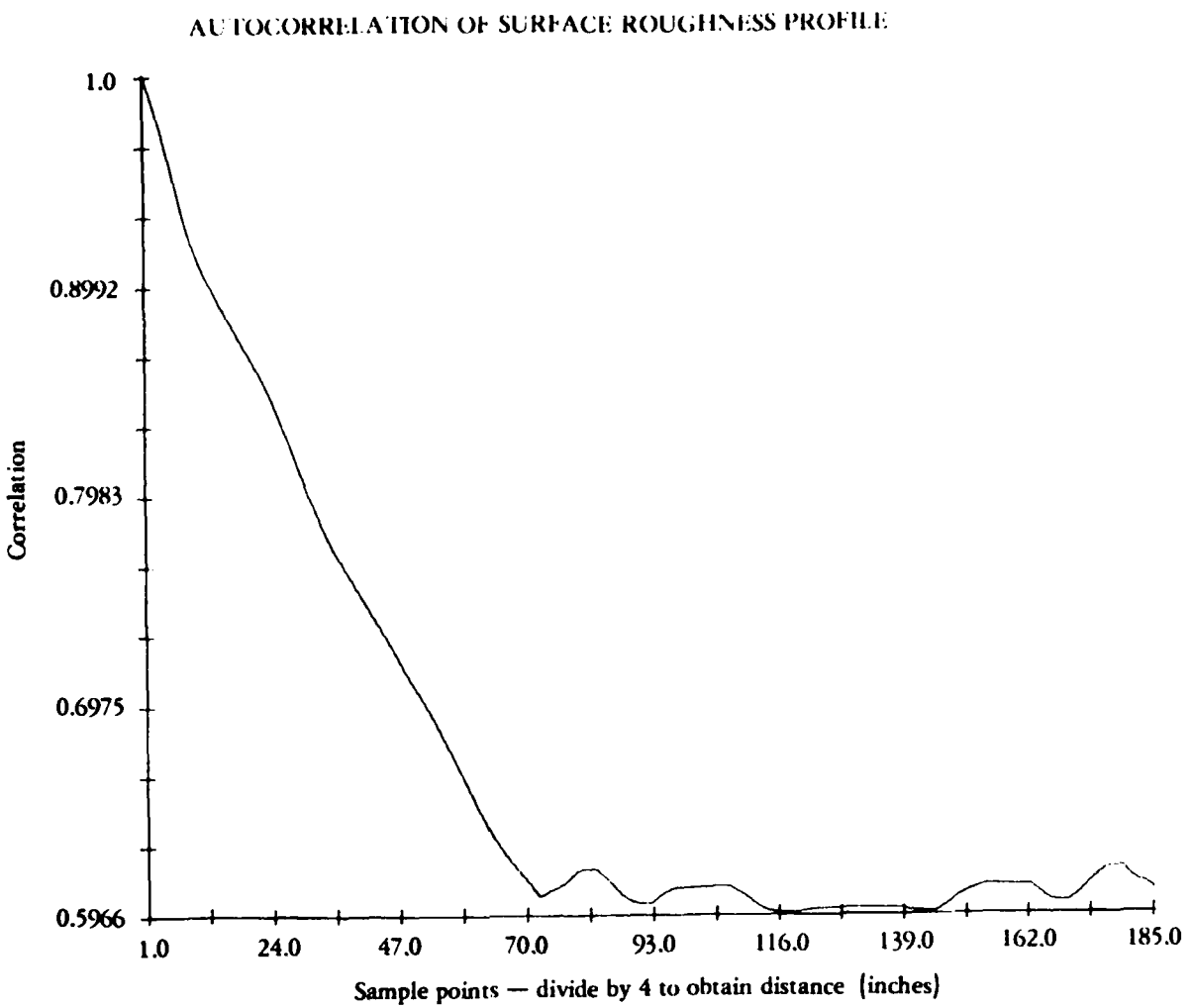

Figure A-47. Potato Field E - Top of Furrows

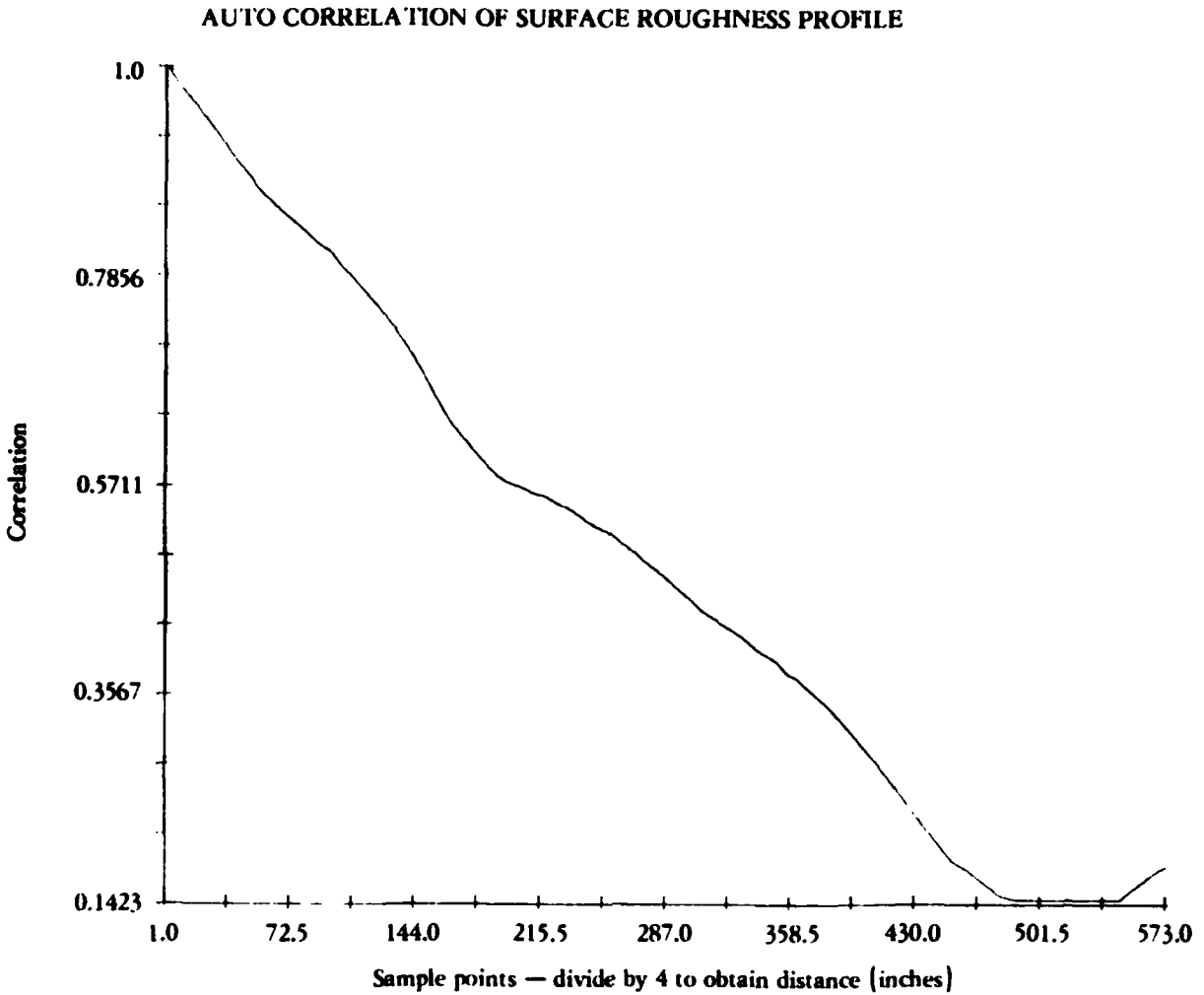

Figure A-48. Grass Field - Reflector Field RFS2

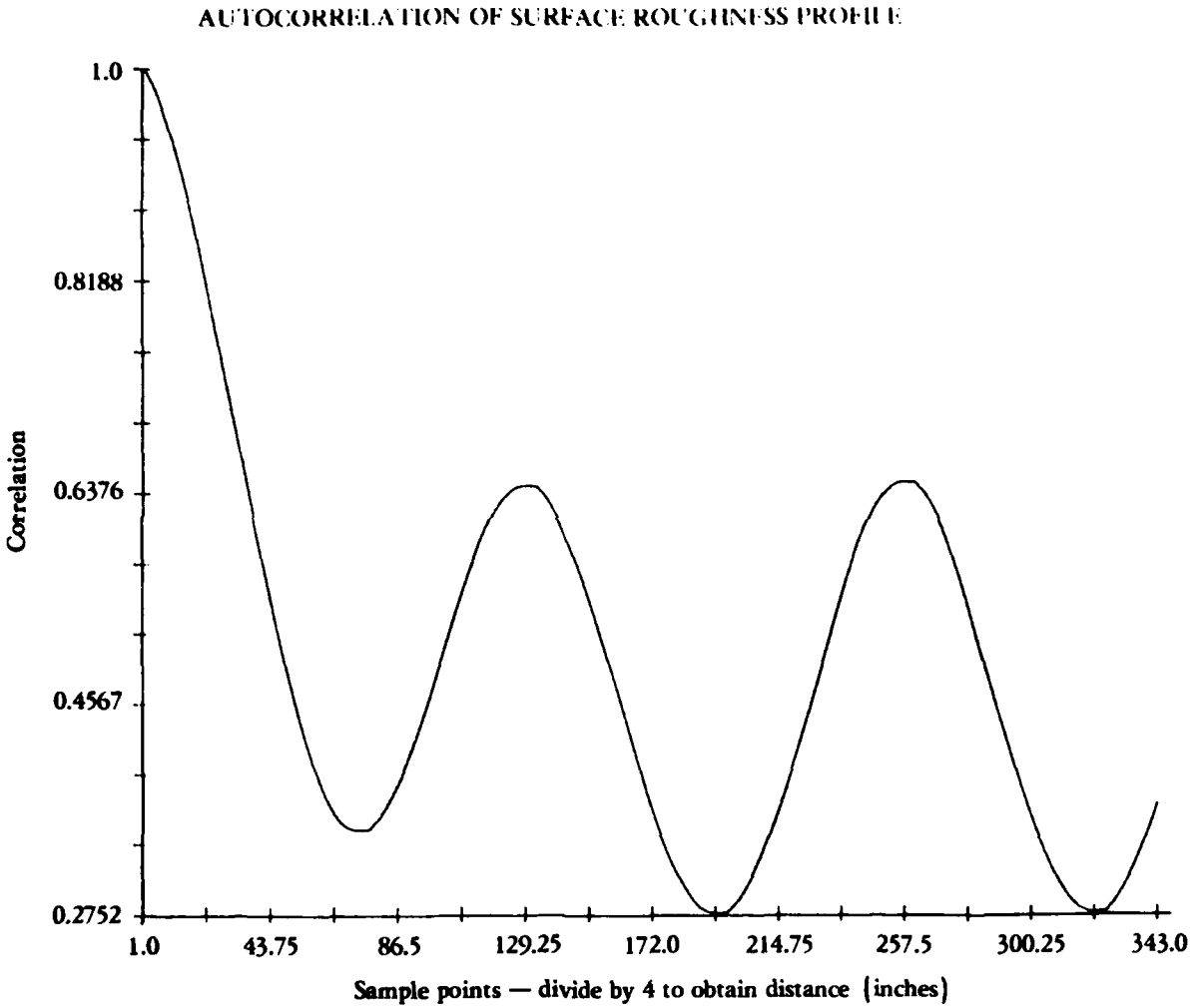

Figure A-49. Potato Field E - Furrows

REFERENCES

Barrick, D.E. and W.H. Peake, Scattering from Surfaces with Different Roughness Scales, Analysis and Interpretation, Battelle Memorial Institute, Rpt. No. BAT 197-A-10-3, AD662751, 1967.

Barrick, D.E., Rough Surface Scattering Based on The Specular Point Theory, Trans. IRE Trans. Ant. Prop., AP-16, No. 4, pp. 449-555, 1968.

Beckman, P. and A. Spizzichino, The Scattering of Electromagnetic Waves for Rough Surfaces, The MacMillan Co., New York, N.Y., 1963.

Burns, B., et al., MIZEX 1984 CV-580 Summary, ERIM Information Report No. 166900-6-T, Ann Arbor, MI, 1985.

Cheng, R.C.H. and N.A.K. Amin, Maximum Liklihood Estimation of Parameters in the Inverse Gaussian Distribution, with Unknown Origin, Technometrics, 23, 257-263, 1981.

Conover, W.J., Practical Nonparametric Statistics, 2nd ed., John Wiley and Sons, New York, 1980.

Cosgriff, R., W. Peake, and R. Taylor, Terrain Scattering Properties for Sensor System Design, Engineering Experiment Station Bulletin 181, Ohio State University, 1960.

Cosgriff, R.L., W.H. Peake, and R.C. Taylor, Terrain Scattering Properties for Sensor System Design (Terrain Handbook II), Engineering Experiment Station Bulletin No. XXIX, No. 3, Ohio State University, Columbus, May 1960.

de Ridder, et al., Project Report CMT-62, Lincoln Laboratory MIT, Lexington, MA 1984.

Folks, J.L. and R.S. Chhikara, The Inverse Gaussian Distribution and its Statistical Application, J. Royal Statist. Soc., B, 40, pp. 263-289, 1978.

Greenstein, L.J., A.E. Brindley, and R.D. Carlson, A Comprehensive Ground Clutter Model for Airborne Radars, IIT Research Institute, Chicago, Illinois, 15 September, AD 861 913L, 1969.

Ishimaru, A., Wave Propagation and Scattering in Random Media, Academic Press, 1978.

Kasischke, E.S., et al., SAR Data Collection and Processing Summary - 1983 Georgia Strait Experiment, ERIM Rept. No. 168400, DARPA/TTO and ONR Contract No. N00014-C-83-0513.

Katz, I. and L.M. Spetner, Polarization and Depression-Angle Dependence of Radar Terrain Return, Journal of Research of the National Bureau of Standards - D: Radio Propagation, Vol. 64D (5), 1960.

Larson, R.W., W. Carrara, and C. Liskow, Amplitude Calibration Techniques Applied to the Environmental Research Institute of Michigan's Airborne Synthetic Aperture Radar System, ERIM Technical Report AFAL-TR-74-239, Ann Arbor, Michigan, 1979.

REFERENCES (Continued)

Larson, R.W., W. Carrara, and J. Haynes, Radar Clutter Data Collection, Calibration, Digitization, and Analysis, ERIM Technical Report AFAL-TR-79-1232, Ann Arbor, Michigan, 1979.

Larson, R.W., R. Hamilton, F. Smith, and J. Haynes, Calibration of Synthetic Aperture Radar, Proc. IGRSS, Washington, DC, June 1981.

Larson, R.W., D. Politis, and J. Walker, Calibration Procedures and Test Plan for SAR, ERIM Final Report No. 157400-10-F, Ann Arbor, MI, 1982.

Larson, R.W. and A.L. Maffett, Calibration Model for SAR Systems, Electromagnetics (in press), 1985.

Maffett, A., et al., L-Band Clutter Statistics for Terrain and Ice, ERIM Final Report No. 128900-9-F1, AD B028457, 1978.

Long, M.W., Radar Reflectivity of Land and Sea, Artech House Inc., 1983.

Peake, W.H. and T.L. Oliver, The Response of Terrestrial Surfaces of Microwave Frequencies, Report Nos. AFAL-TR-70-301 and ESL-2440-7, Ohio State University, Columbus, AD 884 106, May 1971.

Rawson, R., F. Smith, and R. Larson, The ERIM Simultaneous X- and L-Band Dual Polarized Radar, Proc. of IEEE 1975 International Radar Conference, New York, p. 505, 1975.

Ruck, G.T. et al., Radar Cross-Section Handbook, Plenum Press, N.Y., p. 678, 1970

Schroedinger, E., Zur Theorie der Fall-und Steigversche an Teilchen mit Brownscher Bewegung, Physikalische Zeitschrift, 16, pp. 289-295, 1915.

Shuchman, R.A., et al., MIZEX 1983 SAR Data Summary, ERIM Information Report No. 166900-1-T, Ann Arbor, MI, 1983.

Spetner, L.M. and Katz, I., Two Statistical Models for Radar Return, IRE Trans. Ant. Prop., AP-8242, 1960.

Tweedie, M.C.K., Statistical Properties of Inverse Gaussian Distribution, Annals of Math. Statistics, 28, pp. 362-377, 1957.

Ulaby, F.T., R.K. Moore, and A.K. Fung, Microwave Remote Sensing, Addison-Wesley Pub. Co., Reading, Mass., Vol. 1, 1981; Vol. 2, 1982.

Walker, J.L. and R.W. Larson, SAR Calibration Review, ERIM Final Report No. 150400-7-F, Ann Arbor, MI, 1981.

Winebrenner, D. and A. Ishemave, Investigation of Surface Fold Phase Perturbation Technique for Scattering from Rough Surfaces, Radar Science, Vol. 20, No. 2, pp. 161-170, 1985.

MISSION
of
Rome Air Development Center

RADC plans and executes research, development, test and selected acquisition programs in support of Command, Control Communications and Intelligence (C^3I) activities. Technical and engineering support within areas of technical competence is provided to ESD Program Offices (POs) and other ESD elements. The principal technical mission areas are communications, electromagnetic guidance and control, surveillance of ground and aerospace objects, intelligence data collection and handling, information system technology, solid state sciences, electromagnetics and electronic reliability, maintainability and compatibility.

Printed by
United States Air Force
Hanscom AFB, Mass. 01731

DTIC

END

4-86